Architecture and evolution of the Central Eastern Ghats province: Araku-Paderu-Visakhapatnam.

Campbell L. Harvey

E-mail address: campbell.harvey@student.adelaide.edu.au
Tectonics, Resources and Exploration (TRaX), University of Adelaide, SA 5005, Australia

Supervisors: Alan Collins and Guillaume Backé

Abstract

The Eastern Ghats Mobile Belt (EGMB) is a Proterozoic granulite belt extending along the east coast of peninsular India. The EGMB exposes a deep crustal section through a composite orogenic belt that once formed part of the Proterozoic mobile belt system within East Antarctica and East India. A widely distributed megacrystic granitoid suite comprising charnockites and granites forms an important litho-unit of the Central Eastern Ghats (CEG). New U-Pb Laser Ablation Inductively Coupled Mass Spectrometry (LA-ICPMS) ages from zircons and monazite are reported in this study for two megacrystic granitoids, two charnockites and a megacrystic orthogneiss from the Araku-Paderu-Vadaddi region of the CEG. Samples yielded zircon age clusters at ~1000 Ma for cores and ~950 Ma for both cores and metamorphic rims. Monazites from a megacrystic granitoid recorded an age of 949 ± 12 Ma. Zircon rims from one megacrystic granitoid collected proximal to the Narsipatnam Shear Zone yielded metamorphic ages of ~850 Ma, ~750 Ma and ~550 Ma.

LA-Multicollector-ICPMS analysis of Lu/Hf isotopes in zircon reveals negative εHf values for all samples indicating crustal contamination of the source melts. Hf model ages indicate crustal residence times of between 1.98 and 2.5 Ga.

Geochemical discrimination plots of these megacrystic granitoids suggest an S-type nature and a post-collisional, within plate granite petrogenesis. The new ages presented for the Central Eastern Ghats Belt in this study are similar to published ages for the Rayner Complex and the Mawson Coast of Eastern Antarctica. These similar ages lend support to the proposition that these areas were complimentary parts of an extensive orogenic belt formed during the Grenvillean Orogeny around 1 Ga. The Central Eastern Ghats Belt also shows evidence of a localised Pan-African overprint proximal to the Narsipatnam Shear Zone.

Table of Contents

1. Introduction

The Eastern Ghats Mobile Belt (EGMB) is a polycyclic granulite terrain extending NE-SW along the east coast of peninsular India for ~ 900km with an average width of 100km. The EGMB exposes a deep crustal section through a composite orogenic belt that once formed part of the Proterozoic mobile belt system within East Antarctica and East India (Dobmeier & Raith, 2003). The western boundary of the EGMB is marked by a shear zone along which the granulites are thrust over the Archean Bastar and Dharwar cratons. In the north it is bound by the Archean Singhbum craton (Fig.1).

The EGMB comprises mainly upper amphibolite to granulite facies rocks. The principal rock types include a wide variety of pyroxene bearing gneisses (enderbites, mafic granulites and charnockites), a group of garnet-sillimanite-bearing gneisses and associated metasediments (khondalites, calc-granulites and quartzites) (Chetty, 2001). In the central part of the EGMB, intensely migmatised supracrustal granulites are intruded by voluminous plutons of megacrystic, garnet and orthopyroxene-bearing granitoids.

The EGMB is a highly reworked terrain, having been subjected to multiple events of magmatism and metamorphism throughout the Proterozoic. Of relevance to this study are the events associated with the Grenvillean orogeny (1.1 – 0.95 Ga) which inflicted pervasive deformation and granulite facies metamorphism throughout the central EGMB. This HT-phase of metamorphism is believed to be linked to the voluminous intrusion of megacrystic granitoids between 985 and 955 Ma (Aftalion et al. 1988, Paul et al., 1990).

The area of the Central Eastern Ghats (CEG) covered by this study has limited temporal constraints on the timing of emplacement of this syn-orogenic granitoid suite. The age of emplacement these late Mesoproterozoic granitoids is of significance as their intrusion was coeval with collisional events in other cratons associated with the amalgamation of the Rodinia supercontinent. The ages of emplacement of these granitoids have been used as a line of evidence for the hypothesis that the EGMB was contiguous with the Rayner Complex during Grenvillean time. Therefore, understanding the tectonometamorphic history of the CEG is vital for reconstruction of the supercontinent assembly during the Precambrian and the early Palaeozoic (Mukhopadhyay & Basak, 2009).

In this study we present new geochronological and geochemical data for the megacrystic granitoids of the CEG. Precise U-Pb zircon and monazite ages were determined using LA-ICPMS. Lu-Hf isotope analyses were undertaken with LA-MC-ICPMS and whole rock geochemistry for major elements, trace elements and REEs was performed. This data is used to constrain the age of emplacement and determine the provenance of the granitoid suite.

2. Geological Setting

The EGMB comprises two major rock groups: one charnockitic and the other khondalitic. The charnockitic group consists of mafic to acidic charnockites, hypersthene-bearing granulites, gneisses and leptynites while the khondalitic group includes garnet-sillimanite gneisses, quartzites and calc-silicates.

Ramakrishnan et al. (1998) divided the EGMB into five longitudinal zones based on the relative abundance of the lithological units. These zones are the Transition zone (TZ), the Western Charnockite zone (WCZ), the Western Khondalite zone (WKZ), the Eastern Khondalite zone (EKZ), and the Central Charnockite-Migmatite zone (CMZ) (Fig. 1). Chetty (2001) identified several mega-lineaments in Landsat TM imageries and used this network of shear zones to subdivide the EGMB into 9 large terranes. At the same time as Chetty was dividing the EGMB using shear zones Rickers et al. (2001) distinguished 4 crustal domains within the EGMB using the combination of Nd crustal ages with Sr whole-rock characteristics and Pb signatures. These crustal domains were not in agreement with the longitudinal zones delineated by Ramakrishnan et al. (1998).

Dobmeier and Raith (2003) proposed to divide the EGMB into 4 provinces, each with a distinct geological history. The provinces are subdivided into a total of 12 domains, each being characterised by specific lithology, structure and metamorphic grade (Mukhopadhyay & Basak, 2009). The four provinces are the Jeypore Province, Krishna Province, Eastern Ghats Province, and Rengali Province. For the purposes of this study we have chosen to adopt this classification system. Consequently, the area covered by this project is located within their Eastern Ghats Province (EGP) and the Visakhapatnam domain. The study area comprises a ~100km transect from the city of Visakhapatnam to the town of Araku via the towns of Anakapalle, Vadaddi and Paderu (Fig. 2). The transect cuts across the general strike of the EGMB heading from the coast inland towards the Bastar Craton. Vaddadi is in the area proposed by Chetty (2010) to be dissected by the Narsipatnam Shear Zone.

The principal rock types of the EGP are garnet sillimanite quartzo-feldspathic (QF) gneiss (khondalite), small bodies of high-Mg-Al granulite, calc-silicate gneiss and mafic granulite. These are interspersed with massif-type anorthosite and intrusive granite-charnockite (opx-free and opx bearing granitoid) complexes (Mukhopadhyay & Basak, 2009). The Araku-Paderu transect is a representative sector of the entire EGMB, and consists of almost all the major and minor lithologies in the EGMB except anorthosites (Divakara Rao and Murthy, 1998).

The megacrystic, garnet and orthopyroxene-bearing granitoids show a clear intrusive relationship with the metasedimentary khondalites of the area. These garnet sillimanite bearing QF gneisses have a pervasive fabric which is defined by garnet and biotite rich bands.

From regionally limited structural studies, it has been concluded that the EGMB experienced three discrete major episodes of regional deformation. The first episode (D_1) resulted in the formation of strongly appressed isoclinal folds (F_1) with axial trends in the east-northeast-west-southwest and northeast southwest directions. D_1 is coeval with ultrahigh-grade metamorphism (Dobmeier & Raith, 2003). The second episode (D_2) led to open cross-folds (F_2) trending north-south and north-northwest-south-southeast. D_2 is associated with the pervasive Late-Grenvillian tectonothermal event. The third episode (D_3) resulted in cross folding (F_3) of the earlier folds along approximately east-west trending axes into gentler antiforms and synforms. D_3 is believed to be a Pan-African thermal overprint associated with the assembly and breakup of Gondwana (Sarkar et al., 1981, Lal et al., 1987). The multi-intrusive granite-charnockite complexes present in the EGP were not affected by the early pervasive deformation (D1) observed in the khondalites of the area.

3. Sampling, analytical methods and data treatment

3.1 Field work and data collection

Field work was conducted over a period of 3 weeks in January 2010. Structural data and representative samples were collected along the Araku-Paderu-Visakhapatnam transect (Fig. 2). Data collected included foliation and lineation measurements, fold geometry and kinematic indicators. Foliations were measured as dip/dip direction. Figure 4 presents structural measurements collected along the Paderu-Vaddadi transect. Much of the outcrop in the khondalite zone was highly weathered making mineral lineations difficult to ascertain.

Five of the samples collected were chosen for geochronological and geochemical analysis. These consisted of two charnockites (CG10-044, CG10-133), two K-feldspar megacrystic granitoids (CG10-087, CG10-142) and one megacrystic orthogneiss (CG10-006). The locations for individual samples and field data locations are provided in Figure 2.

3.2 U-Pb geochronology

Mineral separations were carried out at the University of Adelaide. Hand sized samples were cleaned with a steel wire brush, cut down with a diamond saw and crushed using a standard jaw crusher. Samples were next split and sieved using a combination of 75 and 425 μm mesh. The 75-425 μm fraction was then hand-panned to isolate heavy mineral components. Once dried, magnetic fractions were removed by a Nd hand magnet. A representative collection of zircon and monazite grains were then handpicked under a binocular microscope. Zircon grains (~ 100-200 per sample) and monazite grains (~10) chosen for analysis were mounted in 25 mm epoxy resin discs and polished until their centres were exposed. The mounts were then cleaned, carbon-coated and imaged via cathodoluminescence (CL) and backscattered electron (BSE) (acc. V 12kV, spot size 7) with a Phillips XL20 SEM coupled with a Gatan CL detector at Adelaide Microscopy.

U-Pb geochronology of zircons and monazite was conducted by Laser Ablation Inductively Coupled Plasma Mass Spectrometry (LA-ICP-MS) at Adelaide Microscopy. Analyses were performed using an Agilent 7500cs ICPMS coupled with a New Wave UP-213 Nd-YAG laser ablation sampling system (λ=213 nm). Ablation was performed in a helium atmosphere with a repetition rate of 5 Hz and laser intensity of 75%. Spot sizes of 30 μm and 40 μm were employed for zircons and monazites, respectively. $^{206}Pb/^{238}U$, $^{207}Pb/^{235}U$, $^{207}Pb/^{206}Pb$ and $^{208}Pb/^{232}Th$ isotope ratios were measured. Each analysis involved 30 seconds of background measurement, 10 seconds for beam and crystal stabilisation, 60 seconds of sample ablation, followed by a 30 second delay to purge the previous sample.

For zircon analysis calibration against a standard zircon GEMOC GJ-1 (published $^{207}Pb/^{206}Pb$ age of 607.7 ± 4.3 Ma, $^{206}Pb/^{238}U$ age of 600.7 ± 1.1 Ma, Jackson et al. 2004) involved a typical run of four analyses followed by two analyses of the internal standard, Plesovice as an independent control. (published $^{207}Pb/^{206}Pb$ age of 339.22 ± 0.25 Ma, $^{206}Pb/^{238}U$ age of 337.13 ± 0.37 Ma, Slama et al., 2008), Analysis of up to 12 unknowns followed initial calibration, followed by four further analyses of the GJ-1 standard to correct for instrument drift.

Monazite analysis utilised the 440 external standard for calibration and the 222 internal standard as an independent control. Runs for monazite analysis were performed as per zircons.

Age determination of individual zircons and monazites was performed with the real-time correction program GLITTER version 3.0 (Van Achterbergh *et al*. 2001).

Concordia diagrams and weighted average plots ages were constructed using the ISOPLOT version 4.11 software (Ludwig, 2009). Probability distribution plots were created using AgeDisplay software (Sircombe, 2004).

3.3 Lu/Hf isotope analyses

Lu/Hf isotope analyses were conducted on zircons previously targeted for U/Pb age data. Analyses were undertaken at the University of Adelaide, Waite (CSIRO) campus. Only zircons which gave concordant ages of >90% were targeted for analyses. Where possible, both cores and rims were targeted. The Hf isotope data were acquired with a Thermo-Scientific Neptune multi-collector ICP-MS coupled to a New Wave UP-193 Excimer laser ablation sampling system (λ =193 nm). Laser repetition rates of 5 Hz and spot sizes of 50 µm diameter were employed. Laser fluence was maintained at ~ 8 J/cm2. Ablation was conducted in the standard New Wave sample cell, with the He carrier gas mixing with Ar sample gas upstream of the ablation cell prior to transport into the ICP-MS.

^{171}Yb, ^{173}Yb, ^{175}Lu, ^{176}Hf, ^{177}Hf, ^{178}Hf, ^{179}Hf and ^{180}Hf were measured on Faraday detectors with $10^{12}\Omega$ amplifiers. An integration interval of 0.232 seconds was employed. The present study follows the interference and mass bias correction protocols recommended by Woodhead et al. (2004).

Hf mass bias was corrected using exponential law fractionation correction using a stable Hf isotope ratio of ^{179}Hf/^{177}Hf=0.7325. Yb isobaric interference on ^{176}Hf was corrected by direct measurement of Yb fractionation using ^{171}Yb/^{173}Yb coupled with the Yb isotopic values of Segal et al. (2003). The applicability of these values were verified by analysing JMC 475 Hf solutions doped with varying levels of Yb with interferences up to ^{176}Yb/^{177}Hf= ~0.5.

Lu isobaric interference on ^{176}Hf was corrected using a ^{176}Lu/^{175}Lu ratio of 0.02655 with the assumption that the mass bias behaviour of Lu is analogous to that of Yb.

For Yb signals below 10 mV interference corrections were made using an empirically derived 176Yb/173Yb ratio and the Hf mass bias factor similar to the method described by Griffin et al. (2000). This was done as the potential errors involved in the method are outweighed by the significantly greater uncertainty caused by the small Yb beam. In this case an empirically derived ratio of 0.739689 was used. This was derived by analysis of a series of Yb and Hf doped glass beads.

Set-up of the system prior to ablation sessions was conducted using analysis of JMC475 Hf solution and an AMES Hf solution. Confirmation of accuracy of the technique for zircon analysis was monitored using a combination of the Plesovice (Slama et al., 2008), Mudtank (Black and Gulson, 1978) and QGNG standards. The average $^{176}Hf/^{177}Hf$ Plesovice value for all runs is 0.282496 (2SD=0.000022, n=27). This compares to the published value of 0.282482 +/- 0.000013 (2SD) by Slama et al (2008). The long term average is 0.282488 (2SD=0.000044, n=44).

3.4 Whole-rock geochemistry

Representative whole-rock analyses were conducted on one Major element analysis (SiO2, MgO, Fe2O3, MnO, CaO, TiO2, Na2O, K2O and P2O5) was performed on 5 samples of charnockites and megacrystic granitoids. Samples were crushed as per preparation of geochronology samples (3.2) at the University of Adelaide. Crushate was milled in a tungsten carbide mill (a possible source of Ta contamination) until the powder could pass a 75 µm mesh. The powder was sent to Amdel analytical laboratories (Wingfield, South Australia) for analysis. Four different methods of analysis were employed. For measuring the major oxides (Al, Ca, Fe_t (total Fe), K, Mn, Mg, Na, P, S, Ti) and Cr, V, Sc and Zr, a 0.1g subsample of the analytical pulp was fused with lithium metaborate followed by dissolution to give a total concentration for the given element. The solution was then analysed using an Inductively Coupled Plasma-Optical Emission Spectroscope (ICPOES) for determination of major element concentrations. The resulting solution was then analysed with an ICPMS for Ba, Be, Hf, Sn and Ta. To measure the concentrations of Cs, Ga, Zn, Ce, La, Mo, Nb, Rb, Sr, Th, U, and Y a small subsample (~0.5g) was digested in an HF/multi acid solution and then analysed with an ICPMS. Concentrations of Dy, Er, Eu, Gd, Ho, Lu, Nd, Pr, Sm, Tb, Tm and Yb were measured by IC3R.

4. Results

4.1 Structure

The area between Araku and Paderu is dominated by large charnockite and megacrystic granitoid massifs, khondalites and quartzo-feldspathic gneisses. The dominant foliation of the khondalites and gneisses in the area dips steeply to the south-southeast (62/154) and the lineation plunges steeply south (45→167) (Fig. 4A-B). Although lacking foliation, the megacrystic granites intermittently display magmatic flow directions sub-parallel to the dominant foliation. These are characterised by the sub-horizontal alignment of K-feldspar porphroblasts. These flow directions trend NNE-SSW. The intrusive nature charnockites and megacrystic granites is well displayed in various outcrops in the Paderu area where massive granitoid bodies can be seen to contain enclaves of partly digested foliated and folded khondalite (Figs. 5A,B). This relationship suggests that the granitoid plutons intruded subsequent to deformation or late in the pervasive fabric defining metamorphic event. The area south of Paderu towards Vaddadi is dominated by well foliated garnet sillimanite quartzo-feldspathic gneisses (khondalites). Figure 4 presents a structural map of the northern half of the Paderu-Vaddadi transect. The dominant foliation in this area dips steeply towards the south (70/181) and the lineation plunges south (38→172) (Fig. 3C and 3D). A structural map of the Paderu-Vaddadi is presented in Figure 4.

4.2 Geochronology

4.2.1 U/Pb LA-ICPMS zircon analysis

U/Pb LA-ICPMS zircon analysis results are presented in Tables 1-5, and Figures 6-34. CL images of selected zircons are displayed in Figures 6, 15, 20, 25 and 30.

To rule out skewed results of ages due to lead-loss during metamorphic events only the 95-105% concordant analyses are considered in detail. All errors on quoted ages are one standard deviation.

4.2.1.1. Sample CG10-006

Sample CG10-006 is K-spar megacrystic orthogneiss that was collected 2km WNW of Araku. (18°20'29.86"N 82°50'51.91"E) (Fig. 2). The foliation of this orthogneiss dipped 74°/230° and the rock cropped out adjacent to migmatitic mafic gneisses and charnockites. The sample is composed of K-feldspar phenocrysts (up to 4cm) in a fine grained matrix of plagioclase, biotite and hornblende. Plagioclase shows myrmekitic textures with quartz. Accessory minerals are apatite and monazite.

The zircons from this sample range in morphology from equant to tabular euhedral crystals with clear faces to sub-rounded grains. Cores display clear oscillatory zoning indicating their igneous origin. Local recrystallisation of cores leading to convolute zoning cross-cutting oscillatory zones is common. Rims range in size from small to large with the majority being homogenous with low CL response.

47 analyses were carried out on 33 zircons targeting 29 cores and 18 rims (Table 1). Of the analyses 45% were between 95-105% concordant, and 94% between 90-110% concordant. All data and 95-105% concordant data are presented on two separate Wetherill concordia diagrams (Figs. 7 and 8). The oldest concordant analysis (07_01) was from a fractured equant euhedral core with frequent narrow magmatic oscillatory zones and a high CL response recrystallised rim with ghost zoning (Fig. 6A). This core yielded a $^{207}Pb/^{206}Pb$ age of 1087 ± 27 Ma. The youngest analysis (28_02) came from a rim and yielded a $^{206}Pb/^{238}U$ age of 911 ± 11 Ma (Fig. 6B).

The $^{206}Pb/^{238}U$ probability density distribution plot for all data and concordant (95-105%) data displays age maxima at 945 Ma, 1019 Ma, and 1080 Ma (Fig. 9).

All analyses were plotted in Th/U age space. Rims have a consistently lower Th/U ratio than cores, with rims displaying a maximum Th/U ratio of ~0.66 and cores of ~1.1 (Fig. 10). This suggests the rims were formed under metamorphic conditions. Weighted mean of $^{206}Pb/^{238}U$ concordant (95-105%) data for cores yields an age of 981 ± 13 Ma (MSWD = 7.4, n=27). This mean disregards the two oldest concordant cores, which together yield a mean $^{207}Pb/^{206}Pb$ age of 1067 ± 33 Ma (MSWD = 0.95) (Fig. 11). Cores were grouped together according to morphology for age analysis, but this failed to yield MSWDs indicative of discrete populations. Concordant cores were therefore sorted into three groups corresponding to the three probability density distribution age maxima. The oldest of these three groups consists of the two cores previously mentioned. The middle group (n=7) cluster around the 1019 Ma age maxima and yield a $^{206}Pb/^{238}U$ mean weighted age of 1019 ± 16 Ma (MSWD = 1.9, prob. = 0.078) (Fig. 12) As this age is within error of the age of the two oldest zircons, this can be considered to be a single event. The youngest group (n=10) cluster around the 945 Ma age maximum and yield a $^{206}Pb/^{238}U$ mean weighted age of 955 ± 11 Ma (MSWD = 1.7, prob. = 0.073) (Fig. 13).

A weighted mean of $^{206}Pb/^{238}U$ concordant (95-105%) data for rims yields an age of 943 ± 13 Ma (MSWD = 2.7, n=11) (Fig.14). One of the twelve concordant rim analyses was rejected in calculating this mean age as it gives a result outside of two standard deviations of the mean. This analysis (11_01, 105% conc.) may have drilled through a rim into a core. The weighted mean of the tightest clustered concordant $^{206}Pb/^{238}U$ ages for rims yields a more precise age of 943 ± 8 Ma (MSWD = 0.77, n=9) and a $^{207}Pb/^{206}Pb$ age of 932 ± 18 Ma (MSWD= 0.77).

The crystallisation age of this orthogneiss is interpreted to be ca. 1050 Ma, with the ca. 950 Ma age recorded in the youngest cores and the rims interpreted to represent the timing of the fabric forming metamorphic event for this orthogneiss. The cores giving this younger 950 Ma age appear to be recrystallised.

4.2.1.2. Sample CG10-044

Sample CG10-044 is a charnockite which was collected from a charnockite massif alongside the road between Araku and Paderu (18°15'3.81"N, 82°47'55.24"E) (Fig.2). This charnockite had what appeared to be a magmatic flow foliation trending east-west.

This greasy green charnockite is composed of quartz, K-feldspar, garnet, two pyroxene, plagioclase (myrmekitic), and biotite. In biotite rich domains, biotite flakes are deflected around the garnets suggesting the biotite crystallised post garnet crystallisation.

The zircons from this sample range in morphology from equant to tabular euhedral crystals with clear crystal faces to sub-rounded equant grains. Cores of nine zircons display clear oscillatory zoning indicating their igneous origin, whereas the majority of cores display convolute and chaotic zoning typically observed in zircons from granulites (Corfu et al., 2003). Rims range in size from small to large with the majority displaying growth zones of medium to high CL responses. Sub-rounded metamorphic ‘soccer ball’ style zircons displaying sector zoning also occur in this sample (Figs. 15 A-F).

48 analyses were carried out on 33 zircons targeting 24 cores and 18 rims and 6 recrystallised zones (Table 2). Of the analyses 54% were between 95-105% concordant, and 85% between 90-110% concordant. All data and 95-105% concordant data are presented on two separate Wetherill concordia diagrams (Figs. 16 and 17). The oldest concordant core analysis came from a zoned core showing very limited recrystallisation (25_01). This core yielded a $^{207}Pb/^{206}Pb$ age of 1000 ± 27 Ma (Fig 15 A). This is interpreted as the crystallisation age of this charnockite. The youngest concordant analysis (09_02) came from a rim of zircon with a clearly recrystallised core (Fig. 15 B) yielding a $^{206}Pb/^{238}U$ age of 879 ± 11 Ma (95% conc.).

The $^{206}Pb/^{238}U$ probability density distribution plots for CG10-044 display age maxima at 940 Ma for 95-105% concordant data and 940 Ma and 1094 Ma for all data (Fig. 18).

A plot of Th/U ratio versus $^{206}Pb/^{238}U$ age for all data reveals that cores from CG10-044 plot consistently lower than rims and recrystallised zones (Fig.19). Cores have a maximum Th/U ratio of ~1.0 whereas rims range in Th/U ratios of ~0.2 - 3.6. Recrystallised zones range from ~1.2 - 3.2.

The 95-100% concordant data plotted on a standard Weatherill plot defines a discordia with a upper intercept at 1087±100 Ma and a lower intercept of 817±84 Ma (MSWD = 0.85). This upper intercept is interpreted to be the crystallisation age of this charnockite. The cores which plot within 5% of concordancy have a weighted mean $^{206}Pb/^{238}U$ age of 939 ± 16 Ma (MSWD=6.1) and a $^{207}Pb/^{206}Pb$ age of 954 ± 16 Ma (MSWD=1.6). The latter age is interpreted as a metamorphic event which recrystallised the majority of cores in this sample and formed the rims. The 95-105% concordant data for rims and recrystallised zones yielded a weighted mean $^{206}Pb/^{238}U$ age of 938 ± 14 Ma (MSWD=2.8) and a $^{207}Pb/^{206}Pb$ age of 958 ± 16 Ma (MSWD=1.0). This indicates that rims and cores in this sample were formed during the same event.

This charnockite is interpreted to have crystallised at ca. 1000 Ma or earlier and subsequently experienced a high grade metamorphic event at 958 ± 16 Ma followed by a lesser event at ca. 900 Ma.

4.2.1.3. Sample CG10-087

Sample CG10-087 is a K-feldspar megacrystic granitoid that was collected from a road cutting approximately 20 km west of Paderu (18° 3'44.99"N, 82°35'6.04"E) (Fig. 2).

This granitoid consists of K-feldspar megacrysts (up to 5 cm), quartz, plagioclase, garnet, biotite and opaque oxides (magnetite and ilmenite). Accessory minerals are apatite, monazite and zircon. Optical properties indicate biotite and garnet are high temperature.

56 spots on 36 zircons targeting 28 cores and 15 rims and 13 recrystallised zones (Table 2). Of the analyses 70% were between 95-105% concordant. All data and 95-105% concordant data are presented on two separate Wetherill concordia diagrams (Figs. 21 and 22). The zircons show a common lead loss trend and a smear of ages near concordia from 1000 Ma to 880 Ma. The $^{206}Pb/^{238}U$ probability density distribution plot for all data and concordant (95-105%) data displays one major age maximum at 955 Ma with an irregularity at 895 Ma and a minor peak at 768 Ma represented by one concordant analysis (Fig. 23).

Th/U ratio versus $^{206}Pb/^{238}U$ age plot for all data shows the majority of cores plotting below Th/U ratios of 0.4 and the majority of rims plotting above 0.4 with a maximum value of 1.5. Recrystallised zones also have higher Th/U ratios than the cores, the majority plotting between 0.7 – 1.3. There is no clear relationship between $^{206}Pb/^{238}U$ age and Th/U value.

The oldest concordant zircon (23_01, Fig. 20 A) returned a $^{206}Pb/^{238}U$ age of 1019 ± 14 Ma (102% conc.) and the youngest concordant zircon (30_01, Fig. 20 B) returned a $^{206}Pb/^{238}U$ age of 768 ± 10 Ma (95% conc.).

Zircons from this sample were sorted into morphologically distinct groups. Group 1 is characterised by euhedral zircons with well defined oscillatory zoned cores. Cores have undergone little or no recrystallisation and rims are small or non-existent (Figs. 20 A, F). Group 2 is characterised by partially resorbed low CL-response cores with large sub-rounded high-CL response metamorphic rims (Figs. 20 C,D).

Group 1 cores (95-105% concordance, n= 7) return a weighted average $^{207}Pb/^{206}Pb$ age of 998 ± 16 Ma (MSWD = 1.04) and a $^{206}Pb/^{238}U$ age of 994 ± 13 Ma (MSWD = 1.3, n=19). Group 2 cores (95-105% concordance, n= 10) return a weighted average $^{207}Pb/^{206}Pb$ age of 966 ± 17 Ma (MSWD = 1.2) and a $^{206}Pb/^{238}U$ age of 954 ± 16 Ma (MSWD = 3.5).

A weighted average of all concordant (95-105%) rims and recrystallised zones returns a $^{206}Pb/^{238}U$ age of 939 ± 13 Ma (MSWD = 5, n=19) and a $^{207}Pb/^{206}Pb$ age of 947 ± 16 Ma (MSWD = 1.9).

These ages are interpreted to represent a crystallisation age of ca. 1000 Ma, a metamorphic recrystallisation event at ca. 950 Ma for this megacrystic granitoid.

4.2.1.4. Sample CG10-133

Sample CG10-133 is a 2 pyroxene charnockite that was collected approximately 1 km south of Paderu (Fig. 2) (18° 4'16.85"N, 82°41'23.65"E).

This charnockite consists of quartz, K-feldspar, garnet, orthopyroxene, clinopyroxene, plagioclase, biotite, opaque oxides (including ilmenite), apatite and zircon. The optical properties of the biotite are indicative of very high temperatures.

Zircons from this sample range in morphology from sub-rounded to sub-angular shapes with low-CL response xenocrystic cores and large high-CL response rims. Euhedral tabular zircons with large dark oscillatory zoned cores and small high-CL rims. Some cores show evidence of recrystallisation of oscillatory zones and localised enrichment of REEs (Fig. 25 D). The zircons from this sample display rims with external morphologies ranging from sub-rounded and highly resorbed shapes to euhedral in nature (Fig. 25 A-D). All characterise metamorphically grown rims, but euhedral shaped rims suggest formation in the presence of carbonic or aqueous fluids (Corfu et al., 2003). Zircon 12_01 is an example of the sub-rounded multifaceted ‘soccer-ball’ morphology typical of metamorphic zircons (Corfu et al., 2003) (Fig. 25 E).

A total of 44 spots on 27 zircons were analysed, targeting 27 cores, 15 rims and 2 recrystallised zones (Table 4). Of these analyses 32% were between 95-105% concordant, and 73% between 90-110% concordant.

The oldest concordant core (08_01) was within a sub-rounded equant zircon with a large homogeneous recrystallised core (Fig. 25 A). This xenocrystic core yielded a $^{207}Pb/^{206}Pb$ age of 1575 ± 23 Ma, with the rim giving a $^{206}Pb/^{238}U$ age of 881 ± 11 Ma. Being the only zircon in this sample of this age, this core is interpreted as being inherited from the khondalite metasediment into which the charnockite intruded.

Zircon 06 (Fig. 25 B) shows 3 wide zones of dark CL response and gives a $^{206}Pb/^{238}U$ age of 984 ± 12 Ma and a large broadly zoned high CL response rim with a $^{206}Pb/^{238}U$ age of 910 ± 11 Ma. This rim displays the characteristic morphology of a composite grain which has been metamorphically grown or modified (Corfu et al., 2003). This zircon, therefore, shows clear evidence for two discrete episodes of zircon growth in sample CG10-133. One event of igneous crystallisation at ca. 985 Ma followed by a metamorphic event leading to zircon recrystallisation at ca. 910 Ma.

Weighted means of the concordant (95-105%) data for cores yields a $^{206}Pb/^{238}U$ age of 947 ± 19 Ma (MSWD = 5.2, n=9) and a more robust $^{207}Pb/^{206}Pb$ age of 962 ± 14 Ma (MSWD = 0.85, n=9). The latter $^{207}Pb/^{206}Pb$ age is interpreted as the crystallisation age of this charnockite at ca. 950 Ma.

A weighted mean of the concordant (95-105%) data for rims gives a $^{207}Pb/^{206}Pb$ age of 925 ± 29 Ma (MSWD = 0.22, prob. = 0.88, n=4) and a $^{206}Pb/^{238}U$ age of 896 ± 11 Ma (MSWD = 0.75, n=4). The $^{206}Pb/^{238}U$ age is interpreted as a discrete metamorphic event leading to zircon rim growth at ca. 900 Ma.

4.2.1.5. Sample CG10-142

Sample CG10-142 is a megacrystic granitoid that was collected from the Vellavilla Agram quarry, situated 3.5 kilometres northwest of the township of Vadaddi. (17°51'51.80"N, 82°50'39.13"E). This granitoid has a porphyritic texture and consists of K-feldspar megacrysts, quartz, plagioclase, garnet, biotite and opaque oxides (ilmenite and magnetite). Accessory minerals are sphene, monazite and zircon.

The zircons of this sample are displayed in Figure 30 (A-F). They range in morphology from blocky euhedral cores with little or no rims (Figs. 30 A,B) to amoeboid shaped cores with totally random recrystallisation patterns (Fig. 30 E).

A total of 81 spots on 66 zircons were analysed, targeting 58 cores, 20 rims and 3 recrystallised zones (Table 5). Of these 48% were between 95-105% concordant, and 62% between 90-110% concordant.

Greater than 55% and 95-105% concordant data are presented in two combined Wetherill concordia diagrams (Fig. 31). The oldest concordant analysis (14_01, Fig. 30 A) has a $^{206}Pb/^{238}U$ age of 981 ± 12 Ma and the remaining data define a trend towards the ages of two cores and a metamorphic rim at ca. 560Ma. A discordia line for all 95-105% concordant analyses yields upper and lower intercepts of 933 ± 16 Ma and 579 ± 35 Ma, respectively (MSWD = 1.3). The discordia for concordant (95-105%) cores alone returns upper and lower intercepts of 946 ± 18 Ma and 569 ± 57 Ma, respectively (MSWD = 1.2). This ca. 950 Ma upper intercept is interpreted as a minimum emplacement age of this granitoid and the ca. 550 Ma lower intercept is interpreted as the last metamorphic event witnessed by this sample.

A weighted mean of 25 concordant (95-105%) cores yields a $^{206}Pb/^{238}U$ age of 916 ± 20 Ma (MSWD = 17) and $^{207}Pb/^{206}Pb$ age of 931 ± 17 Ma (MSWD = 1.6). The more precise $^{207}Pb/^{206}Pb$ age constitutes further evidence toward the interpretation of a ca. 950 Ma crystallisation age for this granitoid.

A weighted mean for 90-110% concordant for rims (n=17) yields a $^{206}Pb/^{238}U$ age of 746 ± 77 Ma (MSWD = 215) and $^{207}Pb/^{206}Pb$ age of 828 ± 70 Ma (MSWD = 18). These imprecise ages and large MSWDs indicate that these rims do not constitute a single population.

The $^{206}Pb/^{238}U$ probability density distribution plot for all data and concordant (95-105%) data is displayed in Figure 32. Four general age maxima for 95-105% concordant data occur at 950 Ma (965 Ma and 917 Ma combined), 850 Ma, 680 Ma and 550Ma. Rims were sorted into four groups corresponding to these four age peaks.

The three younger peaks are interpreted as episodes of subsequent zircon growth after the initial ~950 Ma event. A weighted mean of the concordant (90-110%) rims which cluster at the 950 Ma peak return a weighted mean $^{207}Pb/^{206}Pb$ age of 936 ± 41 Ma (MSWD = 1.7) and a $^{206}Pb/^{238}U$ age of 927 ± 10 Ma (MSWD = 1.12). The latter more precise age is interpreted to correspond to the earliest episode of metamorphic rim growth. A weighted mean of the concordant (90-110%) rims which cluster at the 850 Ma peak return a weighted mean $^{207}Pb/^{206}Pb$ age of 857 ± 46 Ma (MSWD = 1.4, n=5) and a $^{206}Pb/^{238}U$ age of 850 ± 10 Ma

(MSWD = 1.4, n=9). As the $^{206}Pb/^{238}U$ age is more precise and contains more data, this is interpreted to represent the age of the second episode of metamorphic rim growth.

The rims which cluster at the 680 Ma peak give a weighted mean $^{207}Pb/^{206}Pb$ age of 707 ± 36 Ma (MSWD = 0.33, n=4, 90-110% conc.) and the two rims at 550 Ma return a $^{207}Pb/^{206}Pb$ age of 529 ± 48 Ma (MSWD = 0.018, n=2, 90-110% conc.)

These ages are consistent with the discordia defined by the 95-105% concordant rims and recrystallised zones (n=14) that has a lower intercept of 539 ± 38 Ma and an upper intercept of 897 ± 32 Ma (MSWD = 1.06). The intercepts for the concordant rims are within error of the intercepts defined by discordia for 95-105% concordant cores, stated earlier. The lower intercept of 539 ± 38 Ma is taken to represent the final metamorphic event witnessed by this granitoid as it is more accurate and contains much more data than the weighted average calculated from the two rims at the ca. 550 peak.

When plotted in Th/U-age space, rims display a much smaller range Th/U values to cores. Rims range in value from 0.1 to 0.8 and cores range in value from 0.1 to 2.1. This indicates the likely metamorphic origin for most rims, but could also suggest a number of cores have been recrystallised by metamorphic events.

In summary, the U-Pb data for CG10-142 indicate that the granitoid crystallised at 946 ± 18 Ma with further discrete episodes of metamorphic zircon growth at 850 ± 10 Ma, 707 ± 36 Ma and 539 ± 38 Ma.

4.2.2 U/Pb LA-ICPMS monazite analysis

22 analyses were performed on 13 monazites from sample CG10-087, a megacrystic granitoid. The monazites ranged in morphology from equant sub-rounded to sub-angular grains from 100 μm up to 350 μm across. All analyses were between 98-105% concordant.

All data is presented on a standard Wetherill concordia diagram (Fig. 35). A tight cluster of ages is evident at approximately 950 Ma. Weighted means of the concordant $^{206}Pb/^{238}U$ and $^{207}Pb/^{206}Pb$ ages in this cluster return ages of 945 ± 16 Ma (MSWD = 6.1, n=17) and 949 ± 12 Ma, respectively (MSWD = 0.93, n=18) (Figs. 36 and 37). The latter more precise age is interpreted as the crystallisation age of monazite in this sample.

4.3 Lu/Hf LA-MC-ICPMS zircon isotope analysis

Lu/Hf LA-MC-ICPMS zircon analysis results are presented in Table 7. 47 analyses were made on 41 zircons from the five samples.

Figure 83 shows epsilon Hf (εHf) versus zircon U–Pb age and includes an interpretation of the inferred crustal model ages (T^{c}_{DM}) for the cluster of data. These crustal model ages were derived assuming that the protolith of each magmatic rock had the mean $^{176}Lu/^{177}Hf$ of the continental crust (0.015). The inferred crustal model ages are between 2.5 and 1.98 Ga.

All the zircons plot in negative epsilon space indicating a component of crustal contamination. Age can be seen to be inversely proportional to εHf values. The youngest zircon analysed (32_01, 617 Ma), from the megacrystic granitoid CG10-142, returned the most negative εHf value of -14.9. The oldest zircon (07_01, 1087 Ma), from the orthogneiss CG10-006, had the least negative εHf value of -2.1. Most analyses clustered around an εHf value of -5.

4.4 Geochemistry

Representative whole rock analyses are listed in Table 8. When plotted in the classification diagram of Middlemost (1985) for plutonic rocks, the charnockites and granitoids plot in the granidiorite field (Fig. 40). The orthogneiss is richer in alkalis and plots in the quartz monzonite field. The granitoids and charnockites display decreasing alkali concentration as SiO_2 increases. In a Na_2O versus K_2O plot, all the samples lie within the S-type granite field proposed by Misra and Sarkar (1991).

The A/CNK versus A/NK plot illustrates the peraluminous character of the charnockite samples and the highly peraluminous character of the megacrystic granitoids (Fig.41). This peraluminous character is reflected in the presence of aluminous garnet and biotite in these charnockites and megacrystic granitoids. CG10-006 is garnet free and plots in the metaluminous field. In the AFM diagram (Kuno, 1968; Irvine and Baragar, 1971) the samples all plot in a trend subparallel to the AF sideline (Fig. 42).

Chondrite-normalised REE patterns (after Boynton, 1984) of all five samples are very similar with enriched LREE, relatively flat to slightly fractionated HREE displaying relatively smooth igneous-like patterns (Fig.43). Samples CG10-133 and CG10-087, a charnockite and megacrystic granitoid, respectively, have almost identical LREE patterns, and are only slightly separated in the HREEs, with CG10-087 being more enriched. The granitoids are more enriched in HREEs than the charnockites and orthogneiss, CG10-006. Both the charnockites and the megacrystic granitoids display negative Eu anomalies, but it is much more pronounced in the granitoid CG10-142. The orthogneiss has a much flatter REE pattern, being less enriched in LREE and HREE, and displays no Eu anomaly.

Primitive mantle normalised plots (after Sun and McDonough, 1989) of all samples display positive Th anomalies in both the charnockites and granitoids (Fig.44). All samples display a negative Sr and Ti anomalies which is a signature indicative of crustal contamination. Sr depletion and Eu depletion are both indicative of plagioclase having left the magma system from which the suite crystallised. The charnockite CG10-044 has a large negative Nb anomaly suggesting crustal influence or subduction-related magmatism.

Trace element tectonic discrimination diagrams (after Pearce et al., 1984; Pearce, 1996) suggest the within plate granite (WPG) nature of the samples (Fig. 45). In the Rb versus Y+Nb diagram all samples plot within the post-collisional granites field, and in the Nb versus Y plot all except the charnockite CG10-044 plot within the attenuated continental lithosphere field.

Figures 46 and 47 display the two charnockites (CG10-044 and 133) plotted against six representative charnockites from the Paderu area reported by Narayana et al. (1999). The chondrite normalised rare earth element spidergram (after Boynton, 1984) illustrates the almost identical pattern of the two datasets. The combined primitive mantle normalised spidergram (after Sun & McDonough, 1989) also illustrates the geochemical similarities of the two datasets, with the only differences being that the charnockites from this study have relatively small negative Zr anomalies. Plotted together, the two datasets have the appearance of a fractionated igneous suite with the two samples from this study being among the least fractionated.

Figures 48 and 49 display the orthogneiss (CG10-006) and the two megacrystic granitoids (CG10-087 and 142) plotted against seven representative megacrystic granites from the Paderu area reported in the same study by Narayana et al. (1999). The chondrite normalised rare earth element spidergram (after Boynton, 1984) illustrates the similarities between the granites of the two studies and the contrast of the relatively flat signature of the orthogneiss. The combined primitive mantle normalised spidergram (after Sun & McDonough, 1989), once again, illustrates the geochemical similarities of the two datasets. However, like the charnockites, the granitoids from this study display much smaller negative Zr anomalies than those of Narayana et al. (1999). The orthogneiss displays a negative Th anomaly and a positive Zr anomaly which is in contrast to the general pattern of the granites.

Discussion

The U-Pb data from zircons and monazites of all five samples indicate that the study area was subjected to a pervasive metamorphic event at ca. 950 Ma. Three samples (CG10-006, CG10-044 and CG10-087) returned older ages (ca. 1100-1000) in addition to the 950 Ma event. These older ages indicate the possibility that these granitoids were emplaced prior to the pervasive metamorphic event at ca. 950 Ma, or the other possibility is that they contained inherited cores from the khondalite into which they intruded. A comparison with zircon ages from the surrounding khondalites could determine which possibility is more likely.

The ca. 950 Ma metamorphic event recorded in the megacrystic granitoids and charnockites of this study is consistent with the emplacement ages of granitoids from other parts of the EGMB reported between 985 and 955 Ma (Aftalion et al. 1988, Paul et al., 1990). Aftalion et al. (1988) proposes that the charnockitization took place between 1100-950 Ma, and probably ca. 965 Ma ago. These dates are in agreement with the findings of this study.

The 949 ± 12 Ma age reported by this study for monazite is in agreement with monazite ages reported by Simmat and Raith (2008). They reported that the most prominent populations of the chemical dates of monazite fall within the time span of 950-980 Ma for charnockites and augen-gneiss.

The timing of emplacement for the megacrystic granitoids of the CEG reported by this study lends weight to the theory that the CEG were contiguous with the Rayner complex of East Antarctica in the SWEAT (southwest U.S.–East Antarctic) model for Rodinia (Li et al., 2008). Granitoids in the Rayner complex reported by Halpin et al. (2005) are of a similar age to those of this study. The Rayner Complex in Kemp

Land is interpreted to represent Archean crust tectonically reworked during the Rayner Structural Episode (RSE) between 1000 Ma and 900 Ma (Halpin et al., 2005). The emplacement of large charnockite bodies along the Mawson Coast immediately followed peak metamorphic conditions of the RSE at 985 ± 29 Ma and 954 ± 19 Ma (Young and Black, 1991). U-Pb zircon ages from this study are within error of these reported ages. All samples from this study showed evidence of a ca 950 Ma crystallisation event. One zircon's core from the charnockite CG10-133 gave a $^{206}Pb/^{238}U$ age of 984 ± 12 Ma and the weighted mean of $^{206}Pb/^{238}U$ concordant (95-105%) data for cores of the orthogneiss, CG10-006, yielded an age of 981 ± 13 Ma which are within error of the earlier emplacement ages of charnockites along the Mawson Coast.

The post Grenvillean cooling history of the EGMB is characterised by N to NW-S to SE shortening between ca. 950-700 and 550-500 Ma. The 550-500 Ma thermal event was associated with brittle to brittle-ductile reactivation of the Eastern Ghats Boundary Fault and the major intra-province shear zones (Crowe et al., 2001). Rickers et al. (2001) recorded Pan African ages of 513 ± 48 Ma by U-Pb-Th technique in monazites collected proximal to the craton-mobile belt contact. They propose that the Pan-African event is exclusive to zones in the neighbourhood of the craton-mobile belt contact as it is not observed in the age data collected distal to the contact (Rickers et al., 2001). Crowe et al. (2001) reported $^{40}Ar/^{39}Ar$ ages of biotite from granitoids collected from shear zones in the northern Eastern Ghats of 533 ± 2 Ma and 530 ± 2 Ma. They suggest the ca. 550-500 Ma thermal event may be much more extensive in the EGMB due to the widespread occurrence of graphite mineralisation attributed to the Pan-African event (Crowe et al., 2001).

A map of the broad shear zone network in the EGMB (Chetty, 2010) shows the ENE-WSW trending Narsipatnam Shear Zone (NSZ) passes within ~ 10km of the quarry from where CG10-142 was collected. The 550 metamorphic events responsible for the growth of metamorphic rims in this sample could therefore be interpreted to constrain the age of reactivation of the NSZ and intra-cratonic Pan-African tectonism within this area of the CEG.

The negative epsilon values for the five samples after Lu-Hf analysis of zircon indicate a component of crustal contamination and the possible s-type nature of the granitoids. The Hf model ages of between 1.98 and 2.5 Ga suggests that the melts which formed these granitoids came from reworked crustal material with crustal residence times between 1.98 and 2.5 Ga or the melts were formed as a result of mixing Archean crust with input of juvenile Proterozoic material. These ages are in agreement with

Rickers et al. (2001) who reported highly variable Nd model ages between 1.8 and 3.2 Ga for orthogneisses in the central part of the EGMB.

The geochemical data suggests that the charnockites and the megacrystic granitoids are part of a granitoid suite. The granitoids display S-type characteristics in REE spidergram plots. Selective enrichments of Rb, Th, Ce and Sm can be attributed to crustal involvement in the evolution of these granitoids and the pattern could be described as crust-dominated (Narayana et al., 1999). The trace element tectonic discrimination diagrams indicate that the granitoids formed within plate boundaries, possibly in a post collisional regime in thinned continental crust. This suggests that the granitoids were emplaced in a rift setting, however the ca. 1000-950 Ma emplacement ages reported from this study are coeval with Rodinia formation rather than breakup. Rickers et al. (2001) suggest that the geodynamic process for the EGMB at 1 Ga was that of a continent-continent collision.

Conclusions

- The new zircon and monazite ages presented in this study indicate that the megacrystic granitoids, megacrystic charnockites and orthogneiss of the CEG were emplaced between ~1000-950 Ma and underwent high grade metamorphism in the latter stages of this time frame at ~ 950 Ma.
- A lesser discrete thermal event was recorded by metamorphic rims at ~ 900 Ma.
- One megacrystic granitoid collected proximal to the Narsipatnam Shear Zone (NSZ) recorded thermal disturbances at ~850, ~750 and ~550 Ma. The youngest age constrains the timing of the Pan-African reactivation of the NSZ at 539 ± 38 Ma.
- Lu-Hf analysis of zircons returned negative epsilon values for all samples indicating a component of crustal contamination. Hf model ages of between 1.98 and 2.5 Ga were inferred for the megacrystic granitoids and charnockites.
- The megacrystic granitoids and charnockites of the CEG represent a granitoid suite comprised of rocks of an S-type nature with indications they formed within plate boundaries in a post-collisional setting.
- The new ages presented for the Central Eastern Ghats Belt in this study are similar to published ages for the Rayner Complex and the Mawson Coast of Eastern Antarctica. These similar ages lend support to East Antarctica and the Central Eastern Ghats Belt being complimentary parts of an extensive orogenic belt formed during the Grenvillean Orogeny around 1 Ga.

REFERENCES

Black L.P., Gulson B.L.,1978. The age of the Mud Tank carbonatite, Strangways Range, Northern Territory. Bureau of Mineral Resources, Journal of Australian Geology and Geophysics 3:227–232.

Boynton, W.V., (1984) Cosmochemistry of the rare earth elements: meteorite studies. In: Henderson, P. (Ed.), Rare Earth Element Geochemistry. Elsevier, Amsterdam, pp. 63–114.

Crowe W.A., Cosca M.A., Harris L.B. (2001) $^{40}Ar/^{39}Ar$ geochronology and Neoproterozoic tectonics along the northern margin of the Eastern Ghats Belt in north Orissa, India. Precambrian Research, 108, 237-266.

Chetty T. R. K., 2001. The Eastern Ghats Mobile Belt, India: A collage of juxtaposed terranes (?). Gondwana Research, 4, 319-328.

Chetty T. R. K., 2010. Structural architecture of the northern composite terrane, the Eastern Ghats Mobile Belt, India: Implications for Gondwana tectonics. Gondwana Research, 18, 565-582.

Corfu F., Hanchar J.M., Hoskin P.W.O., Kinny P., 2003 Atlas of Zircon Textures. Reviews in Mineralogy and Geochemistry v. 53;1, 469-500

Griffin, W.L., Pearson, N.J., Belousova, E.A., Jackson, S.R., van Achterbergh, E., O'Reilly, S.Y., Shee, S.R., 2000. The Hf isotope composition of cratonic mantle: LAM-MCICPMS analysis of zircon megacrysts in kimberlites. Geochimica et Cosmochimica Acta 64, 133–147.

Halpin, J.A., Gerakiteys, C.L., Clarke, G.L., Belousova, E.A., Griffin, W.L., 2005. In-situ U-Pb geochronology and Hf isotope analyses of the Rayner Complex, east Antarctica. Contributions to Mineral Petrology, 148: 689-706.

Irvine, T.N. and Baragar, W.R.A., 1971. A guide to the chemical classification of the common volcanic rocks. Canadian Journal of Earth Sciences, 8: 523-548.

Jackson SE, Pearson NJ, Griffin WL, Belousova EA. 2004. The application of Laser Ablation-Inductively Coupled Plasma-Mass Spectrometry (LA-ICP-MS) to in situ U–Pb zircon geochemistry. Chem Geol.

Li, Z. X., Bogdanova, S. V.; Collins, A. S.; Davidson, A.; B. De Waele, R. E. Ernst, I. C. W. Fitzsimons, R. A. Fuck, D. P. Gladkochub, J. Jacobs, K. E. Karlstrom, S. Lul, L.M. Natapov, V. Pease, S. A. Pisarevsky, K. Thrane and V. Vernikovsky 2008. Assembly, configuration, and break-up history of Rodinia: A synthesis. Precambrian Research 160: 179–210.

Ludwig, K.R., 2009. Isoplot Ver:3.0.

Misra, S., Sarkar, S.S. 1991. Linear discrimination among M-, I-, S- and A-granites. Indian J. Earth Sci., 18, 84-93.

Nanda, J., Gupta, S., Dobmeier, C.J. (2008) Metamorphism of the Koraput Alkaline Complex, Eastern Ghats Province, India—Evidence for reworking of a granulite terrane. Precambrian Res.

Narayana, B.L., Rama Rao, P., Reddy, G.L.N., Divakara Rao, V., 1999. Geochemistry and origin of the megacrystic granitoid rocks from Eastern Ghats Granulite Belt. Gondwana Research, V.2, 1 : 105-115.

Pearce, J.A., 1996. Sources and settings of granitic rocks. Episodes 19, 120–125.

Pearce, J.A., Harris, N.W., Twindle, A.G. 1984. Trace element discrimination diagrams for the tectonic interpretation of granitic rocks. Journal of Petrology 25, 965-983.

Rickers K, Mezger K, Raith MM, 2001. Evolution of the Continental Crust in the Proerozoic Eastern Ghats Mobile Belt, India and new constraints for Rodinia reconstruction: implications from Sm-Nd, Rb-Sr and Pb-Pb isotopes. Precambrian Res. 112, 183-210.

Sarkar A, Bhanumathi L, Balasubrahmanyan MN, 1981. Petrology, geochemistry and geochronology of the Chilka Lake igneous complex, Orissa state, India. Lithos, 14, 93-111.

Shaw, R.K., Arima, M., Kagami, H., Fanning, C.M., Shiraishi, K., Motoyoshi,Y.,1997. Proterozoic events in the Eastern Ghats Granulite Belt, India: evidence from Rb-Sr, Sm-Nd systematics and SHRIMP dating. Jour. Geol., v.105, pp.645-656.

Simmat, R. and Raith, M.M. (2008) U–Th–Pb monazite geochronometry of the Eastern Ghats Belt, India: Timing and spatial disposition of poly-metamorphism. Precambrian Res.,v.162, pp.16-39.

Sircombe, K.N., 2004. AGEDISPLAY: an EXCEL workbook to evaluate and display univariate geochronological data using binned frequency histograms and probability density distributions. Computers and Geosciences, 30: (1) 21-31.

Slama, J., Kosler, J., Condon, D.J., Crowley, J.L., Gerdes, A., Hanchar, J.M., Horstwood, M.S.A., Morris, G.A., Nasdala, L., Norberg, N., Schaltegger, U., Schoene, B.,Tubrett, M.N., and Whitehouse, M.J., 2008, Plesovice zircon - A new naturalreference material for U-Pb and Hf isotopic microanalysis: Chemical Geology, v.249, p. 1-35.

Sun, S.S. & McDonough, W. F.,1989. Chemical and isotopic systematics of oceanic basalts: implications for mantle composition and processes. Geological Society of London Special Publication 42, 313-345.

Upadhyay D., Gerdes A., Raith M.M., 2009. Unravelling Sedimentary Provenance and Tectonothermal History of High-Temperature Metapelites, Using Zircon and Monazite Chemistry: A Case Study from the Eastern Ghats Belt, India. The Journal of Geology 117, 665-683.

Van Achterbergh E., Ryan C. G., Jackson S. E., Griffin W. L. 2001. Data reduction software for LA-ICPMS. Laser-ablation-ICPMS in the earth sciences; principles and applications. Mineralogical Association of Canada, Ottowa, ON, Canada.

Woodhead, J.D., Hergt, J.M., Shelley, M., Eggins, S. & Kemp, R., 2004. Zircon Hf-isotope analysis with an excimer laser, depth profiling, ablation of complex geometries, and concomitant age estimation. Chem. Geol., 209, 121-135.

Young, D.N., Black, L.P., 1991. U-Pb dating of Proterozoic igneous charnockites from the Mawson Coast, East Antarctica. Antarctic Science, 3(2): 205-216.

Figures and tables

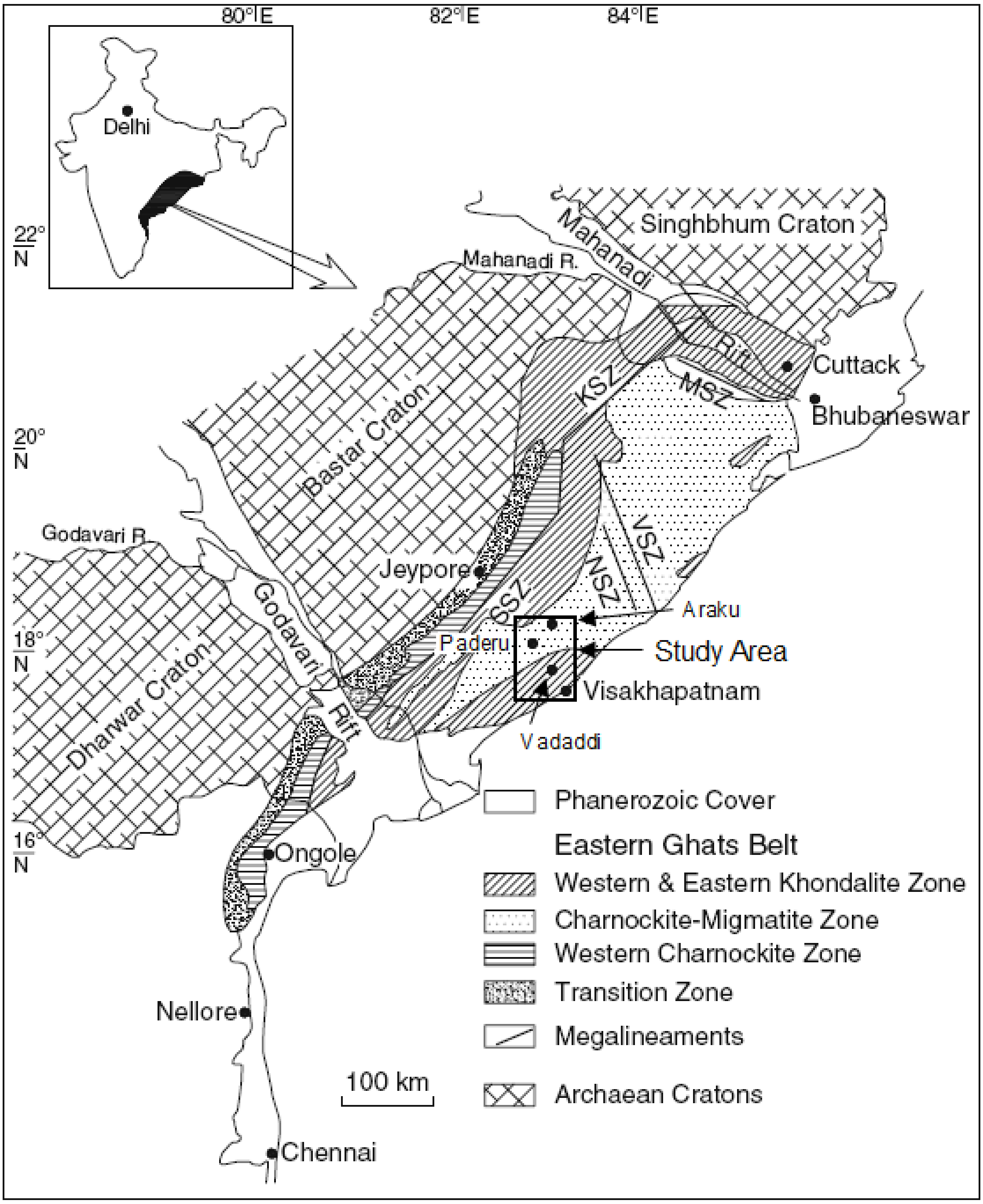

Figure 1. Simplified geological map of the Eastern Ghats Mobile Belt (EGMB) (after Ramakrishnan et al., 1998) highlighting the study area and the locations of Araku, Paderu, Vadaddi and Visakhapatnam. The study area falls within the Charnockite-Migmatite Zone and Western Khondalite Zone. Megalineaments after Chetty (1995). MSZ = Mahanadi Shear Zone; NSZ = Nagavalli Shear Zone; SSZ = Sileru Shear Zone; VSZ = Vamsadhara shear Zone. Inset shows location of the mobile belt within continental India (after Ram, 2009).

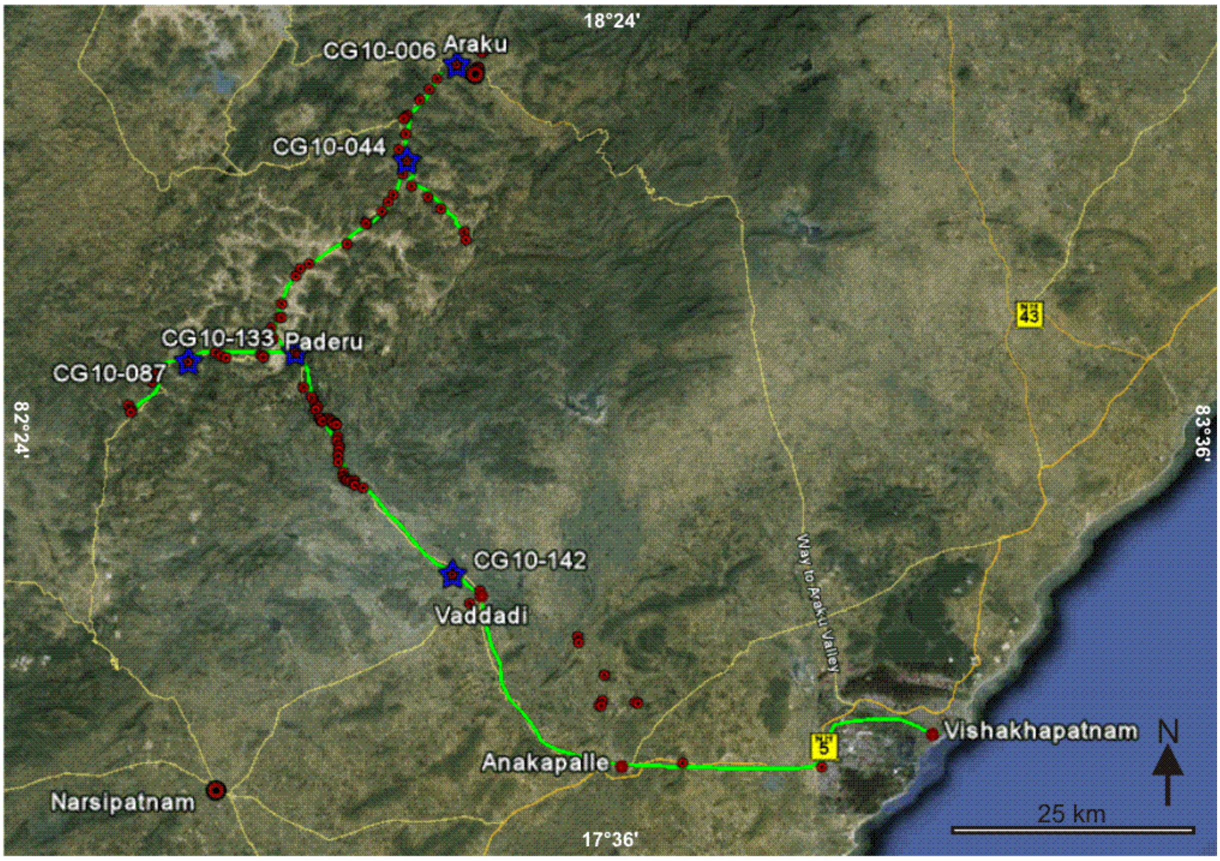

Figure 2. Location map of study area. Blue stars denote sample locations. Small red dots represent field data points. Major roads are marked as yellow lines. Green lines represent field transects.Major cities and towns are highlighted.

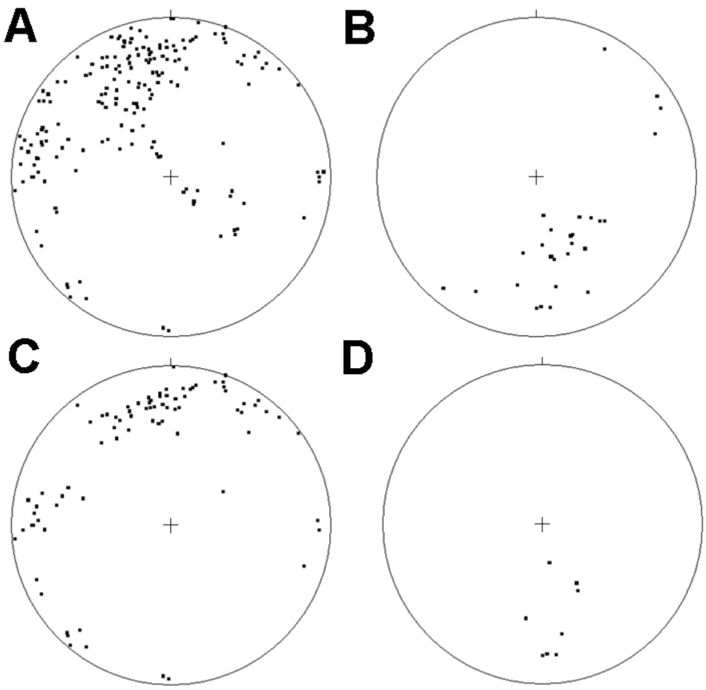

Figure 3. Stereographic projections for field measurements: **(A)** All foliations measured in mapping area shown as poles to foliation (n= 187, Mean Principal Orientation= 62/154). **(B)** Stereographic projection of all lineations measured in mapping area shown as lines (n= 28, Mean Principal Orientation= 45→167) **(C)** Stereographic projection of all foliations measured on Paderu-Vaddadi transect shown as poles to foliation. (n= 81, Mean Principal Orientation = 70/181). **(D)** Stereographic projection of all lineations measured on Paderu-Vaddadi transect shown as lines (n = 8, Mean Principal Direction= 38→172).

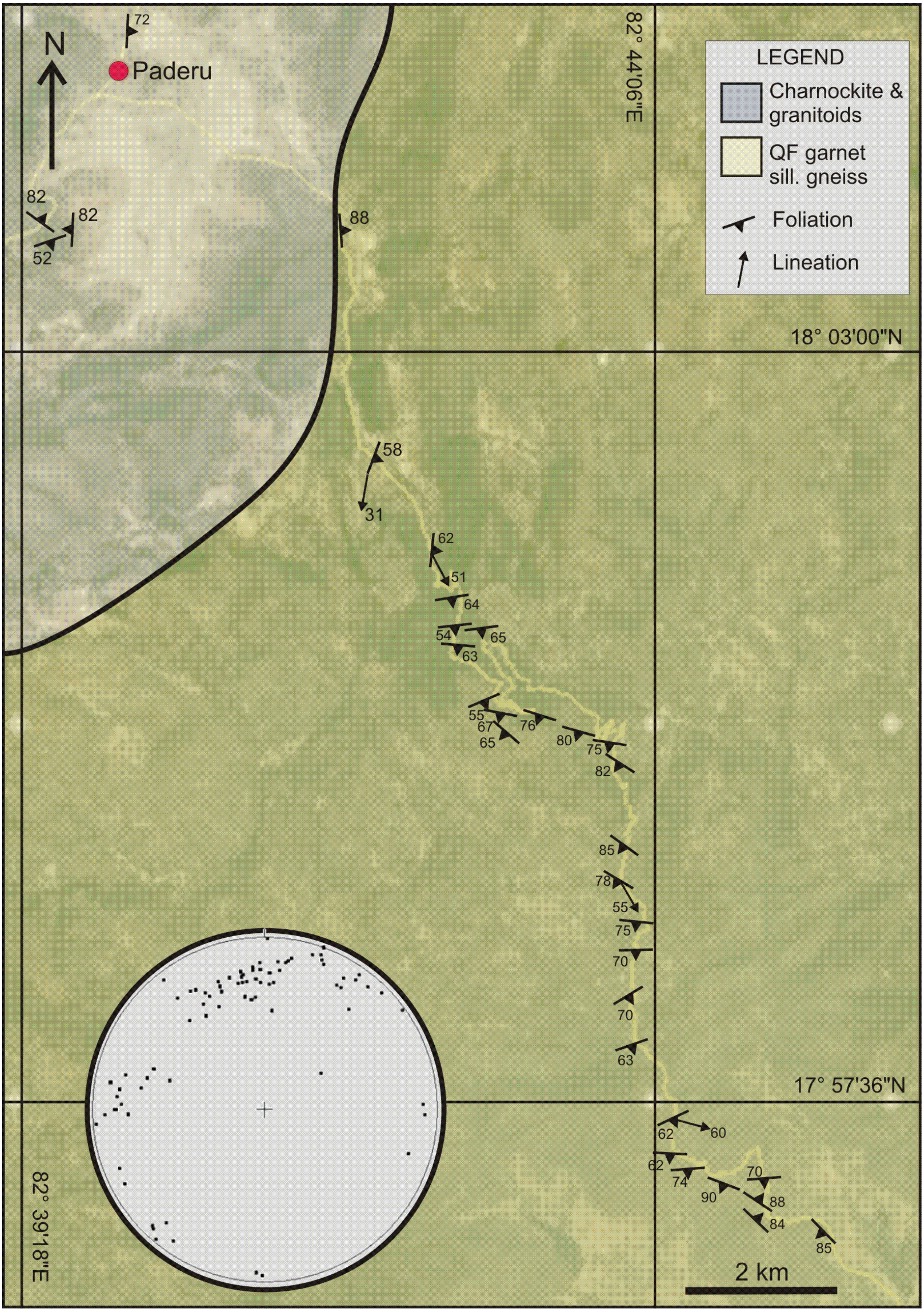

Figure 4. Structural map of the upper portion of the Paderu-Vaddadi transect. Foliations are measured as dip/dip-direction. Foliations and lineations expressed in degrees. Poles to foliation measured along the transect are displayed in a stereographic projection (n= 81, Mean Principal Orientation = 70/181).

(A)

(B)

Figure 5. 2 photographs displaying xenoliths of foliated khondalite (garnet sillimanite quartzo-feldspathic gneiss) partially digested within massive megacrystic granitoid **(A)** 17°51'51.80"N, 82°50'39.13"E. **(B)** 18°20'21.92"N, 82°52'5.56"E.

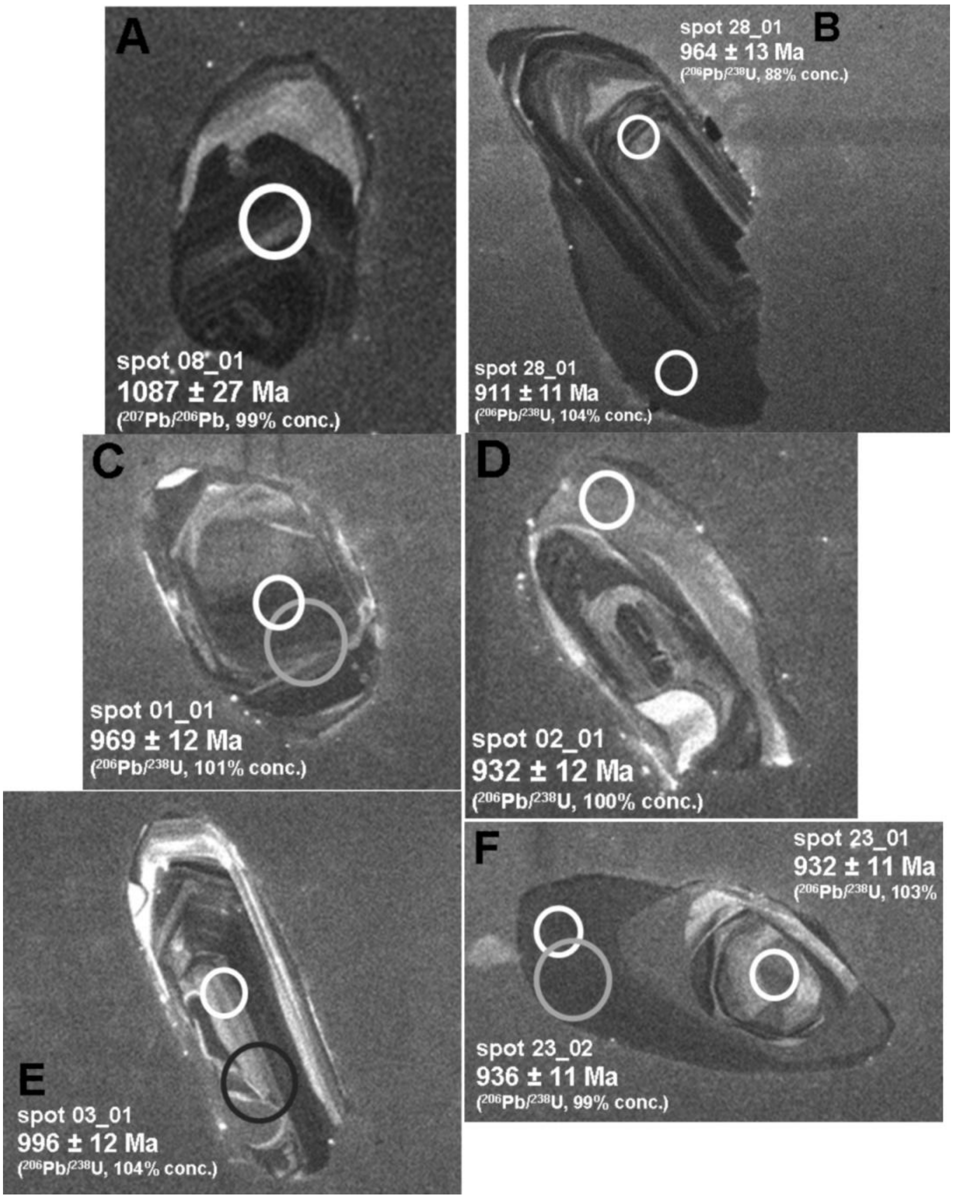

Figure 6. CL images of representative zircons from sample CG10-006, a megacrystic orthogneiss. White rings represent the positions of U/Pb analysis spots (diameter = 30 µm). Larger rings (grey and black) represent locations of Lu/Hf analysis spots (diameter = 50 µm) **(A.)** The oldest concordant zircon analysis (07_01) was from a fractured equant euhedral core with frequent narrow magmatic oscillatory zones and a high CL response recrystallised rim with ghost zoning .This core yielded a $^{207}Pb/^{206}Pb$ age of 1087 ± 27 Ma. **(B.)** The youngest analysis (28_02) came from a recrystallised rim and yielded a $^{206}Pb/^{238}U$ age of 911 ± 11 Ma. Note older euhedral core with remnant oscillatory zoning with evidence of local recrystallisation. **(C.)** Equant euhedral core with broad zones and 'ghost' oscillatory zones suggesting recrystallisation. **(D.)** Rim displaying broad zones with slight differences in CL response. Core displays evidence of recrystallisation with a high CL response convolute zone cross-cutting remnant oscillatory zones. **(E.)** Euhedral oscillatory zoned zircon displaying limited localised recrystallisation and an absence of rim formation. Note $^{206}Pb/^{238}U$ age of 996 ± 12 Ma. This is interpreted as the crystallisation age of the granitoid protolith of this orthogneiss. **(F.)** Recrystallised euhedral core displaying convolute zoning and homogeneous low CL response sub-angular rim. Note $^{206}Pb/^{238}U$ ages of core and rim are both ~ 935 ± 11 Ma indicating one metamorphic event responsible for rim formation and core recrystallisation.

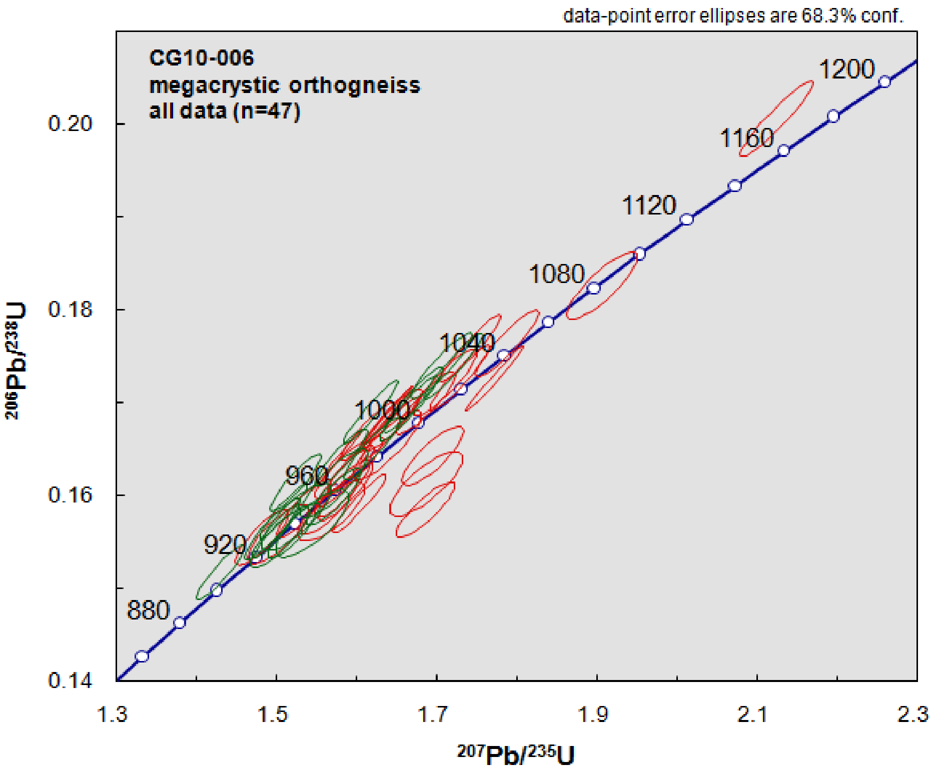

Figure 7. Standard Wetherill concordia diagram of all data (n=47) for sample CG10-006, a megacrystic orthogneiss. Cores (n=29) and rims (n=18) are displayed as red and green ellipses, respectively.

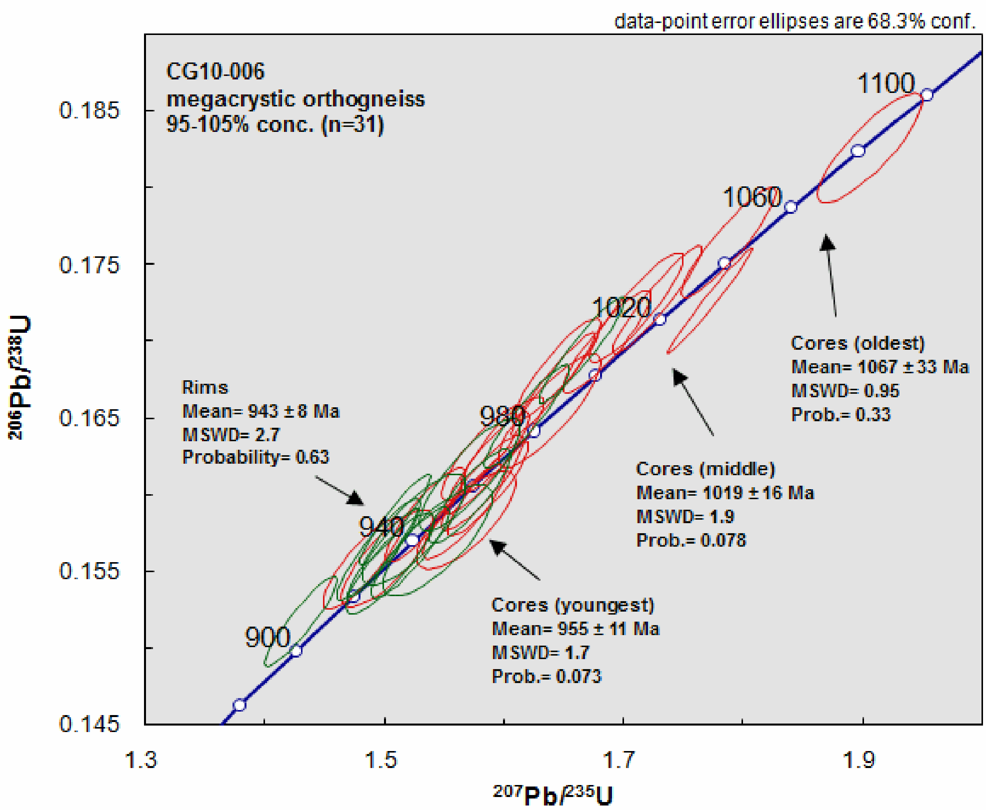

Figure 8. Standard Wetherill concordia diagram of 95-105% concordant data (n=31) for sample CG10-006, a megacrystic orthogneiss. Cores and rims are displayed as red and green ellipses, respectively. Weighted mean ages for rims and groups of cores based on probability density distribution maxima are displayed.

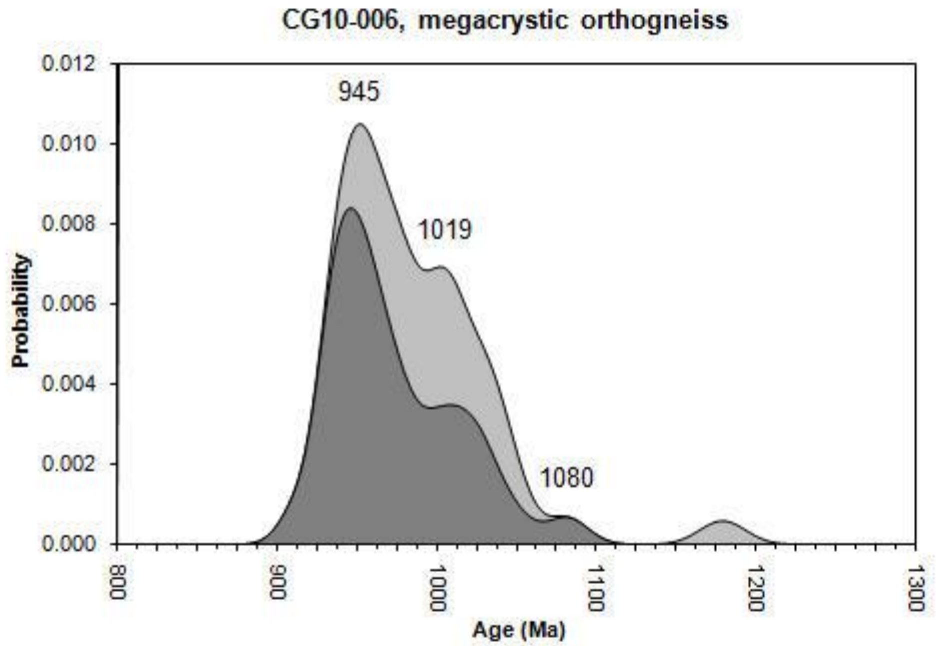

Figure 9. Probability density distribution plot of $^{206}Pb/^{238}U$ ages for sample CG10-006, a megacrystic orthogneiss. Dark grey shaded area represents 95-105% concordant data (n=31), light grey shaded area represents all data (n=47). Age maxima for 95-105% concordant data are labelled.

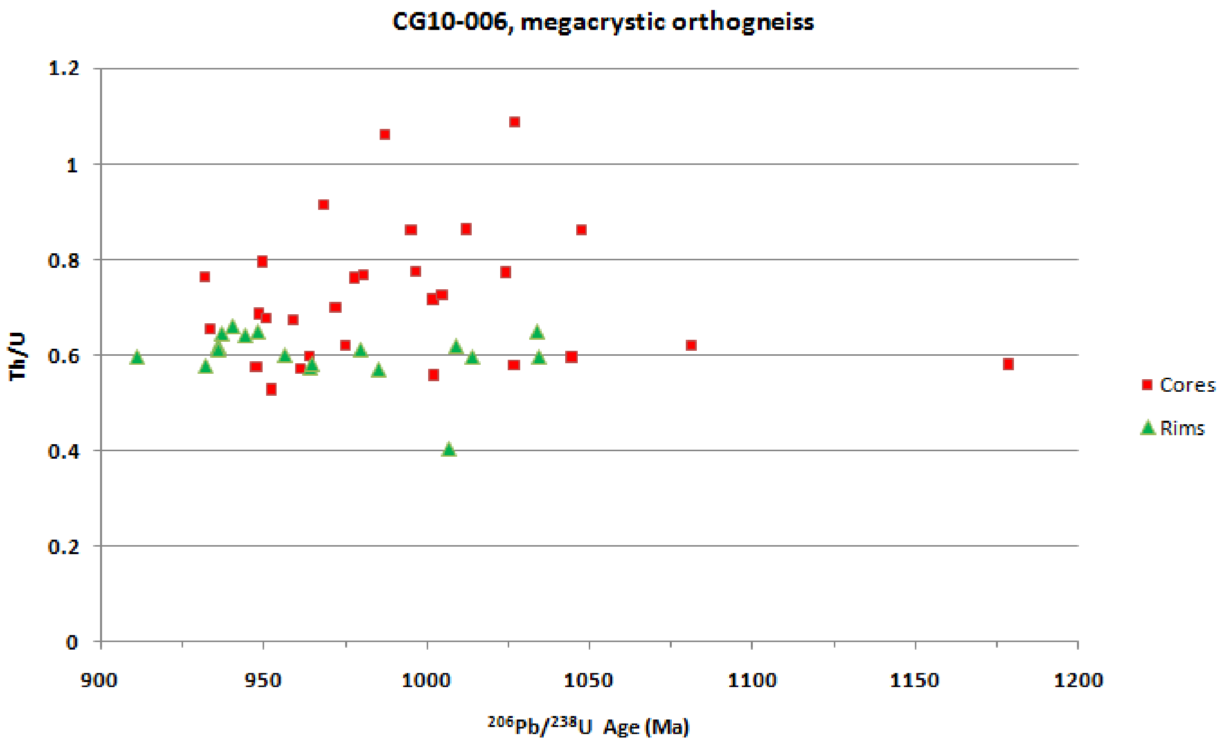

Figure 10. Th/U ratio versus $^{206}Pb/^{238}U$ age plot (all data, n=47) for the megacrystic orthogneiss, CG10-006.
.

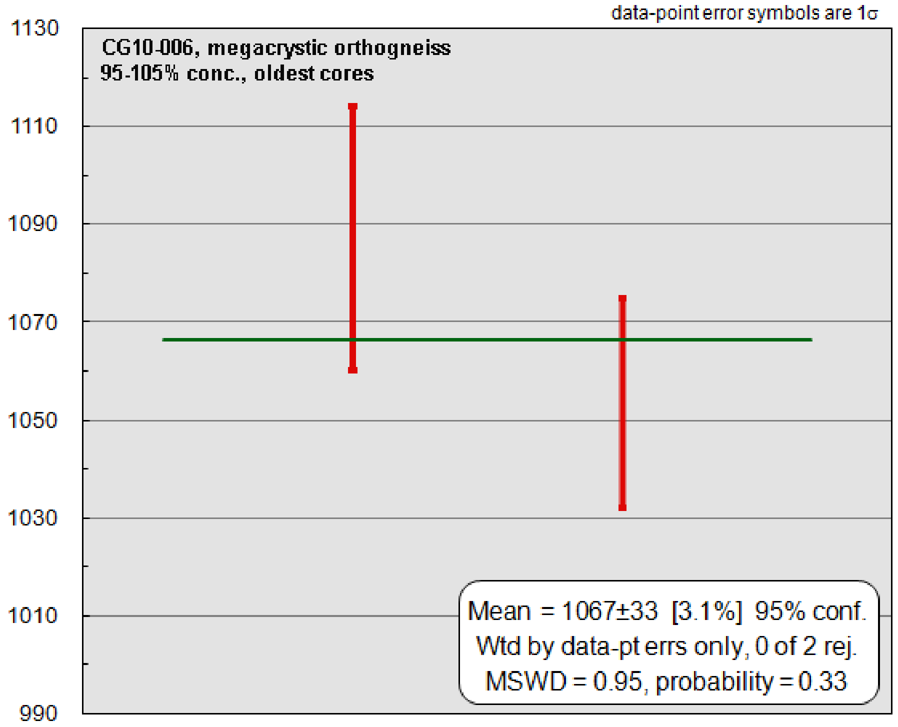

Figure 11. Weighted mean of 95-105% concordant $^{207}Pb/^{206}Pb$ data (n=2) for the oldest cores (>1050 Ma) of sample CG10-006, a megacrystic orthogneiss. These cores correspond to the 1080 age maxima on the PDD (Figure X). MSWD= mean square of weighted deviates.

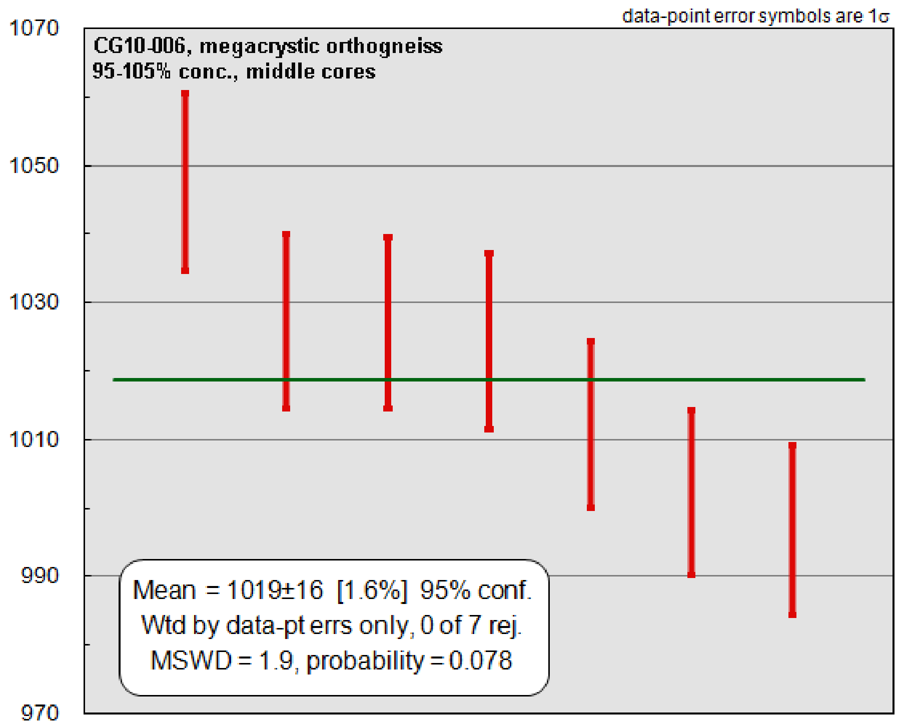

Figure 12. Weighted mean of 95-105% concordant $^{206}Pb/^{238}U$ data (n=7) for the cores of middle-age in sample CG10-006, a megacrystic orthogneiss. These cores correspond to the 1019 Ma age maxima on the PDD (Figure X). MSWD= mean square of weighted deviates.

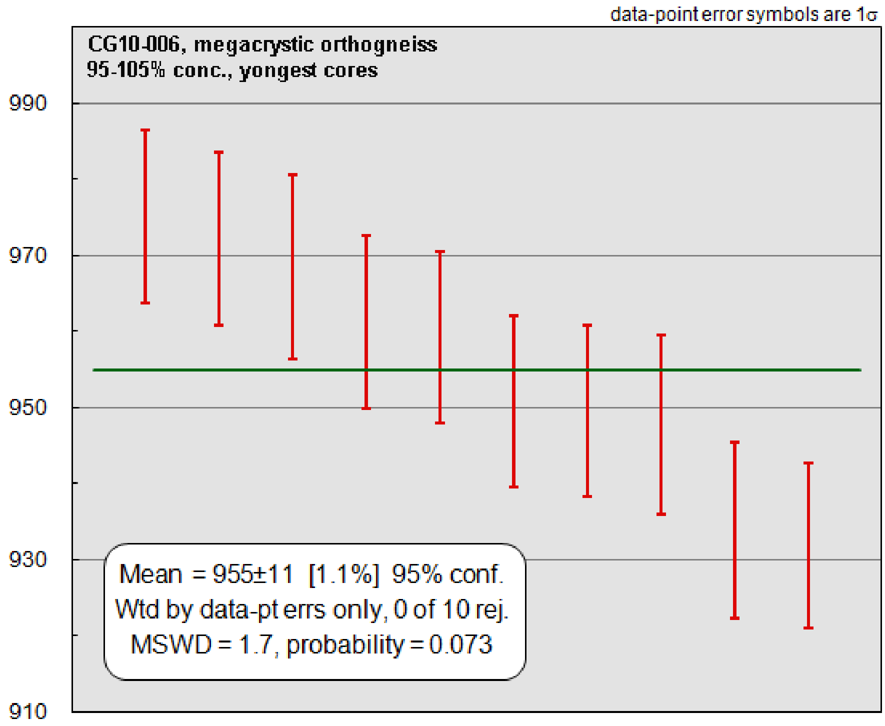

Figure 13. Weighted mean of 95-105% concordant $^{206}Pb/^{238}U$ data (n=10) for the youngest cores of sample CG10-006, a megacrystic orthogneiss. These cores correspond to the 945 Ma age maxima on the PDD (Figure X). MSWD= mean square of weighted deviates.

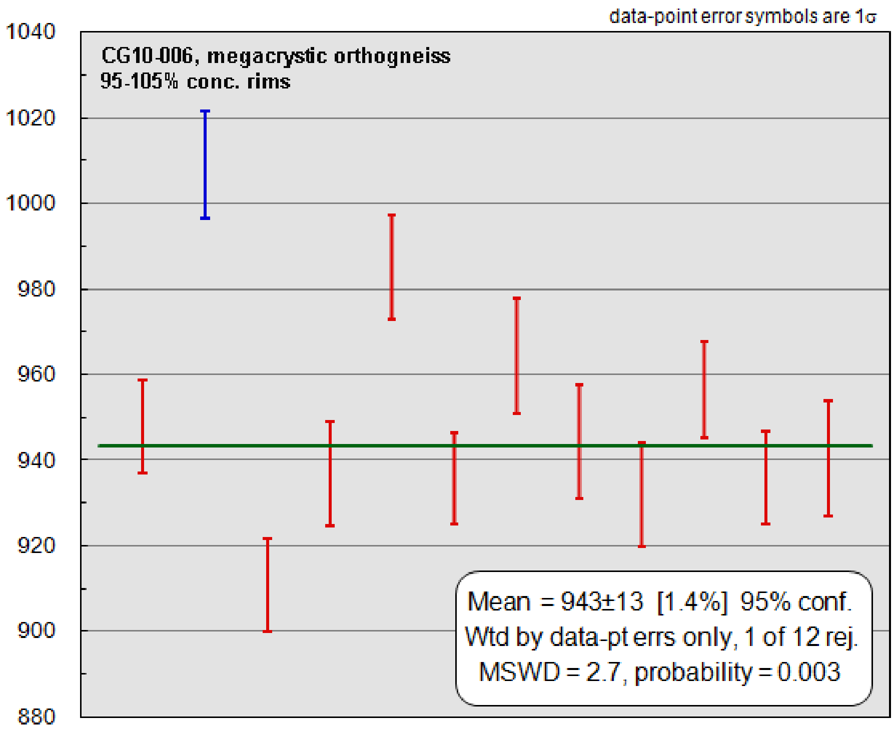

Figure 14. Weighted mean of 95-105% concordant $^{206}Pb/^{238}U$ dates (n=12) for rims of sample CG10-006, a megacrystic orthogneiss. Note 1 of 12 analyses is rejected as it gives a result outside of two standard deviations of the mean. This analysis (22_01) had a concordancy of 105%. MSWD= mean square of weighted deviates

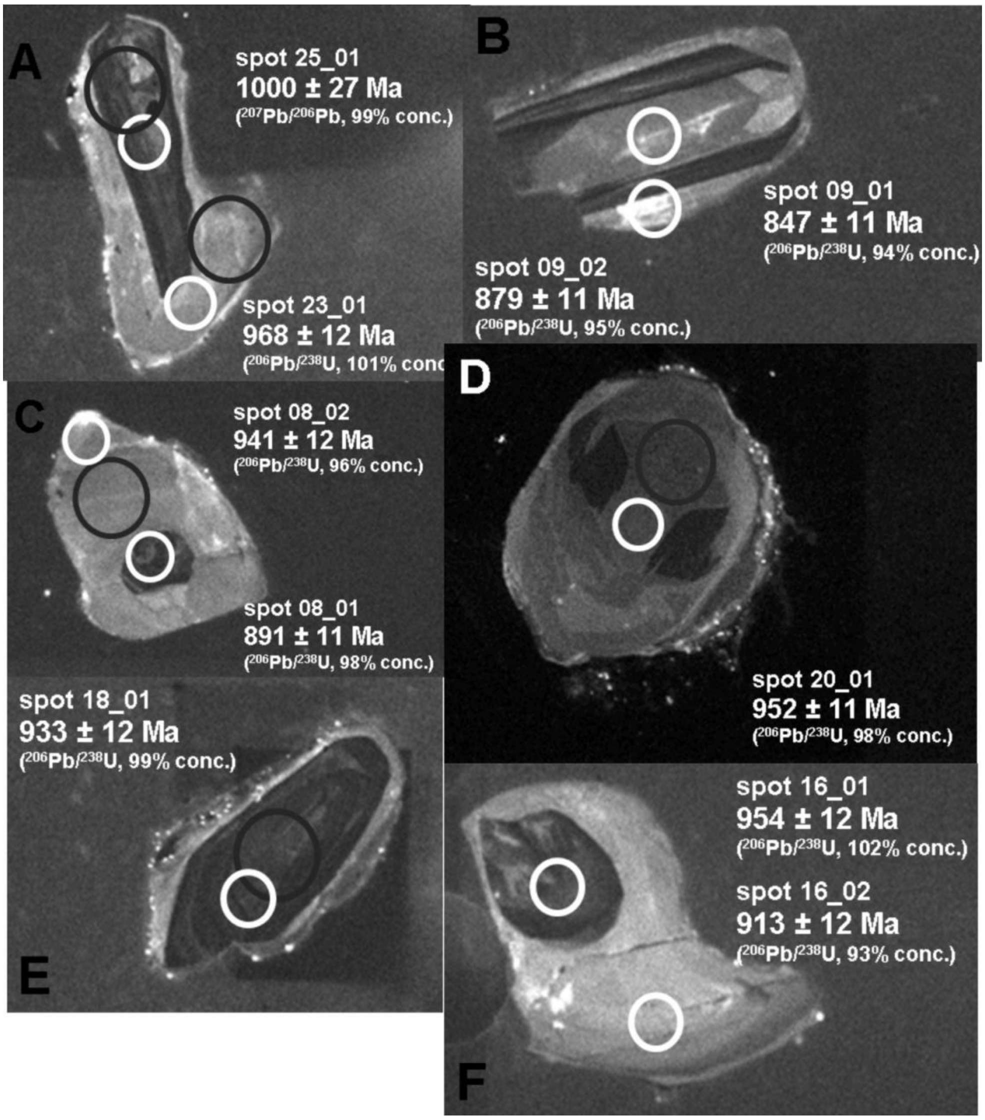

Figure 15. CL images of representative zircons from sample CG10-044, a charnockite. White rings represent the positions of U/Pb analysis spots (diameter = 30 µm). Larger rings (grey and black) represent locations of Lu/Hf analysis spots (diameter = 50 µm) **(A.)** The oldest concordant zircon. **(B.)** Euhedral core with a metamorphic rim and recrystallised central region. Note rim gives older age than recrystallised core. **(C.)** Dark sector zoned with large sector zoned high CL response rim. Note core gives older age than rim. **(D.)** Classic 'soccer ball' style metamorphic zircon displaying sector zones of varying CL responses. Zircon still retains equant euhedral shape indicating its probable magmatic origin. **(E.)** Recrystallised low CL response euhedral core displaying 'ghost' zoning and a thin high CL response rim. **(F.)** Equant recrystallised core with low CL response sector zoning and a large sub-angular rim with bands of high CL response.

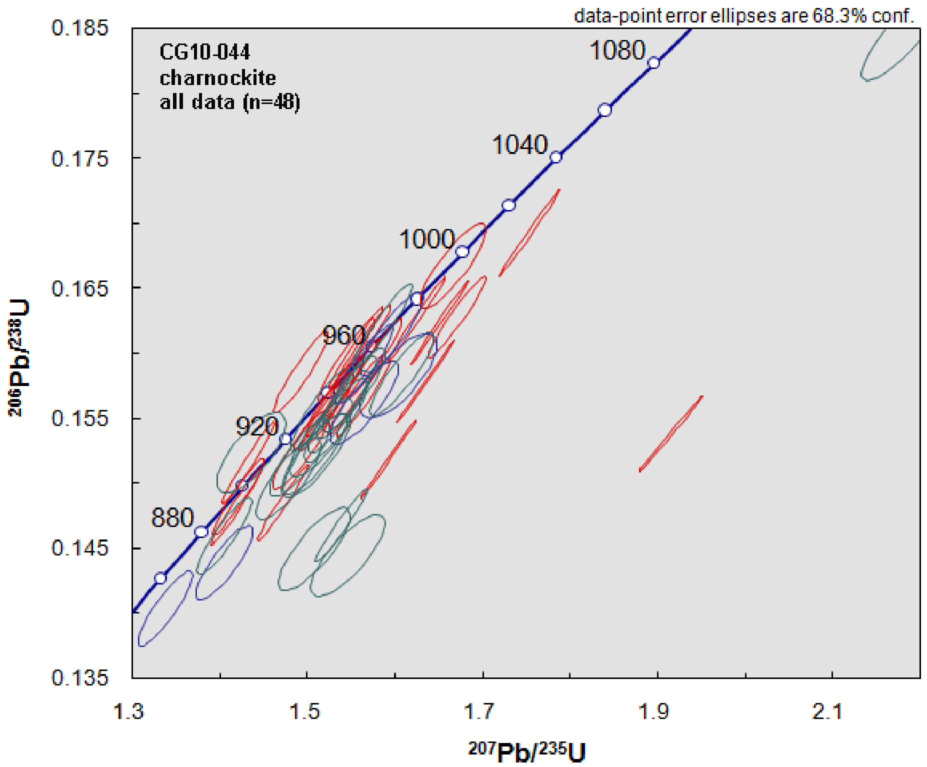

Figure 16. Standard Wetherill concordia diagram of all data (n=48) for sample CG10-044, a charnockite. Cores (n=24), rims (n=18) and recrystallised zones (n=6) are displayed as red, green and blue ellipses, respectively.

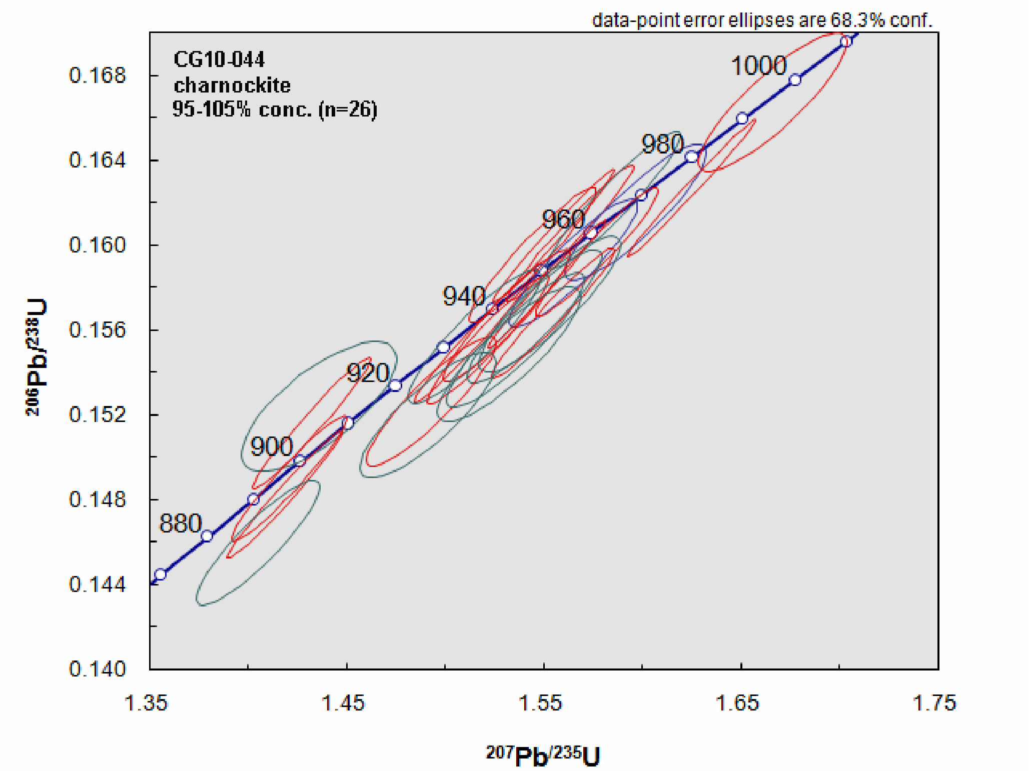

Figure 17. Standard Wetherill concordia diagram of 95-105% concordant data (n=26) for sample CG10-044, a charnockite. Cores, rims and recrystallised zones are displayed as red, green and blue ellipses, respectively.

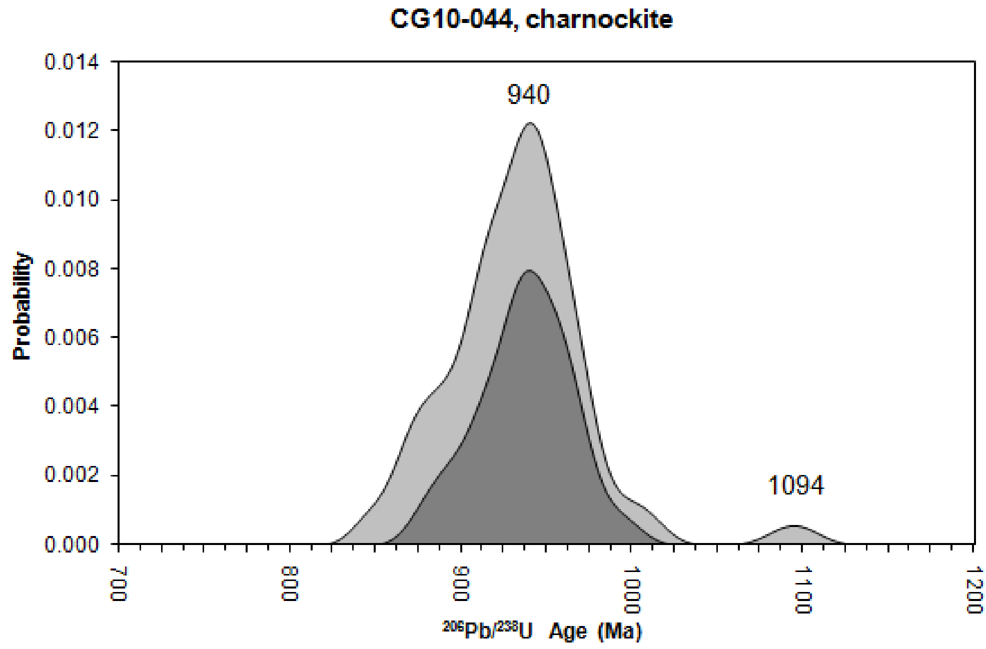

Figure 18. Probability density distribution plot of $^{206}Pb/^{238}U$ ages for sample CG10-044, a charnockite. Dark grey shaded area represents 95-105% concordant data (n=26), light grey shaded area represents all data (n=48). Age maxima for all data and 95-105% concordant data are labelled.

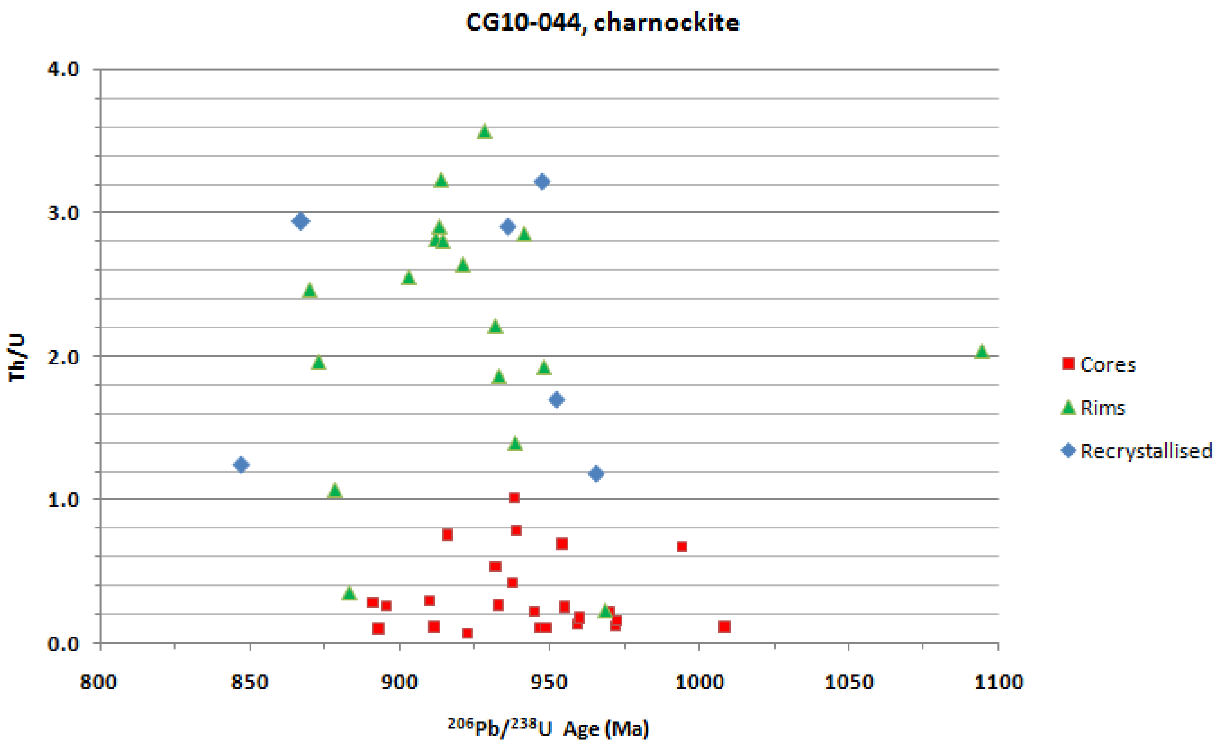

Figure 19. Th/U ratio versus $^{206}Pb/^{238}U$ age plot (all data, n=48) for the charnockite CG10-044.

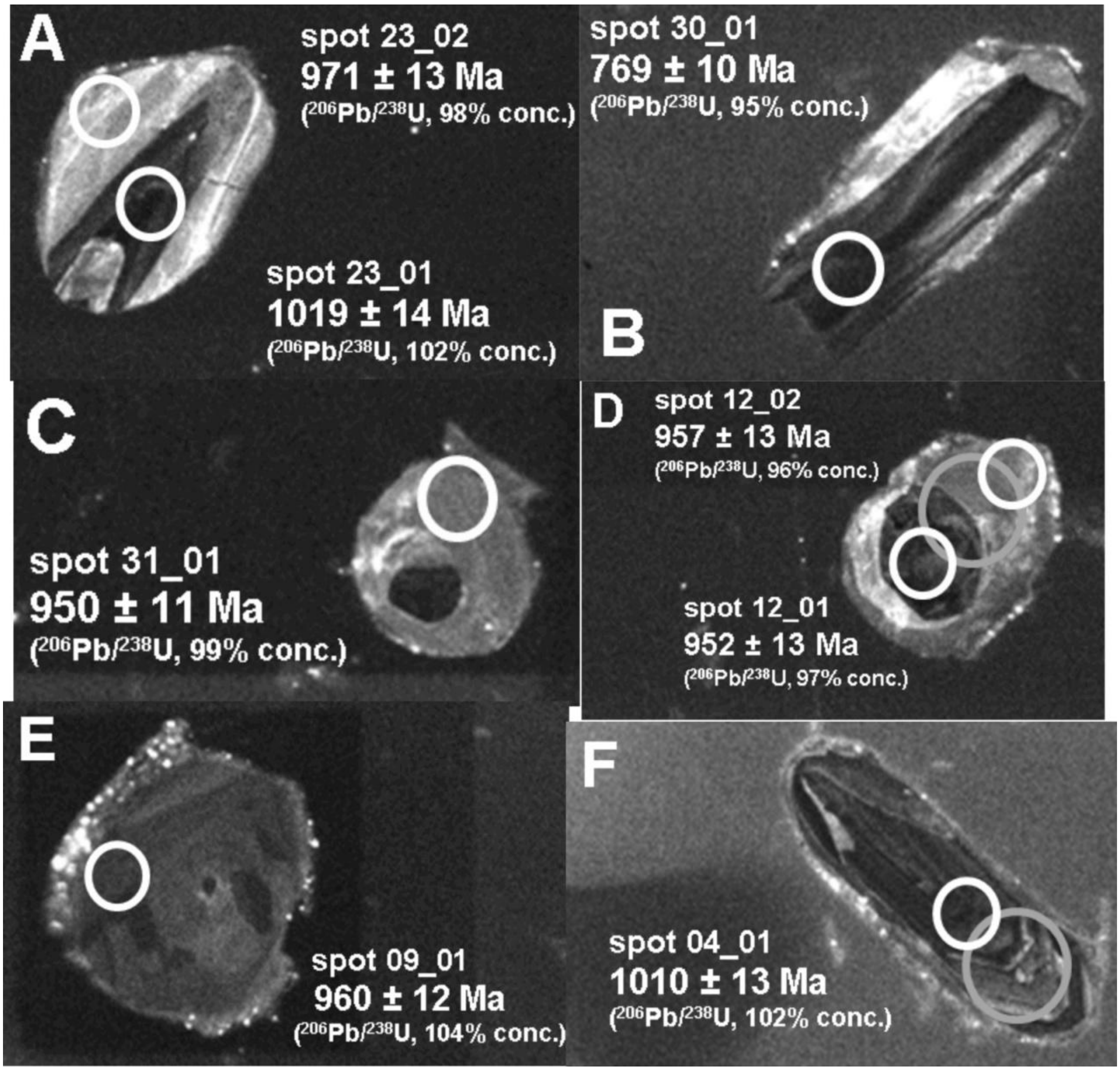

Figure 20. CL images of representative zircons from sample CG10-087, a megacrystic granitoid. White rings represent the positions of U/Pb analysis spots (diameter = 30 µm). Larger rings (grey) represent locations of Lu/Hf analysis spots (diameter = 50 µm).

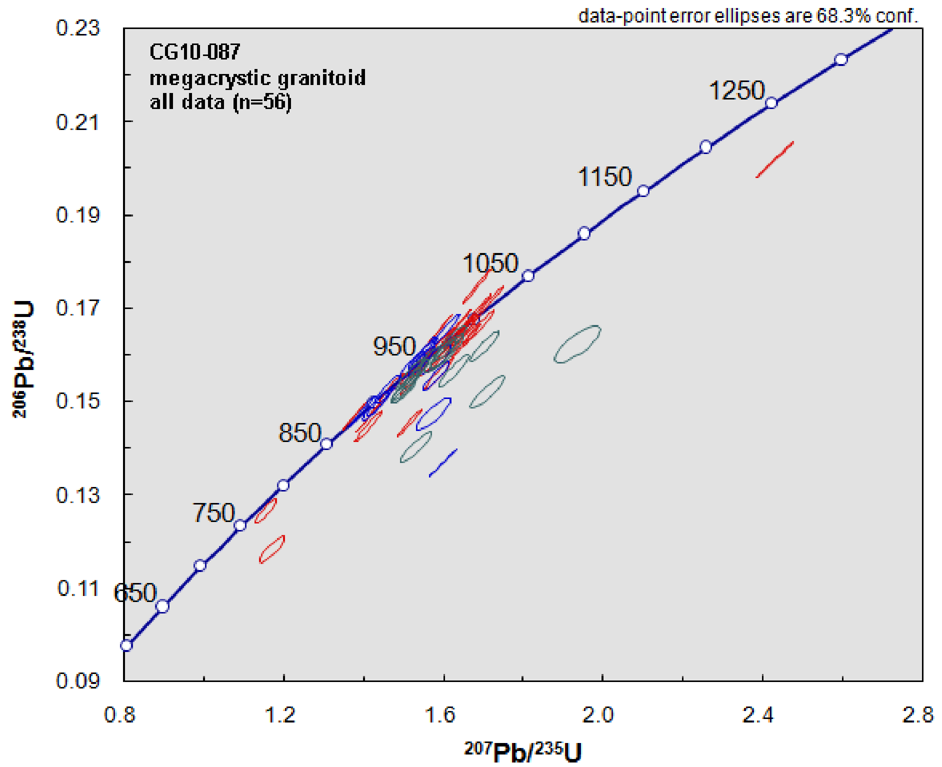

Figure 21. Standard Wetherill concordia diagram of all data (n=56) for sample CG10-087, a megacrystic granitoid. Cores (n=28), rims (n=15) and recrystallised zones (n=13) are displayed as red, green and blue ellipses, respectively.

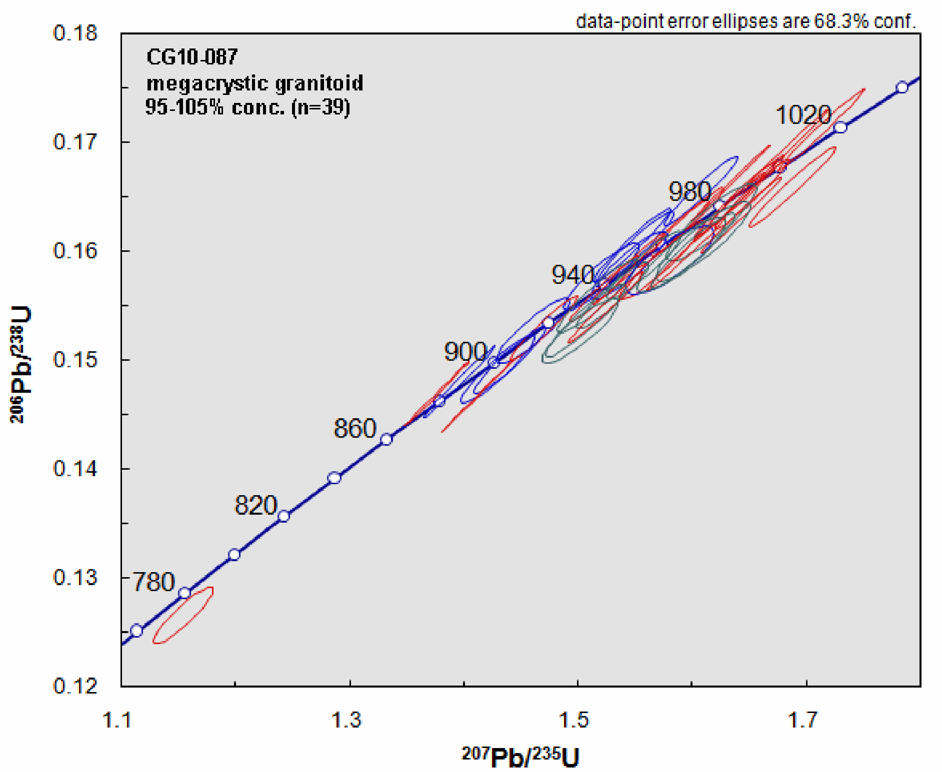

Figure 22. Standard Wetherill concordia diagram of 95-105% concordant data (n=26) for sample CG10-087, a megacrystic granitoid. Cores, rims and recrystallised zones are displayed as red, green and blue ellipses, respectively.

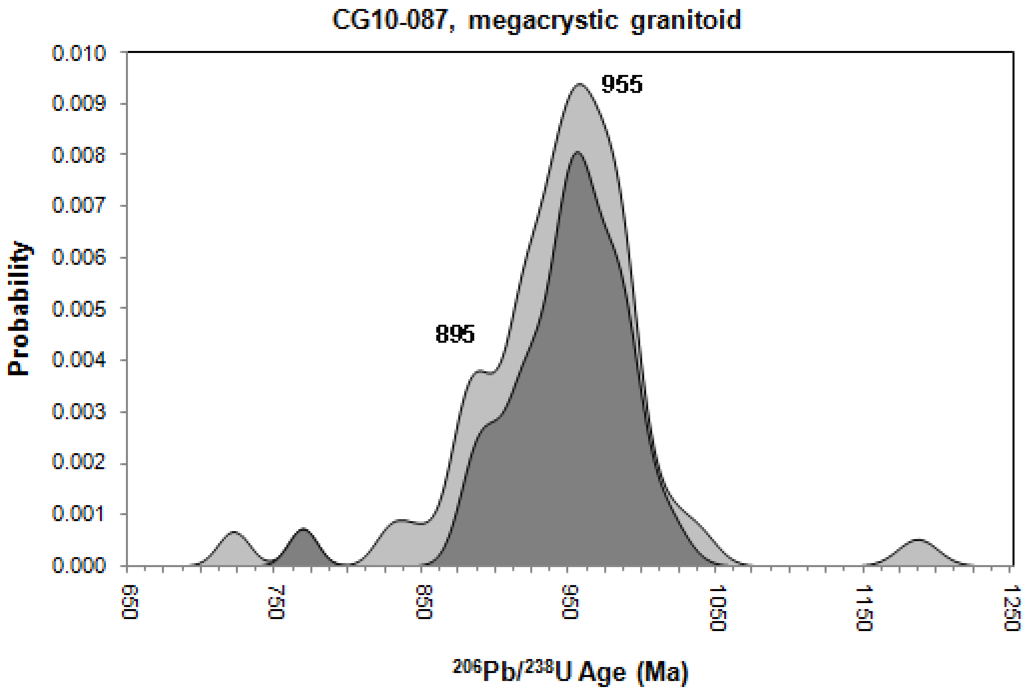

Figure 23. Probability density distribution plot of $^{206}Pb/^{238}U$ ages for sample CG10-087, a megacrystic granitoid. Dark grey shaded area represents 95-105% concordant data (n=39), light grey shaded area represents all data (n=56). Age maxima for 95-105% concordant data are labelled.

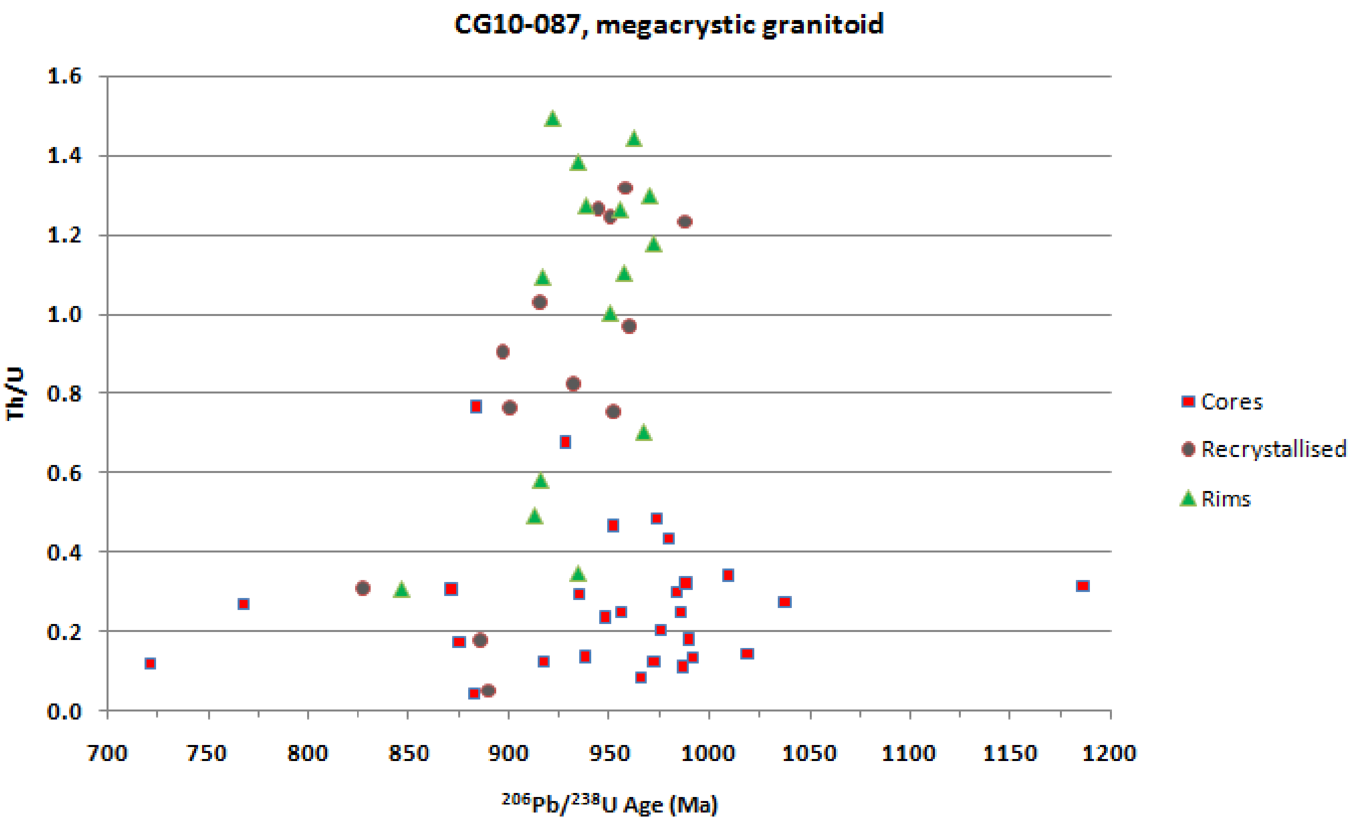

Figure 24. Th/U ratio versus $^{206}Pb/^{238}U$ age plot (all data, n=48) for the megacrystic granitoid, CG10-087.

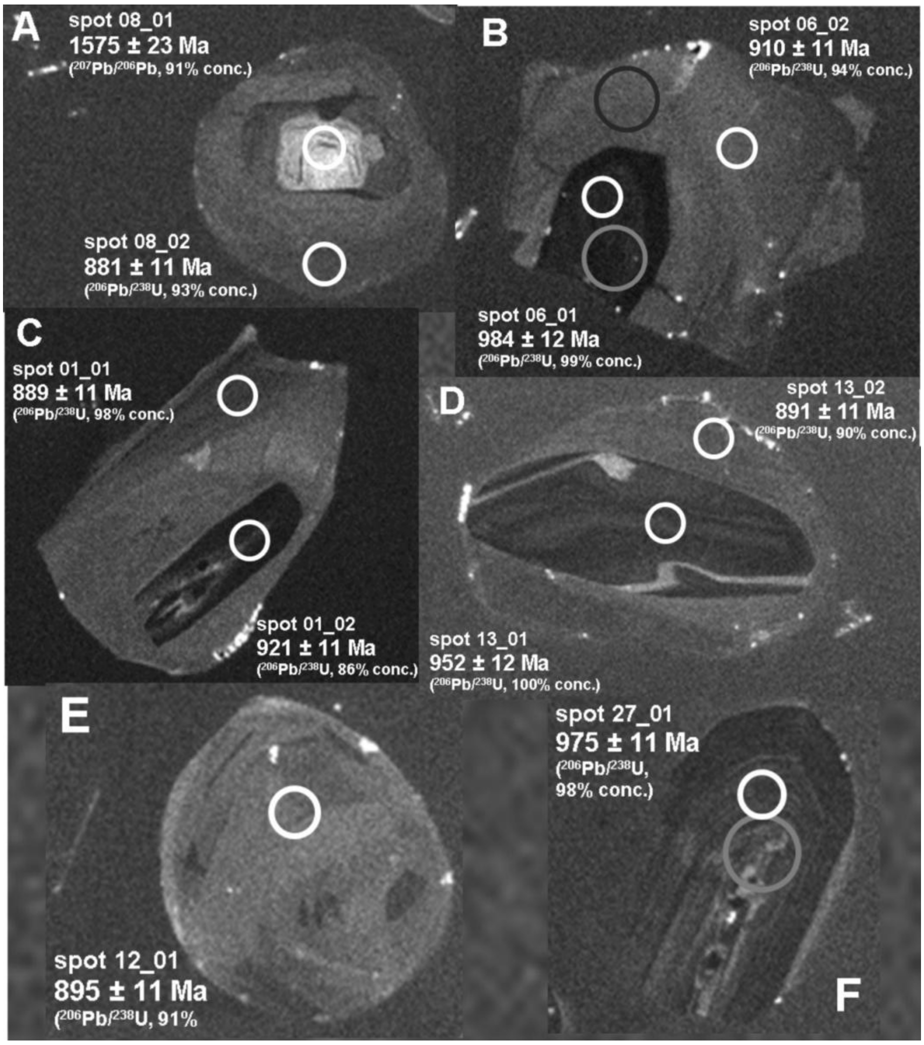

Figure 25 (A-F). CL images of representative zircons from sample CG10-133, a charnockite. White rings represent the positions of U/Pb analysis spots (diameter = 30 µm). Larger rings (grey and black) represent locations of Lu/Hf analysis spots (diameter = 50 µm).

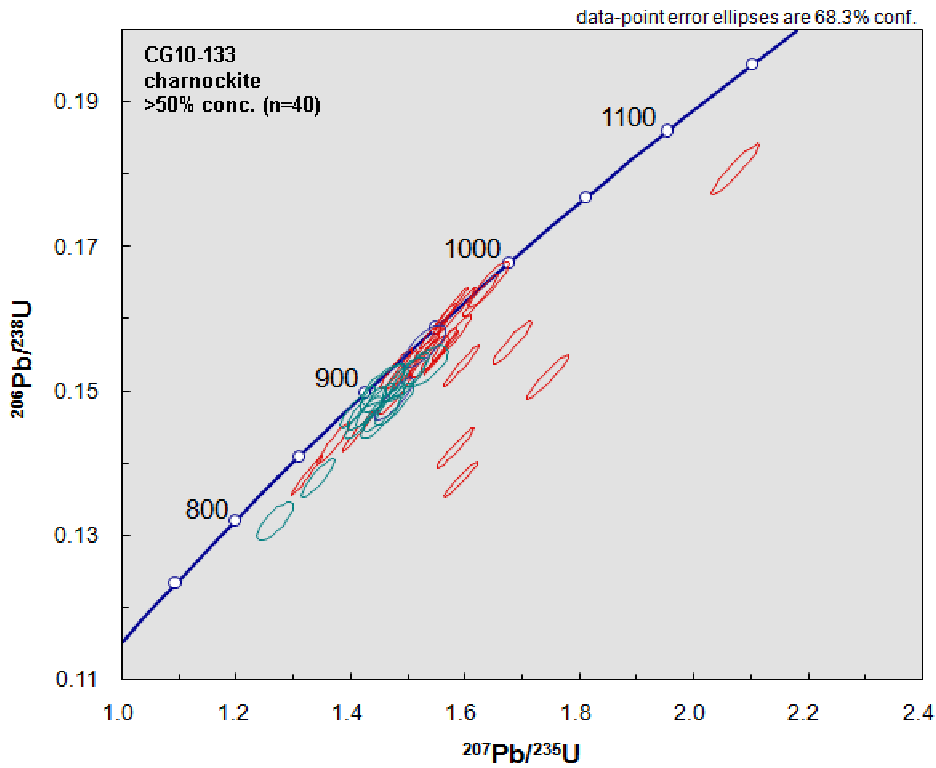

Figure 26. Standard Wetherill concordia diagram of greater than 50% concordant data (n=40) for sample CG10-133, a charnockite. Cores (n=24), rims (n=14) and recrystallised zones (n=2) are displayed as red, green and blue ellipses, respectively. Spot 08_01 ($^{207}Pb/^{206}Pb$ age = 1575 ± 23 Ma, 91% conc.) is not included, as it is off the scale.

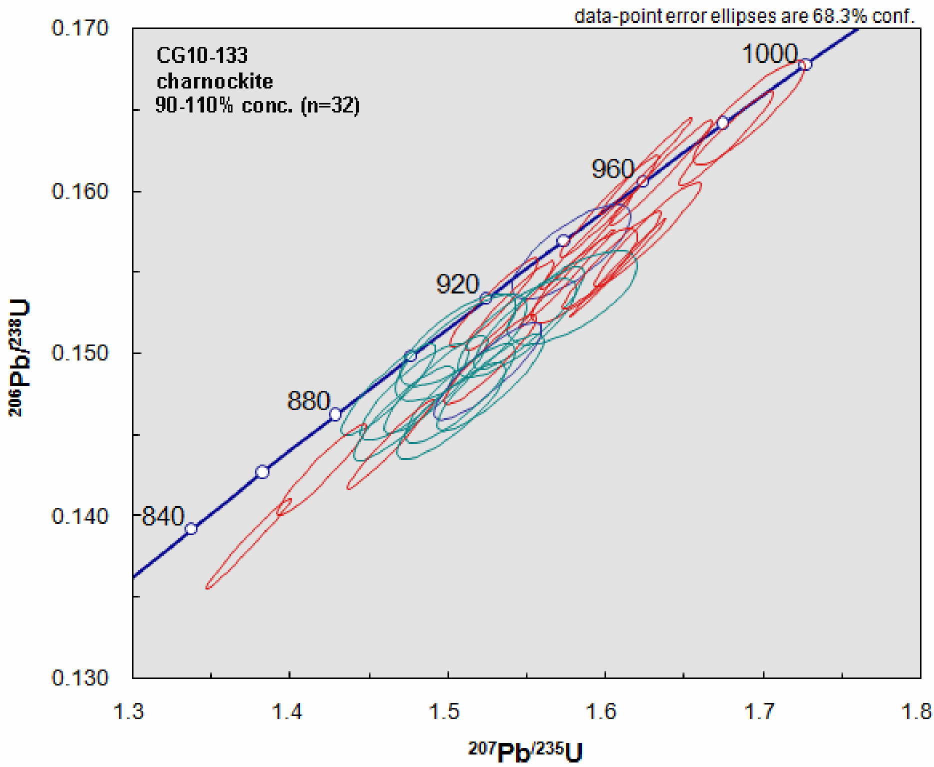

Figure 27. Standard Wetherill concordia diagram of 90-110% concordant data (n=32) for sample CG10-133, a charnockite. Cores (n=18), rims (n=12) and recrystallised zones (n=2) are displayed as red, green and blue ellipses, respectively. Spot 08_01 ($^{207}Pb/^{206}Pb$ age = 1575 ± 23 Ma, 91% conc.) is not included, as it is off the scale.

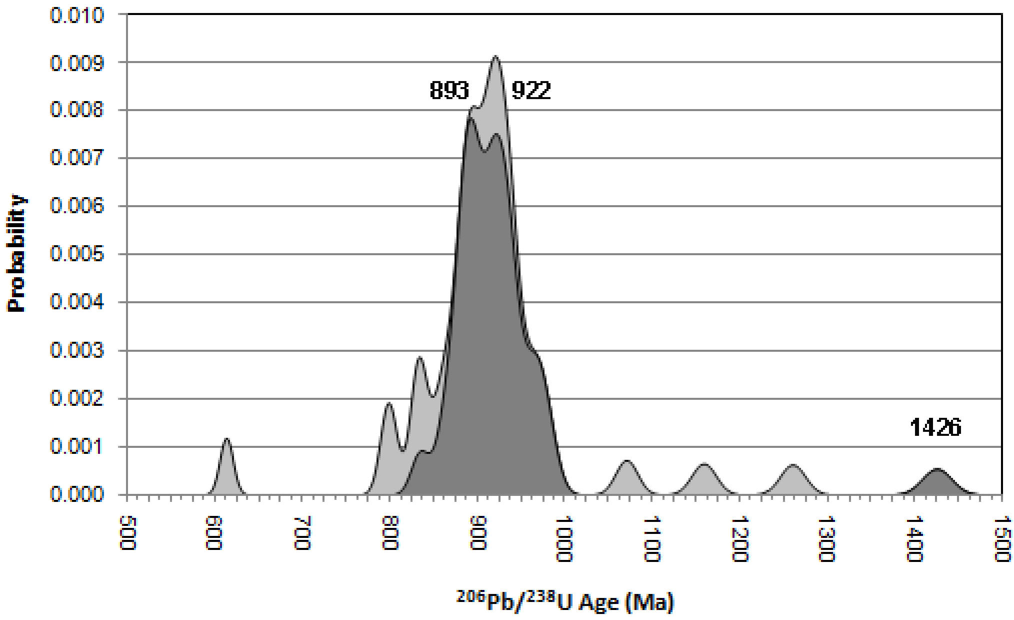

Figure 28. Probability density distribution plot of $^{206}Pb/^{238}U$ ages for sample CG10-133, a charnockite. Dark grey shaded area represents 90-110% concordant data (n=32), light grey shaded area represents all data (n=44). Age maxima for all data are labelled with maxima for 90-110% concordancy highlighted in bold text.

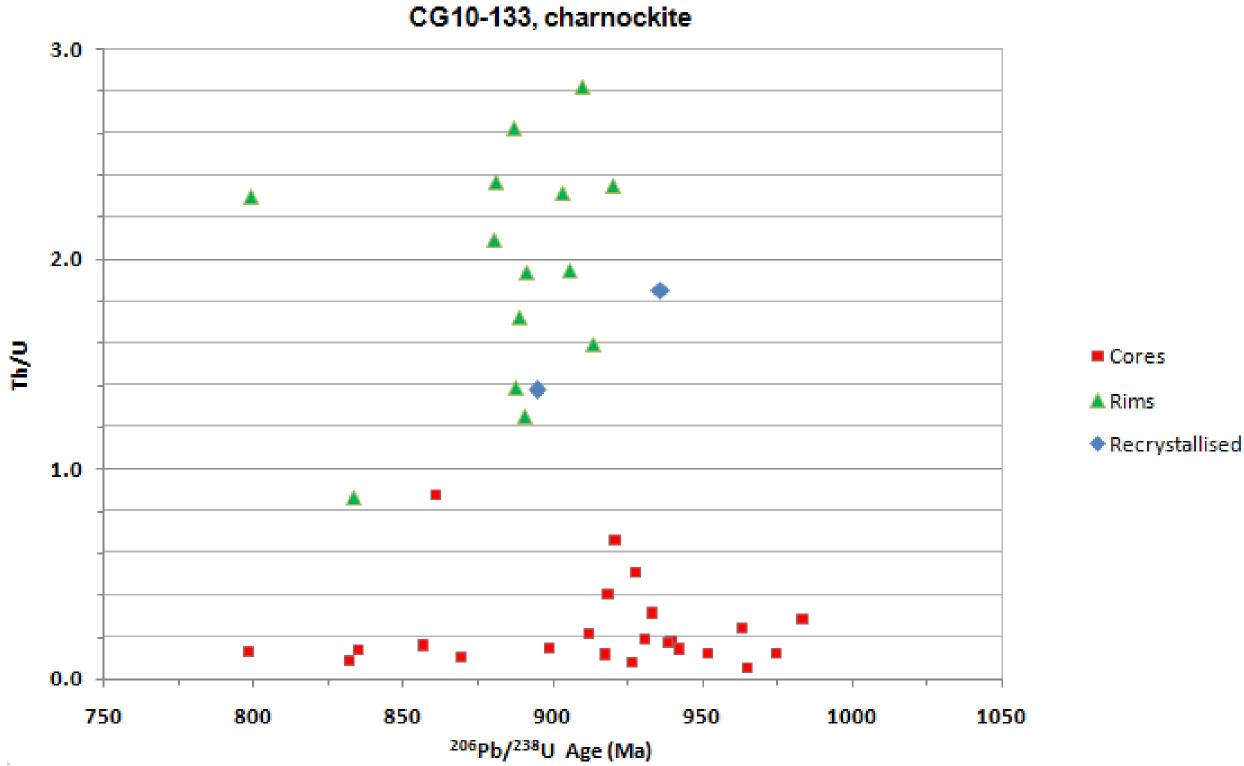

Figure 29. Th/U ratio versus $^{206}Pb/^{238}U$ age plot of >50% concordant data (n=40) for the charnockite, CG10-133.

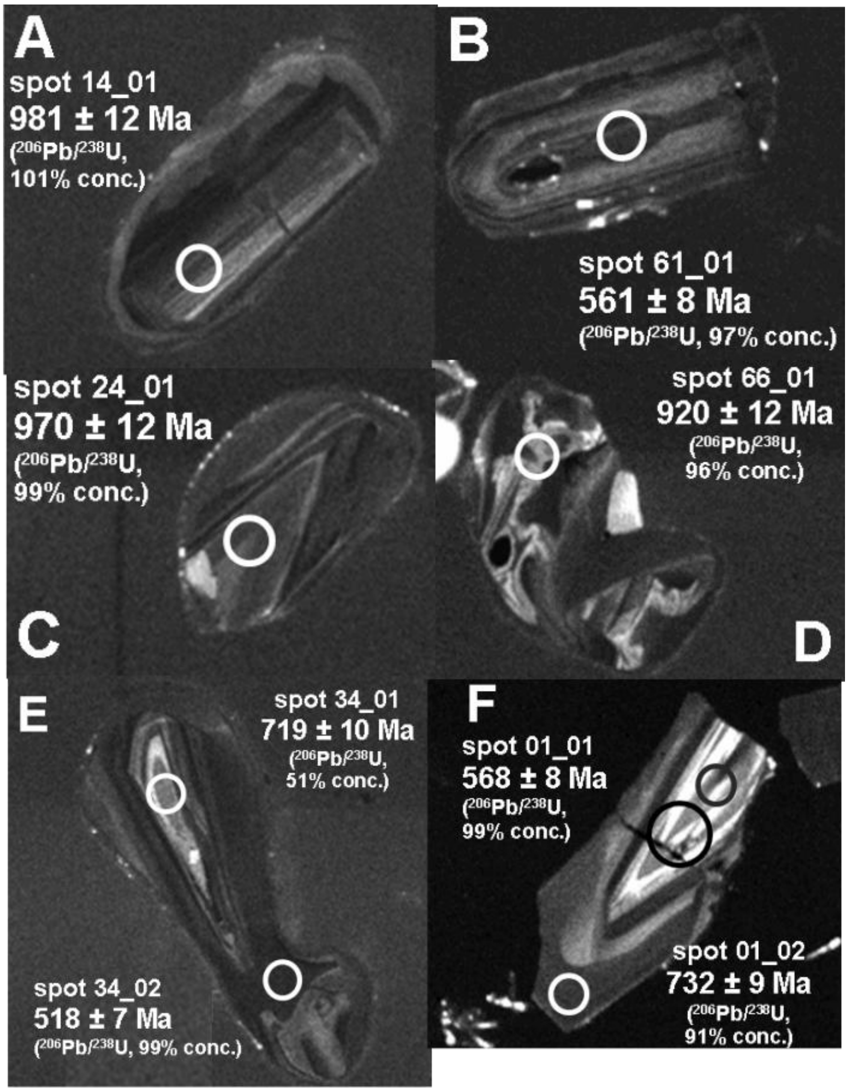

Figure 30. CL images of representative zircons from sample CG10-142, a megacrystic granitoid. Smaller rings (white and grey) represent the positions of U/Pb analysis spots (diameter = 30 µm). Larger rings (black) represent locations of Lu/Hf analysis spots (diameter = 50 µm) **(A.)** The oldest concordant zircon analysis

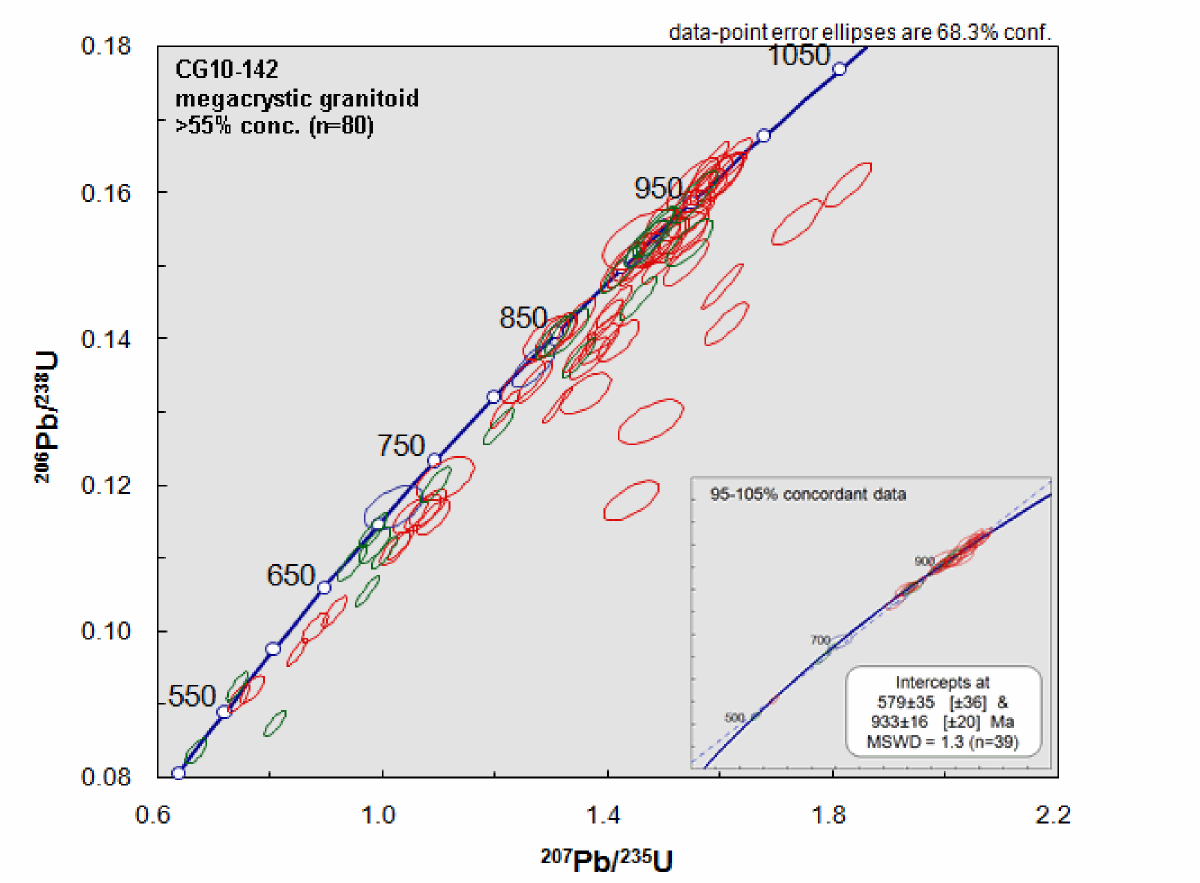

Figure 31. Standard Wetherill concordia diagram of greater than 55% concordant data (n=80) for sample CG10-142, a megacrystic granitoid. Cores (n=57), rims (n=20) and recrystallised zones (n=3) are displayed as red, green and blue ellipses, respectively. Concordia for 95-105% concordant data (n=39) is inset displaying intercepts of 579 ± 35 Ma and 933 ± 16 Ma (MSWD = 1.3).

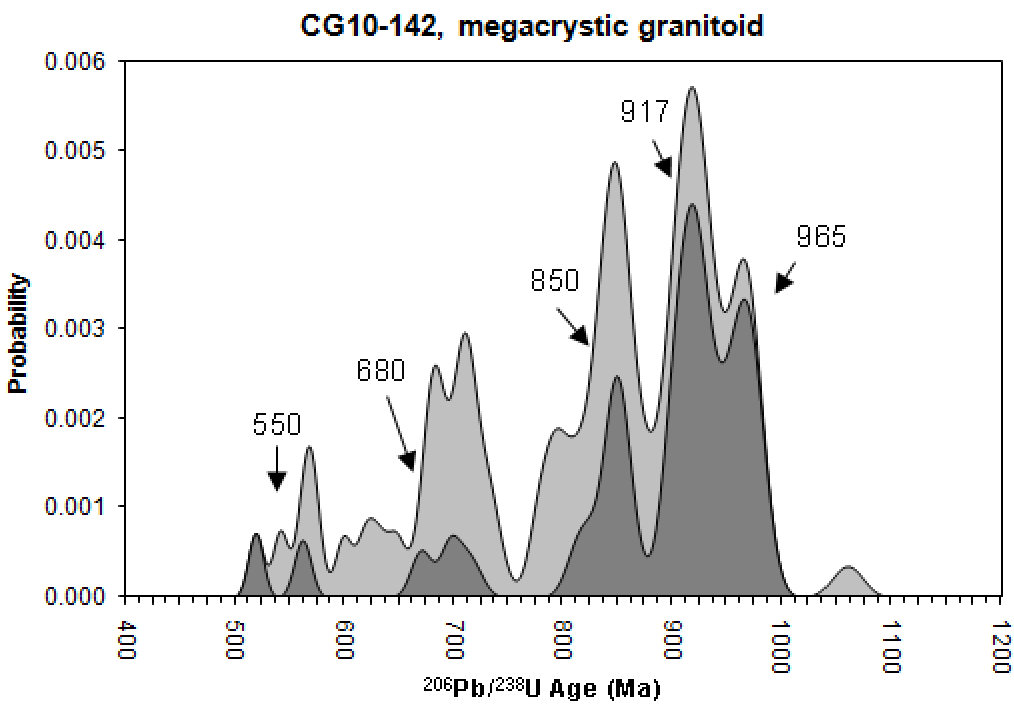

Figure 32. Probability density distribution plot of $^{206}Pb/^{238}U$ ages for sample CG10-142, a megacrystic granitoid. Dark grey shaded area represents 95-105% concordant data (n=39), light grey shaded area represents all data (n=81). Age maxima for concordant data are labelled.

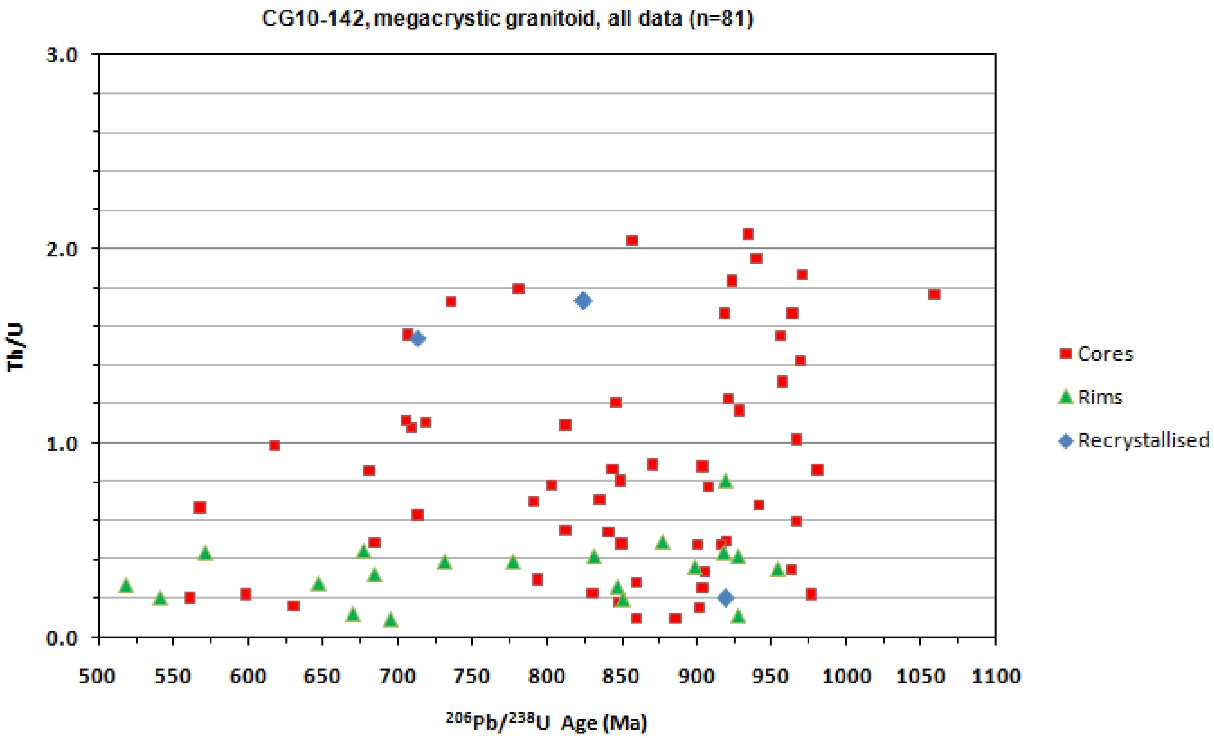

Figure 33. Th/U ratio versus ^{206}Pb/^{238}U age plot of all data (n=81) for the megacrystic granitoid, CG10-142.

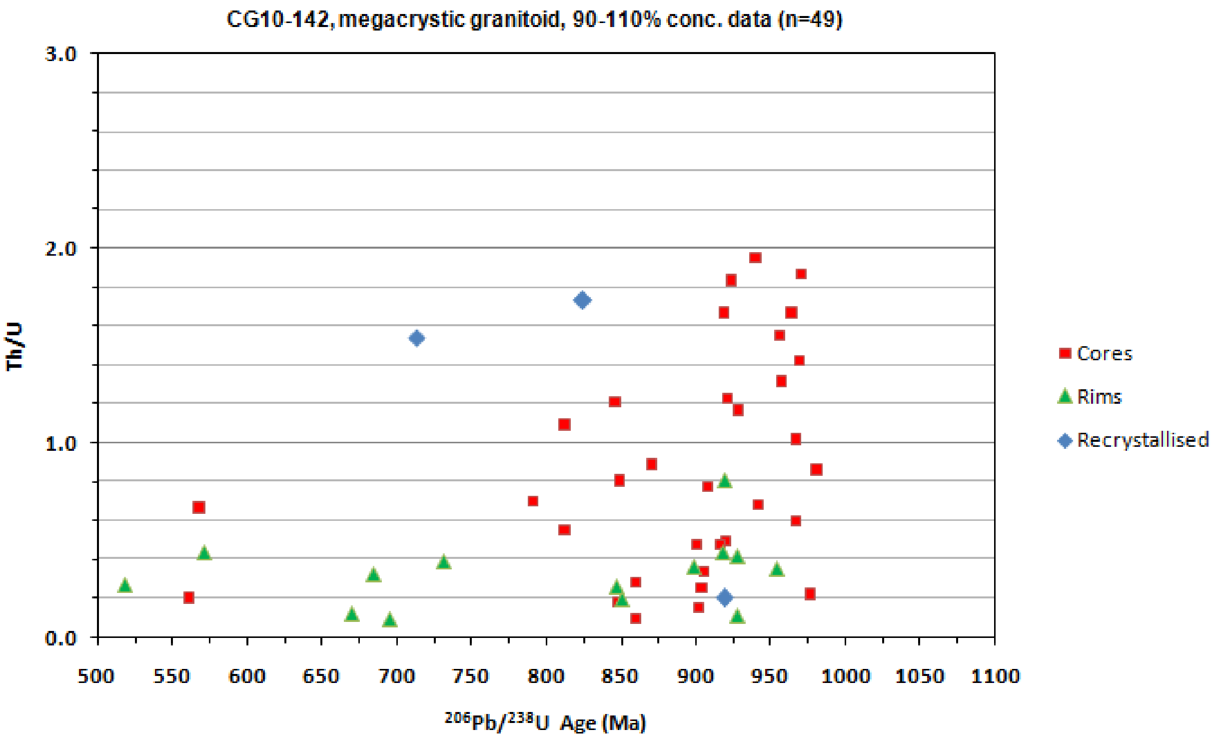

Figure 34. Th/U ratio versus ^{206}Pb/^{238}U age plot (90-110% concordancy, n=49) for the megacrystic granitoid, CG10-142.

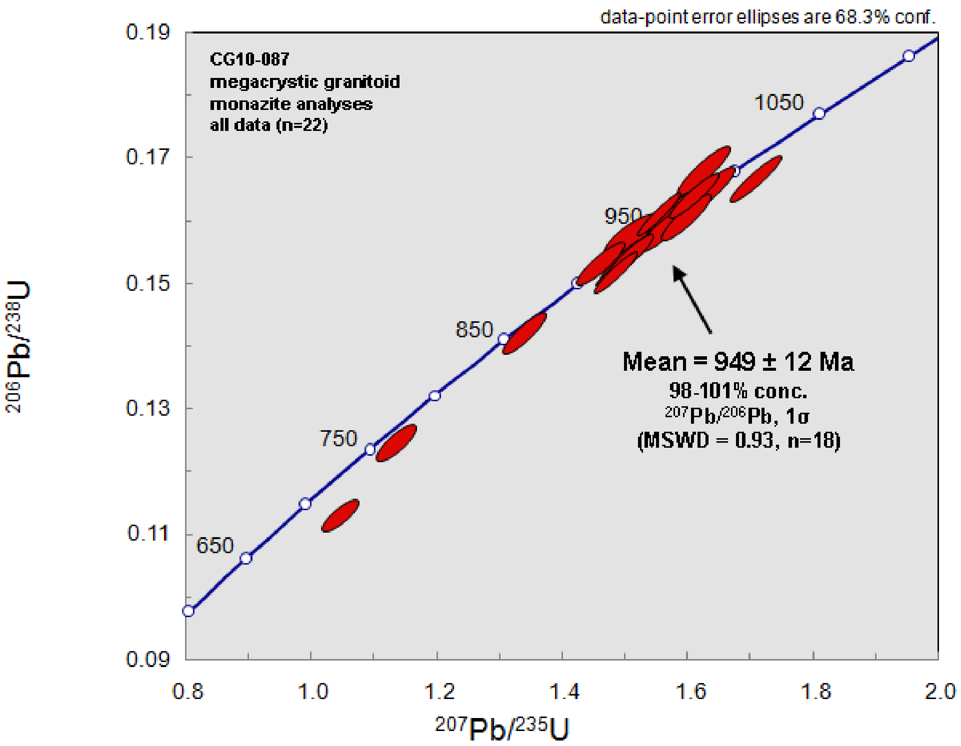

Figure 35. Standard Wetherill concordia diagram for all monazite data (n=22) for sample CG10-087, a megacrystic granitoid. Weighted mean for 98-101% concordant $^{207}Pb/^{206}Pb$ age data is indicated (n=18).

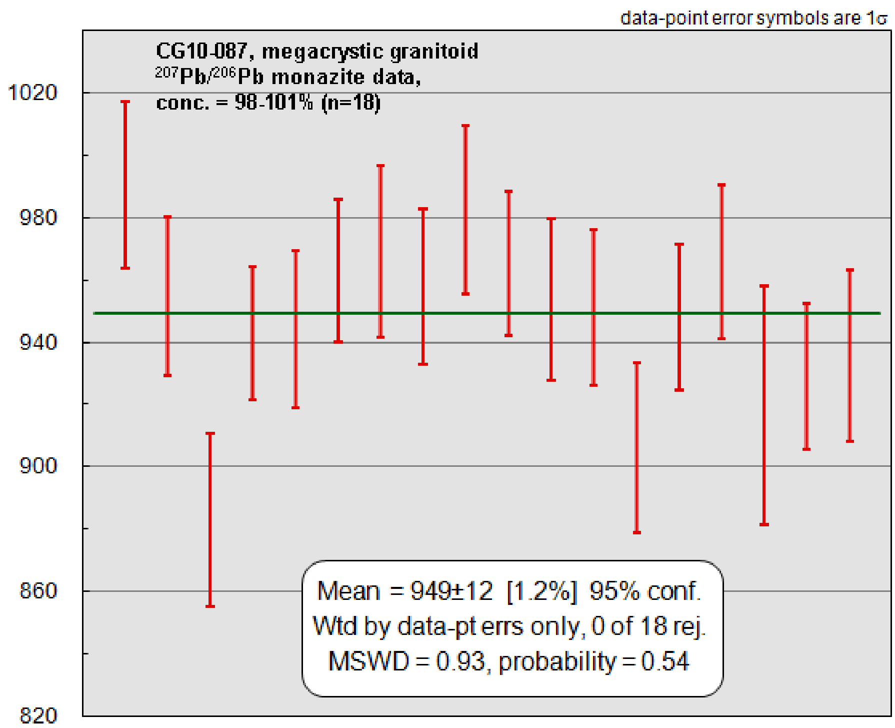

Figure 36. Weighted mean of 98-101% concordant $^{207}Pb/^{206}Pb$ data (n=18) for monazite analyses for sample CG10-087, a megacrystic granitoid. The calculated mean age is 949 ± 12 Ma (MSWD = 0.93).

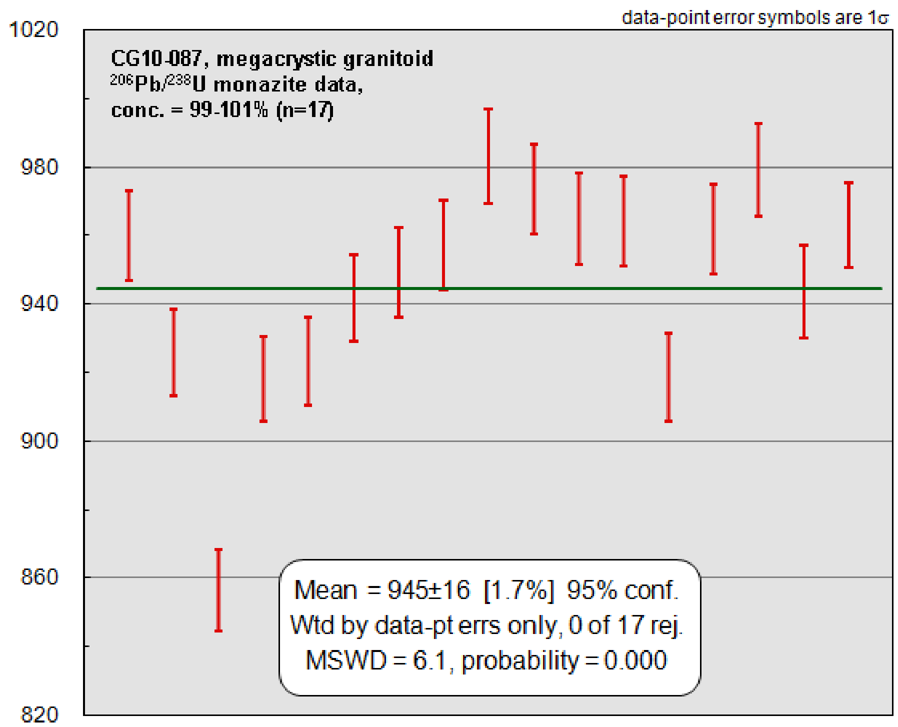

Figure 37. Weighted mean of 99-101% concordant $^{206}Pb/^{238}U$ data (n=17) for monazite analyses for sample CG10-087, a megacrystic granitoid. The calculated mean age is 945 ± 16 Ma (MSWD = 6.1).

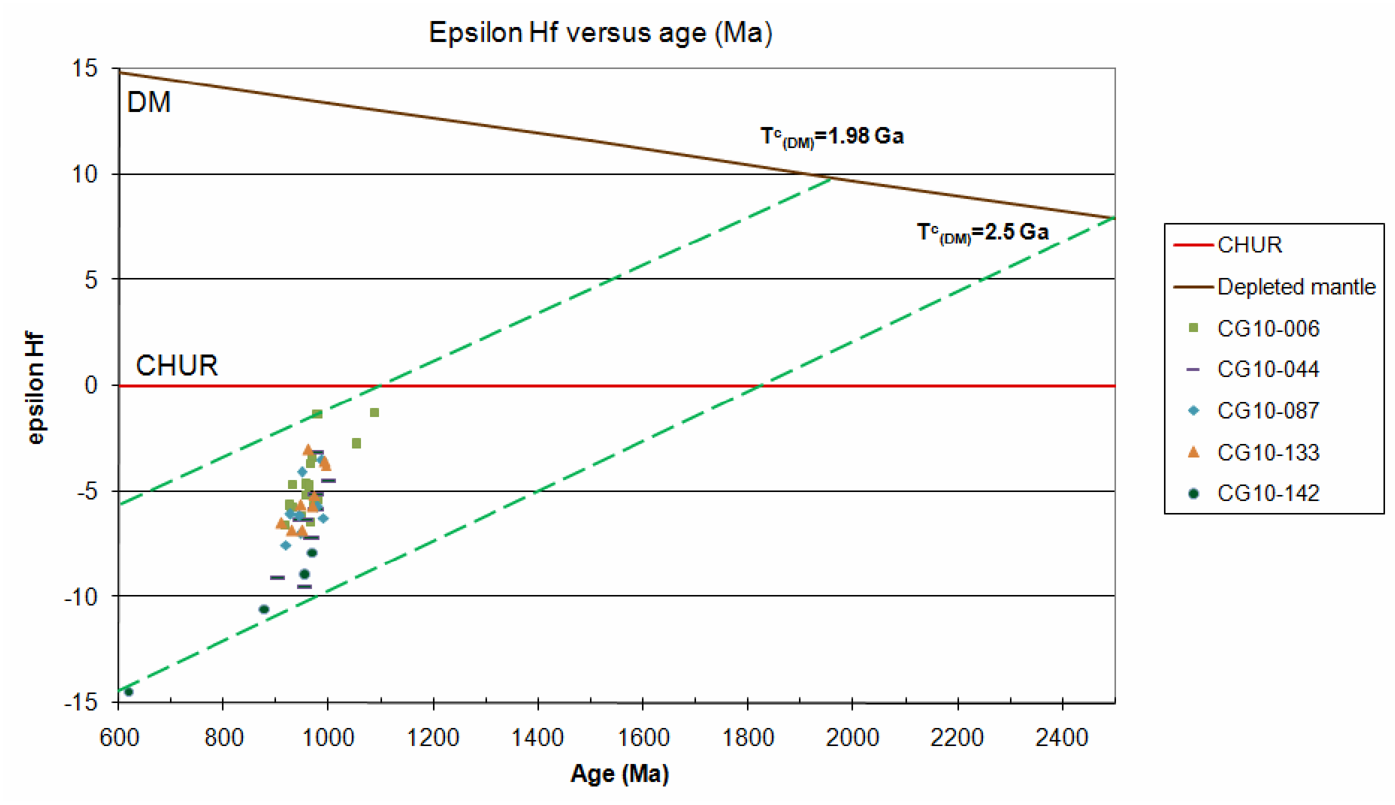

Figure 38. Epsilon Hf versus U/Pb age (Ma) plot for all samples.

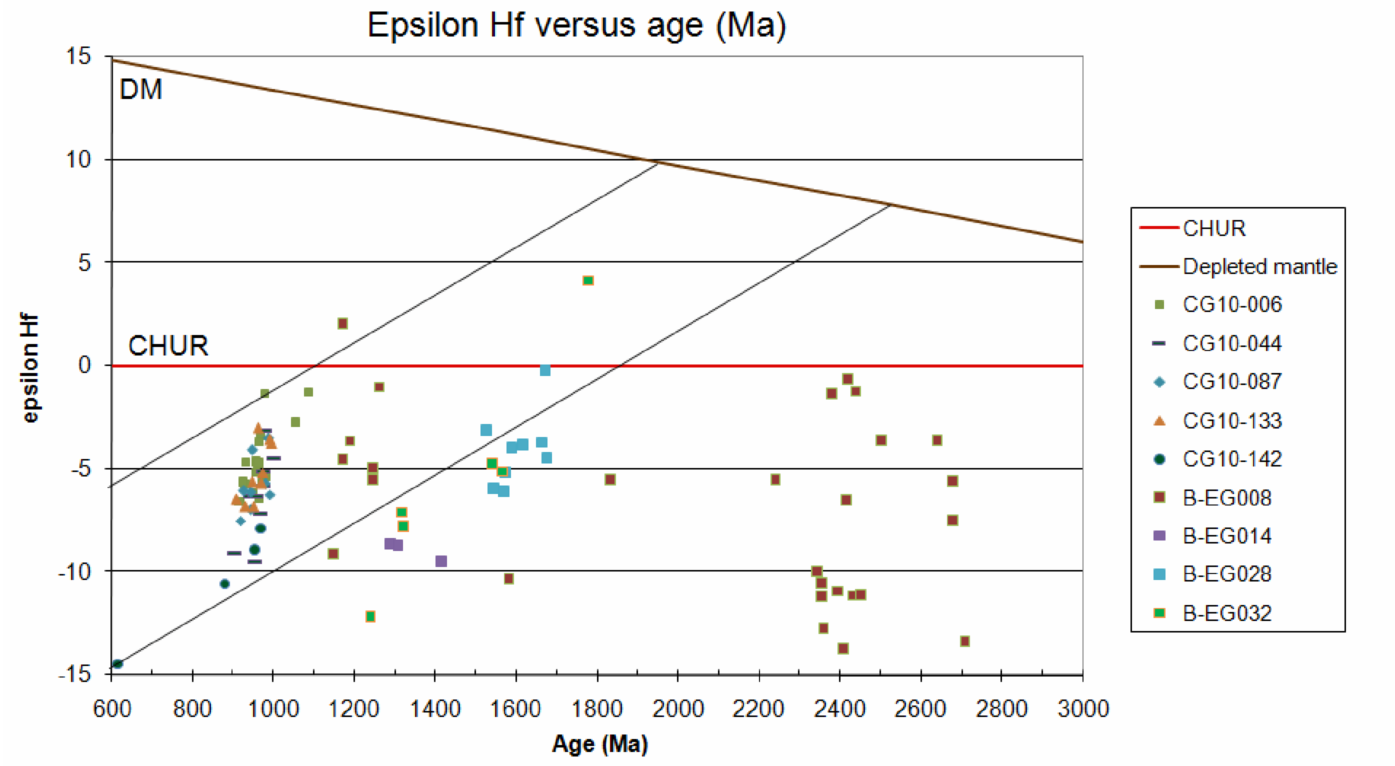

Figure 39. Epsilon Hf versus age plot for all samples from this study plotted with Hf data for metasediments from the Central Eastern Ghats (Reid, 2010). CG10-006 = megacrystic orthogneiss; CG10-044 & 133 = charnockites; CG10-087 & 142 = megacrystic granitoids; B-EG008 & 014 = quartzites; B-EG028 & 032 = metapelites.

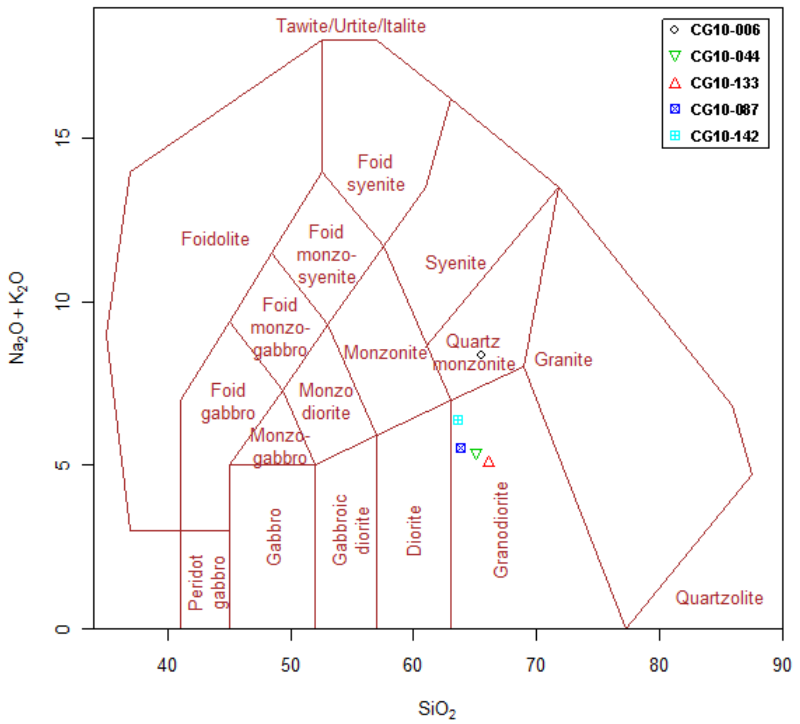

Figure 40. Granite classification plot of all samples (after Middlemost, 1985).

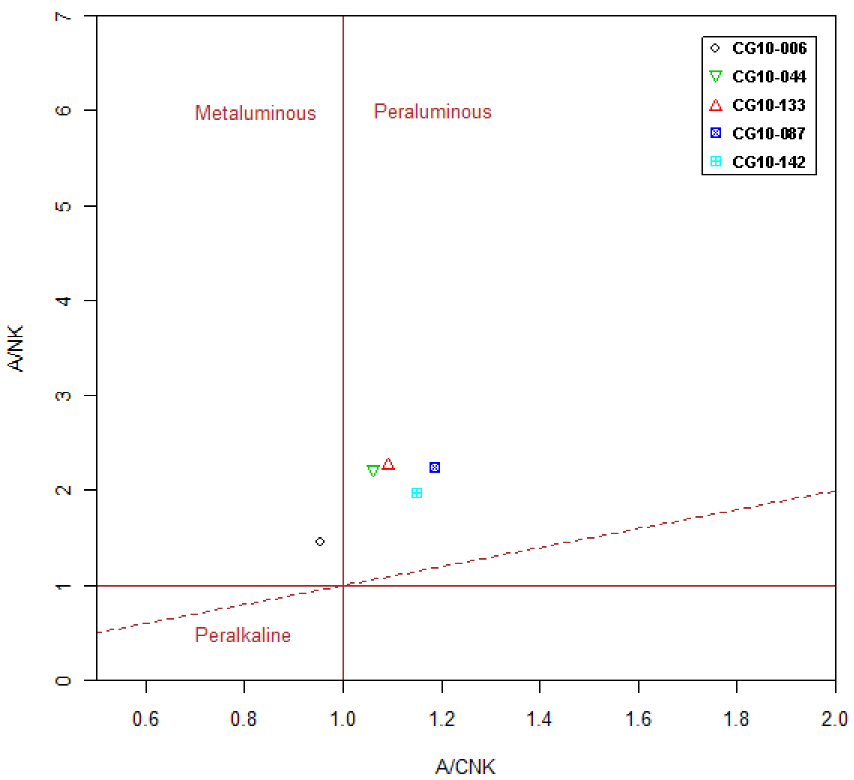

Figure 41. A/CNK-A/NK plot of all samples (after Shand, 1943).

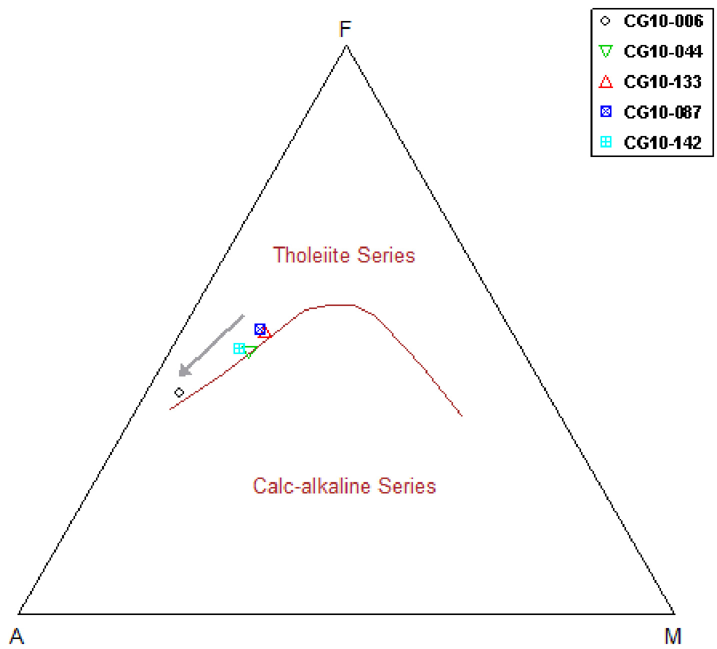

Figure 42. AFM diagram for all samples (after Irvine and Baragar, 1971).

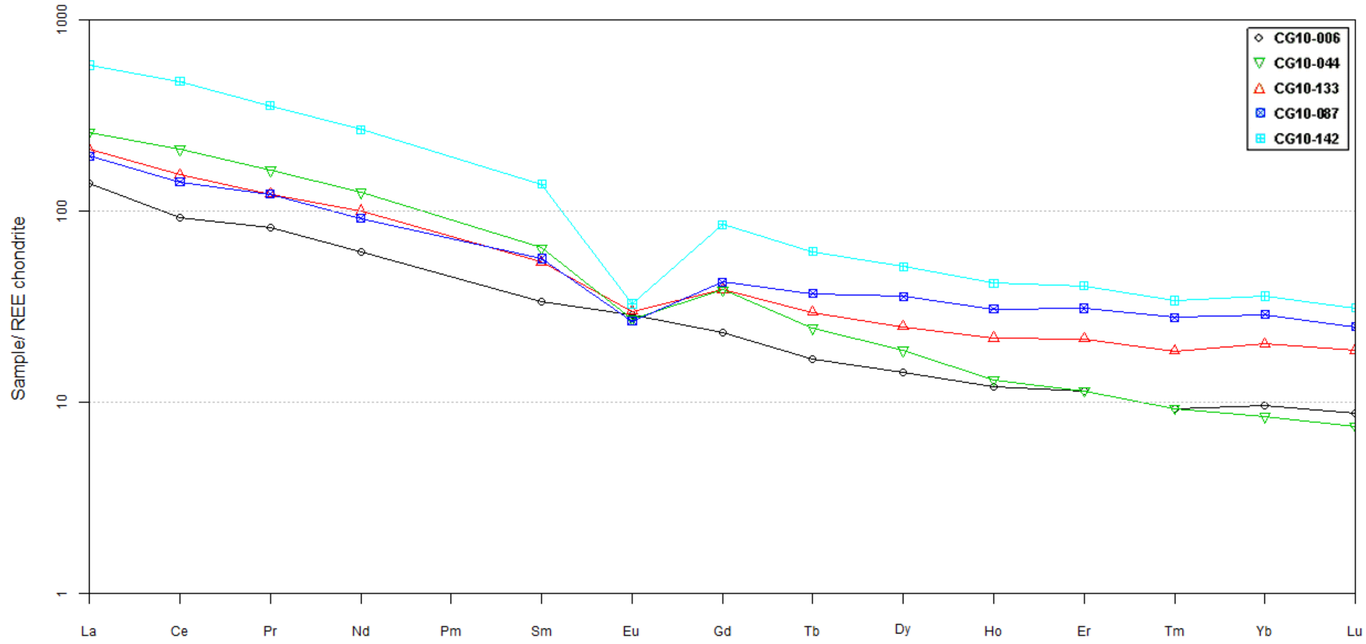

Figure 43. Chondrite normalised rare earth element plot of all samples (after Boynton, 1984).

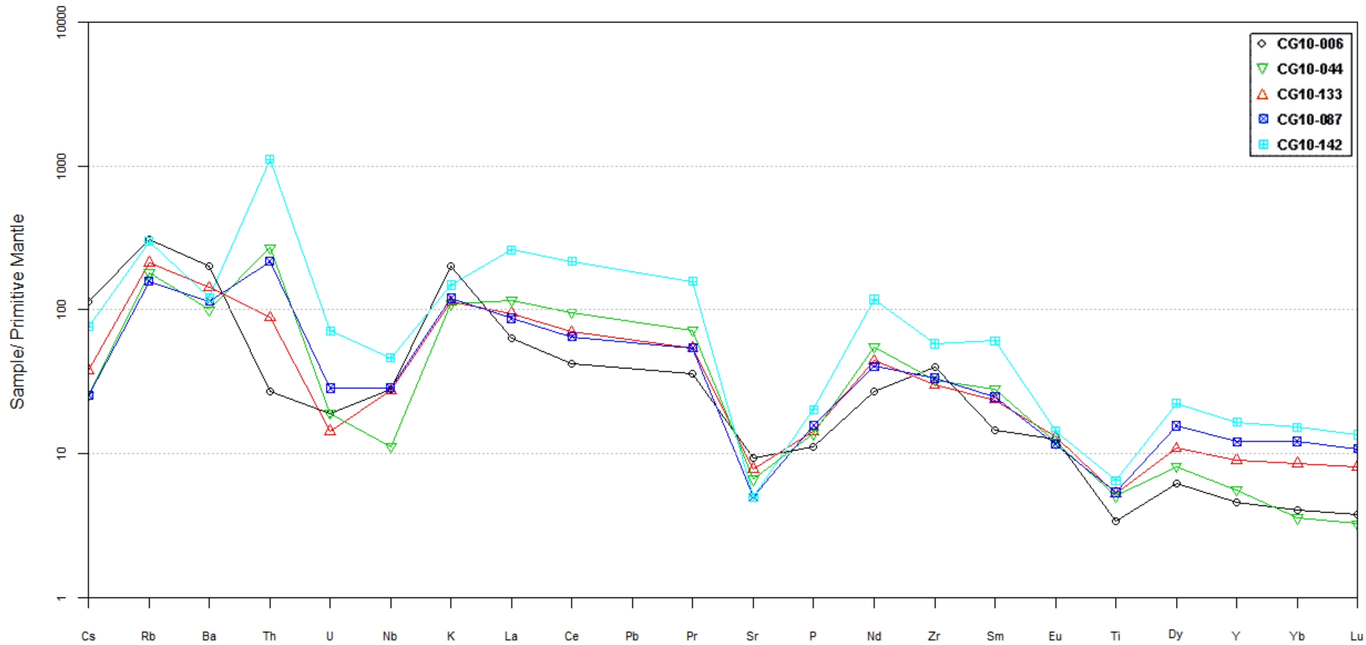

Figure 44. Primitive mantle normalised spidergram plot of all samples (after Sun & McDonough, 1989).

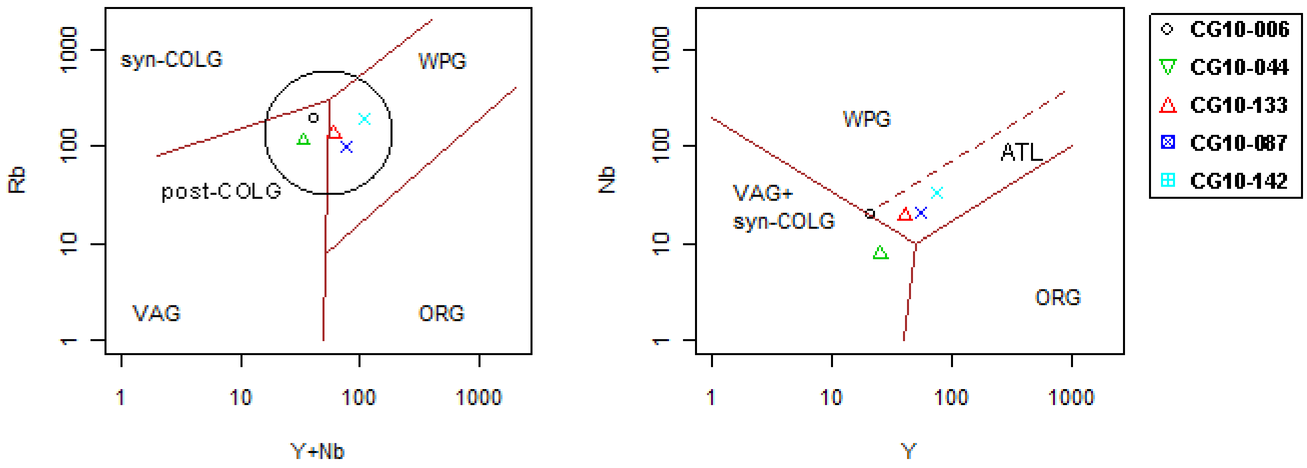

Figure 45. Trace element discrimination diagrams for tectonic interpretation of granitic rocks (after Pearce et al., 1984; Pearce, 1996). WPG: Within plate granites, syn-COLG: syn-collisional granites, post-COLG: post-collisional granites, VAG: volcanic ocean arc granites, ORG: ocean ridge granites, ATL: attenuated continental lithosphere.

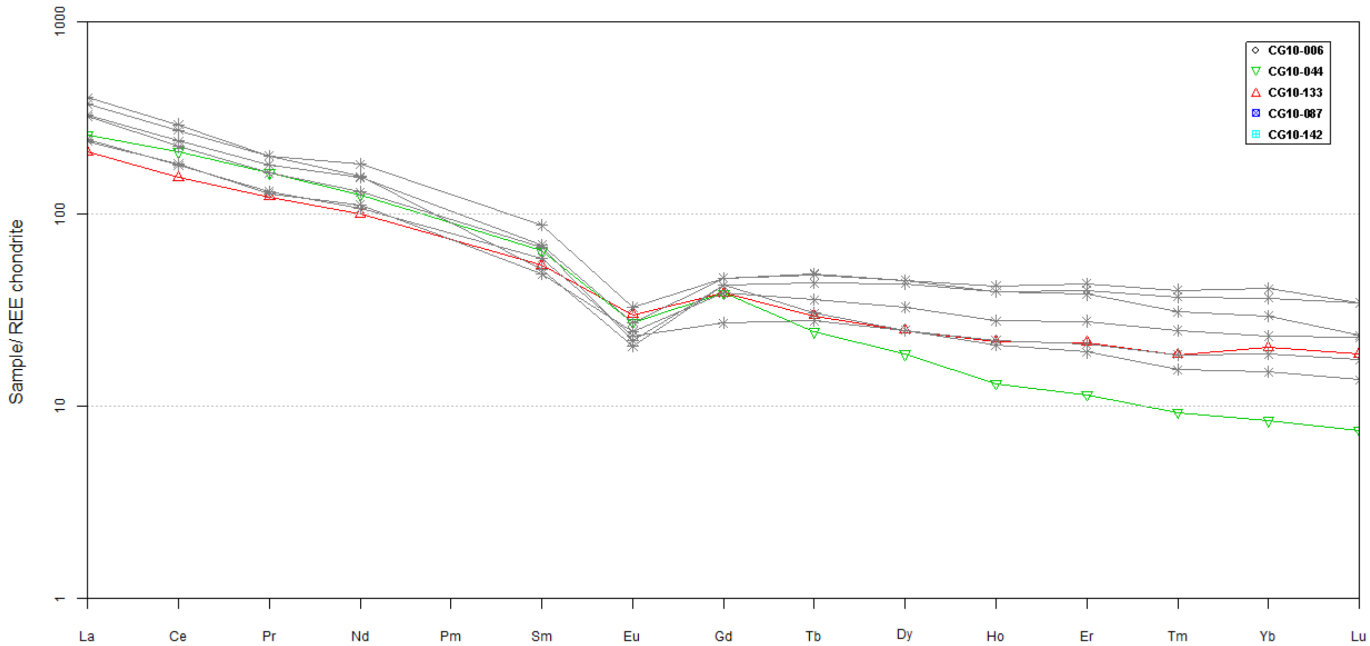

Figure 46. Chondrite normalised rare earth element spidergram (after Boynton, 1984) for charnockite samples CG10-044 (red) and CG10-133 (green) plotted alongside six representative charnockites (grey) from the Paderu area (Narayana et al., 1999).

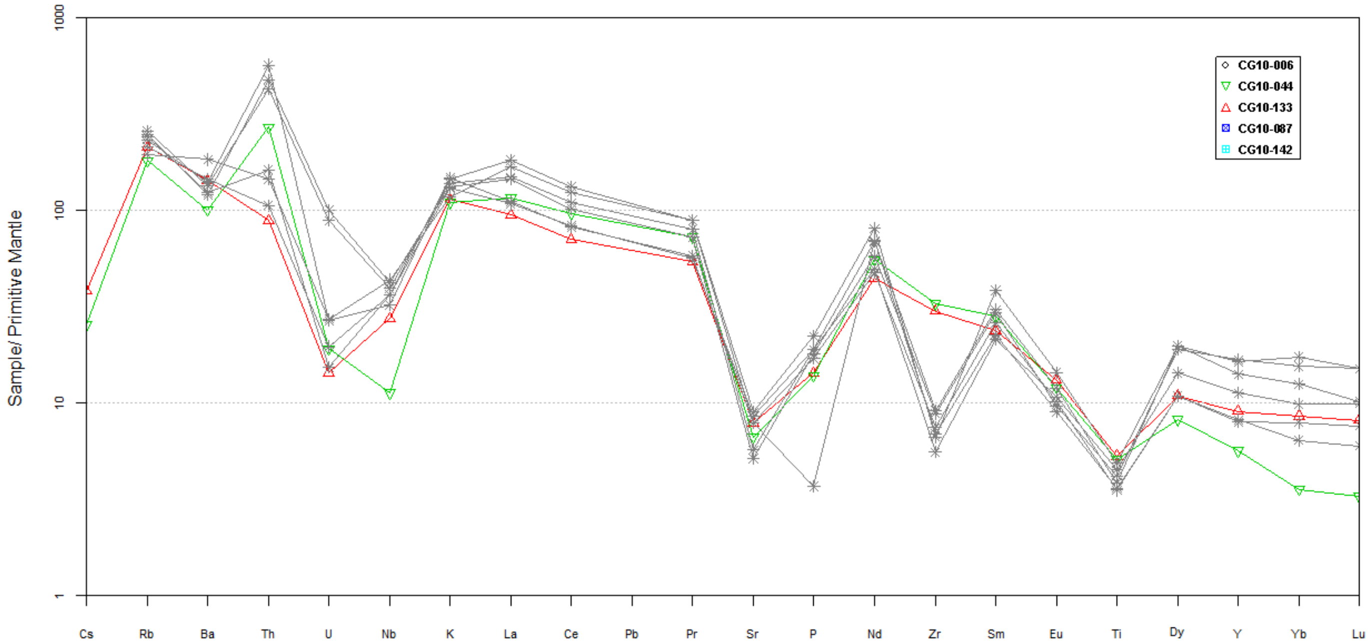

Figure 47. Primitive mantle normalised spidergram (after Sun & McDonough, 1989) for charnockite samples CG10-044 (red) and CG10-133 (green) plotted alongside six representative charnockites (grey) from the Paderu area (Narayana et al., 1999).

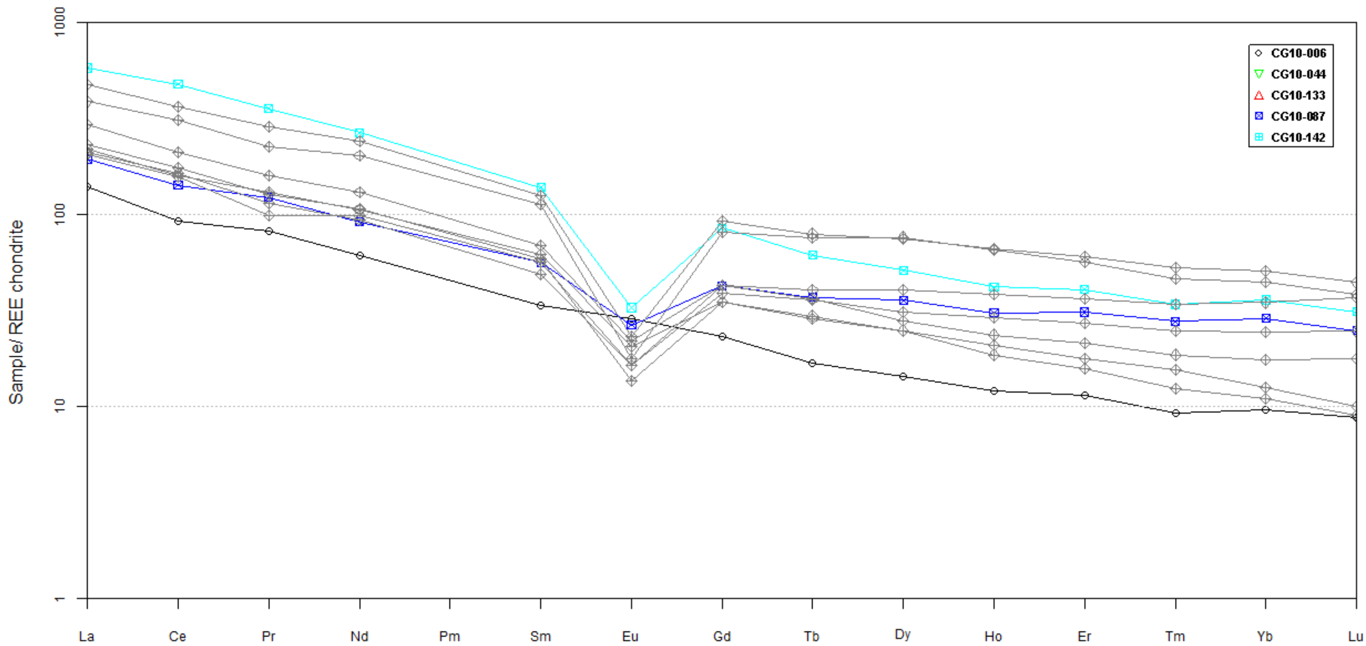

Figure 48. Chondrite normalised rare earth element spidergram (after Boynton, 1984) for the megacrystic granitoids CG10-087 (navy) and CG10-142 (aqua); the orthogneiss, CG10-006 (black); plotted alongside seven representative megacrystic granites (grey) from the Paderu area (Narayana et al., 1999).

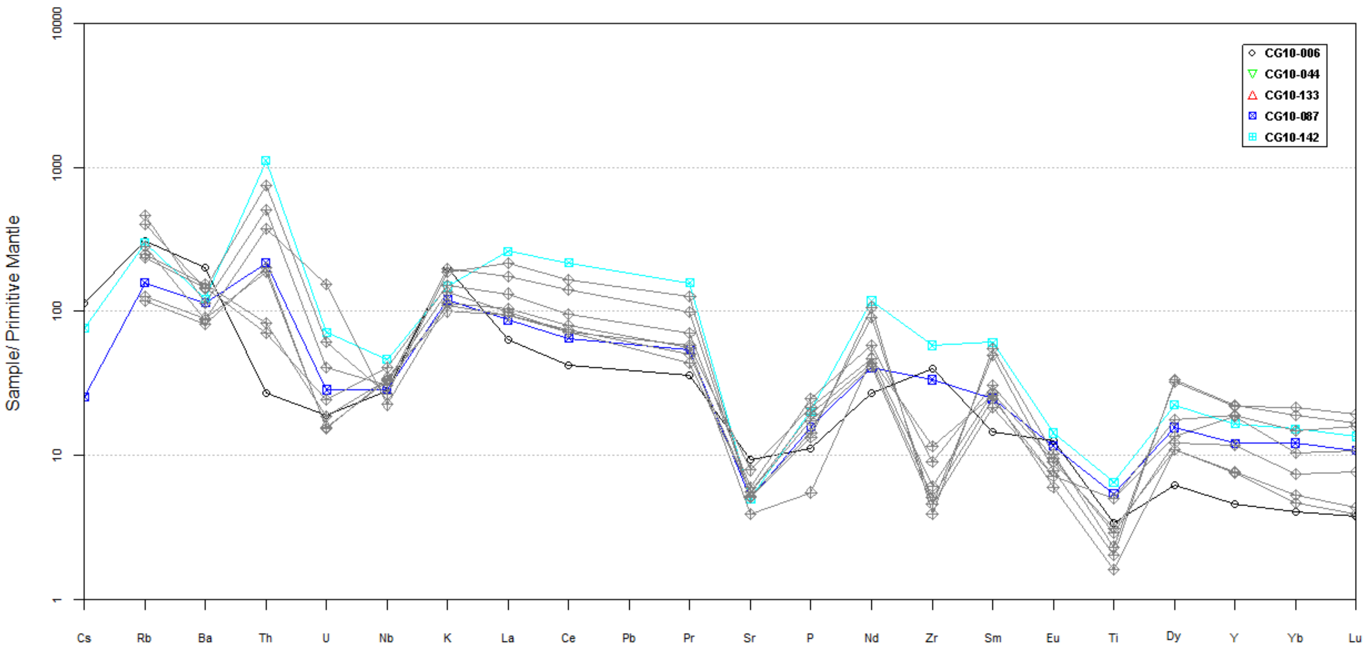

Figure 49. Primitive mantle normalised spidergram (after Sun & McDonough, 1989) for the megacrystic granitoids CG10-087 (navy) and CG10-142 (aqua); the orthogneiss, CG10-006 (black); plotted alongside seven representative megacrystic granites (grey) from the Paderu area (Narayana et al., 1999).

Table 1. CG10-006 U-Pb zircon age data.

Sample Name: CG10-006, megacrystic orthogneiss
GPS co-ordinates: Latitude (N) 18°20'29.86"
Longitude (E) 82°50'51.91"

Spot	Type	Pb207/U235	1σ	Pb206/U238	1σ	rho	Pb207/Pb206 Age (Ma)	1σ ± (Ma)	Pb206/U238 Age (Ma)	1σ ± (Ma)	Concordancy %
01_01	c	1.58608	0.0232	0.16212	0.00217	0.915082485	956.7	24.96	968.5	12.05	101
02_01	r	1.50474	0.02435	0.15557	0.00217	0.861978399	933.5	28.54	932.1	12.09	100
03_01	c	1.64102	0.02296	0.16722	0.00223	0.953144254	963	23.17	996.8	12.3	104
04_01	r	1.49488	0.02294	0.15645	0.00219	0.912181931	908	26.04	937	12.19	103
04_02	c	1.5752	0.02104	0.16385	0.00218	0.996093292	920.8	21.34	978.1	12.05	106
05_01	r	1.54464	0.03023	0.15706	0.0024	0.780790964	965.5	36.07	940.4	13.35	97
05_02	c	1.7726	0.02369	0.1727	0.00228	0.987843607	1053.6	21.46	1027	12.53	97
06_01	r	1.52485	0.02854	0.15775	0.00239	0.809471734	930.3	34.04	944.3	13.3	102
07_01	c	1.9067	0.02901	0.18265	0.00237	0.852831646	1087.3	27.11	1081.4	12.94	99
08_01	c	1.63592	0.02246	0.16819	0.00224	0.970063486	944.7	22.39	1002.1	12.33	106
09_01	r	1.5715	0.02779	0.16137	0.00242	0.848044039	949.4	30.61	964.4	13.44	102
09_02	c	2.12438	0.03014	0.20065	0.0027	0.948448068	1115.8	22.71	1178.8	14.49	106
10_01	r	1.6192	0.02348	0.16513	0.00222	0.927106009	960.9	24.21	985.2	12.28	103
10_02	c	1.7109	0.02592	0.17224	0.00235	0.90058244	987.6	25.55	1024.4	12.92	104
11_01	r	1.66532	0.02372	0.16947	0.00228	0.94455017	965.2	23.37	1009.2	12.56	105
12_01	c	1.7285	0.02463	0.17275	0.00232	0.942485985	1002.1	23.29	1027.3	12.75	103
13_01	c	1.74188	0.02477	0.17591	0.00238	0.951433972	981	22.93	1044.6	13.07	106
13_02	r	1.70652	0.02485	0.17406	0.00234	0.923212907	960.5	24.42	1034.4	12.85	108
14_01	r	1.72072	0.02428	0.17402	0.00233	0.948895268	977.9	23	1034.2	12.81	106
14_02	c	1.78803	0.02617	0.17647	0.00237	0.917589719	1027.2	24.61	1047.6	12.99	102
15_01	r	1.61782	0.02274	0.16905	0.00228	0.959531887	911	22.76	1006.9	12.59	111
15_02	r	1.67066	0.0241	0.17038	0.00232	0.943931334	960.9	23.41	1014.2	12.79	106
16_01	c	1.6382	0.02819	0.16552	0.00244	0.856665337	980.4	29.56	987.4	13.5	101
17_01	c	1.59851	0.02276	0.16332	0.00204	0.877271248	957.2	26.11	975.2	11.31	102
18_01	c	1.50217	0.02516	0.15588	0.00209	0.80050553	925.6	31.24	933.9	11.64	101
19_01	c	1.58258	0.02279	0.16278	0.00204	0.870262903	943.5	26.43	972.2	11.33	103
20_01	c	1.68566	0.02403	0.15853	0.00197	0.87170789	1124.4	25.69	948.6	10.94	84
20_02	c	1.69502	0.02548	0.16432	0.00207	0.838021812	1063.8	27.71	980.7	11.48	92
21_01	c	1.53419	0.02225	0.15872	0.00203	0.881888167	931.9	26.22	949.6	11.3	102
22_01	c	1.58219	0.02268	0.16081	0.00204	0.884978461	968.3	25.94	961.3	11.32	99
23_01	c	1.48142	0.02175	0.15553	0.00195	0.853963644	901.6	27.37	931.9	10.9	103
23_02	r	1.52144	0.0214	0.15625	0.00196	0.891819783	946.9	25.42	935.9	10.95	99
24_01	c	1.56845	0.02749	0.15838	0.00211	0.760112817	981.8	33.44	947.8	11.74	97
25_01	c	1.56646	0.02281	0.15892	0.00202	0.872904711	971.7	26.5	950.8	11.21	98
25_02	r	1.49907	0.01951	0.15625	0.00191	0.939243038	916.5	23.13	935.9	10.68	102
26_01	c	1.58675	0.02243	0.16046	0.00204	0.899378731	978.3	25.19	959.3	11.32	98
26_02	r	1.57126	0.02263	0.15993	0.00201	0.872628958	965.3	26.4	956.4	11.18	99
27_01	c	1.68643	0.02417	0.17002	0.0022	0.902847371	984.6	25.24	1012.2	12.11	103
28_01	c	1.68661	0.03004	0.16131	0.00228	0.793575586	1090.6	32.16	964.1	12.65	88
28_02	r	1.42987	0.01982	0.15177	0.00194	0.922165138	878.9	24.53	910.9	10.87	104
29_01	c	1.61364	0.02166	0.16697	0.00207	0.923591861	931.5	24.21	995.4	11.46	107
29_02	r	1.52382	0.02069	0.16145	0.00201	0.916919453	882.8	24.69	964.8	11.17	109
30_01	r	1.58054	0.02138	0.16414	0.00202	0.909776534	924	24.79	979.7	11.19	106
31_01	c	1.6453	0.02369	0.16823	0.00218	0.899980471	955.8	25.51	1002.3	12.01	105
32_01	c	1.63903	0.0203	0.16869	0.00208	0.995554092	942.3	21.19	1004.9	11.45	107
32_02	r	1.50888	0.01964	0.15842	0.00195	0.9456661	901.4	23.39	948	10.84	105
33_01	c	1.60326	0.02212	0.15921	0.00208	0.946916812	1015.1	22.94	952.4	11.55	94

Table 2. CG10-044 zircon U-Pb age data.

Sample Name: CG10-044, charnockite
GPS Co-Ordinates: Latitude (N) 18°15'3.81"
Longitude (E) 82°47'55.24"

Spot	Type	Pb207/U235	1σ	Pb206/U238	1σ	rho	Pb207/Pb206 Age (Ma)	1σ ± (Ma)	Pb206/U238 Age (Ma)	1σ ± (Ma)	Concordancy %
01_02	c	1.55114	0.0197	0.15819	0.00199	0.990509902	961.8	21.09	946.7	11.05	98
02_01	m	1.40501	0.02155	0.14396	0.00188	0.851428439	952.2	27.83	867	10.61	91
03_01	c	1.91549	0.02386	0.15388	0.00192	0.998323971	1432.5	19.07	922.7	10.75	64
03_02	c	1.47148	0.01923	0.14856	0.00191	0.983799406	982.3	21.21	892.9	10.74	91
04_01	c	1.52145	0.02052	0.15557	0.00201	0.957966967	956.2	22.51	932.1	11.21	97
05_01	c	1.55445	0.02059	0.15682	0.00202	0.972456829	983.7	21.66	939.1	11.27	95
05_02	r	1.50854	0.02398	0.15228	0.00205	0.846873697	982.3	28.46	913.8	11.45	93
06_01	c	1.49281	0.02169	0.15268	0.00201	0.90606403	955.5	25	916	11.26	96
06_02	r	1.51457	0.02229	0.15571	0.00207	0.903302313	944.8	25.39	932.9	11.53	99
07_01	c	1.59243	0.02089	0.15189	0.00199	0.998724733	1096.7	20.28	911.6	11.14	83
07_02	r	1.53205	0.02405	0.15488	0.00209	0.859624539	979.4	27.78	928.2	11.67	95
08_01	c	1.4181	0.01919	0.14826	0.00197	0.981915493	910.5	21.6	891.2	11.08	98
08_02	r	1.55279	0.02376	0.15724	0.00211	0.876971964	975.9	26.67	941.4	11.78	96
09_01	m	1.33723	0.02043	0.14042	0.0019	0.885650509	901.4	26.72	847.1	10.72	94
09_02	r	1.40472	0.02076	0.14601	0.00194	0.899045239	922.3	25.63	878.5	10.93	95
10_01	m	1.56468	0.02568	0.15625	0.00211	0.822797458	1004.1	29.89	935.9	11.76	93
10_02	r	1.53553	0.02302	0.15556	0.00209	0.896192568	974.9	25.84	932	11.63	96
11_01	r	1.54507	0.02259	0.15666	0.00208	0.908107248	973	25.04	938.2	11.59	96
12_01	c	1.55475	0.0204	0.16046	0.00208	0.987931755	936.8	21.23	959.3	11.56	102
12_02	r	1.54597	0.02795	0.1445	0.00207	0.792358549	1136.8	32.26	870.1	11.64	77
13_01	c	1.7541	0.02287	0.16935	0.0022	0.996381519	1072.2	20.39	1008.5	12.14	94
13_02	c	1.65091	0.02171	0.16241	0.00213	0.997310547	1034.1	20.08	970.1	11.81	94
13_03	r	1.53843	0.01996	0.1468	0.00185	0.971321219	1096	21.33	883	10.39	81
14_01	c	1.62493	0.02143	0.16272	0.00213	0.992547166	997.9	20.73	971.9	11.82	97
14_02	r	1.60766	0.02426	0.15845	0.00213	0.890821663	1030.2	25.52	948.1	11.85	92
15_01	c	1.63507	0.02156	0.15791	0.00208	0.998944351	1071.2	20.33	945.2	11.57	88
15_02	r	2.18641	0.03535	0.18503	0.00262	0.875792717	1331.8	26.54	1094.4	14.25	82
16_01	c	1.5441	0.02133	0.15957	0.0021	0.952692217	933.9	22.98	954.4	11.65	102
16_02	r	1.50953	0.02577	0.15221	0.00212	0.815868198	984	30.89	913.3	11.85	93
17_02	c	1.56304	0.02124	0.16057	0.00213	0.976181956	945.9	21.83	959.9	11.85	101
17_03	r	1.47823	0.02454	0.15039	0.00206	0.825117341	965.8	30.06	903.2	11.54	94
18_01	c	1.51516	0.02063	0.15575	0.00209	0.985547361	944.7	21.66	933.1	11.63	99
19_01	c	1.43208	0.01981	0.15164	0.00205	0.977288727	883.5	22.23	910.2	11.5	103
19_02	r	1.50773	0.02693	0.145	0.0021	0.810846255	1079.6	32	872.8	11.82	81
20_01	m	1.5648	0.02164	0.15918	0.002	0.908537958	967.2	24.28	952.2	11.15	98
21_01	c	1.56361	0.02005	0.15655	0.00195	0.971394414	999.5	21.39	937.6	10.9	94
21_02	r	1.51568	0.02381	0.15357	0.00198	0.820742515	975.4	28.8	920.9	11.08	94
22_01	c	1.6711	0.02195	0.16286	0.00206	0.962987621	1053.6	22.04	972.6	11.42	92
23_01	c	1.42052	0.01939	0.14903	0.00195	0.958584613	903.7	22.51	895.5	10.92	99
24_01	c	1.53094	0.02125	0.15671	0.00205	0.942445807	954.1	22.94	938.5	11.44	98
25_01	c	1.66603	0.02492	0.16676	0.00215	0.861948569	999.9	26.81	994.2	11.89	99
25_02	r	1.58557	0.02215	0.16214	0.00213	0.940375107	955.6	23.37	968.7	11.8	101
26_01	r	1.43545	0.02594	0.15241	0.00202	0.733425498	878.4	34.89	914.5	11.33	104
27_01	c	1.57678	0.02057	0.15969	0.002	0.960039464	975.3	21.99	955.1	11.13	98
28_01	c	1.4924	0.02073	0.15859	0.00207	0.939681084	877.2	23.78	948.9	11.49	108
29_01	m	1.59663	0.0237	0.16157	0.00212	0.883956869	976.8	25.8	965.5	11.76	99
30_01	m	1.60354	0.02907	0.15831	0.00214	0.745658874	1026.8	33.99	947.4	11.91	92

Table 3. CG10-087 zircon U-Pb age data.

Sample Name: CG10-087, megacrystic granitoid
GPS Co-Ordinates: Latitude (N) 18° 3'44.99"
Longitude (E) 82°35'6.04"

Spot	Type	Pb207/U235	1σ	Pb206/U238	1σ	rho	Pb207/Pb206 Age (Ma)	1σ ± (Ma)	Pb206/U238 Age (Ma)	1σ ± (Ma)	Concordancy %
01_01	c	1.37683	0.01847	0.147	0.00197	0.998992704	866.5	21.39	884.1	11.07	102
02_01	c	1.54404	0.02115	0.15846	0.00213	0.981314299	948.1	21.93	948.2	11.85	100
03_01	m	1.44032	0.02069	0.15004	0.00204	0.946502167	917.5	23.68	901.2	11.46	98
03_02	r	1.7101	0.0281	0.15214	0.00226	0.904024529	1234.9	26.11	913	12.63	74
04_01	c	1.68385	0.02293	0.16955	0.0023	0.996160664	987.3	20.77	1009.7	12.7	102
05_01	c	1.68203	0.02261	0.17469	0.00236	0.99499951	923.9	20.95	1037.9	12.93	112
06_01	m	1.4299	0.02132	0.14923	0.00207	0.930320674	914	24.73	896.6	11.6	98
07_01	c	1.63353	0.02262	0.16632	0.0023	0.998660503	964.7	21.09	991.8	12.69	103
08_01	m	1.54946	0.02273	0.16028	0.00224	0.952685638	932.1	23.48	958.4	12.43	103
09_01	m	1.54698	0.02219	0.1606	0.00224	0.972366245	924.8	22.4	960.1	12.45	104
10_01	c	1.5883	0.0221	0.16539	0.0023	0.999444888	918.2	20.95	986.6	12.73	107
10_02	r	1.51742	0.02326	0.15594	0.00221	0.924550925	945.2	24.96	934.2	12.3	99
11_01	c	1.68801	0.02523	0.16599	0.00243	0.979449645	1035.1	21.7	990	13.46	96
12_01	c	1.57413	0.02459	0.15919	0.00238	0.957068982	978.5	23.69	952.3	13.22	97
12_02	r	1.60072	0.02388	0.16011	0.00226	0.946174045	1000.4	23.47	957.4	12.56	96
13_01	c	1.64247	0.02319	0.16339	0.00229	0.992674137	1011.4	20.97	975.6	12.68	96
13_02	r	1.53101	0.02573	0.14034	0.00216	0.915820836	1179.5	26.22	846.6	12.19	72
14_01	c	1.638	0.02329	0.16484	0.00231	0.985584314	987.8	21.45	983.6	12.79	100
14_02	r	1.62623	0.02497	0.15673	0.00223	0.926650908	1075.3	24.43	938.6	12.4	87
15_01	c	1.58908	0.02287	0.15611	0.00218	0.970298516	1036.9	21.64	935.1	12.16	90
15_02	r	1.93649	0.03836	0.16239	0.0026	0.80825933	1351.5	33.41	970.1	14.39	72
16_01	c	1.65751	0.02351	0.16312	0.0023	0.994086444	1033.3	20.49	974.1	12.74	94
16_02	r	1.60971	0.02711	0.16097	0.00241	0.888976382	1000.8	27.57	962.2	13.38	96
17_01	c	1.41262	0.02127	0.14683	0.00221	0.999620918	925.4	21.75	883.2	12.43	95
17_02	m	1.39594	0.0206	0.14804	0.00217	0.993299436	880.3	21.68	890	12.18	101
18_01	c	1.59475	0.02252	0.15986	0.00224	0.992275879	996	21.15	956	12.44	96
18_02	r	1.59063	0.02558	0.15973	0.00226	0.879813409	992.3	27.32	955.3	12.56	96
19_01	m	1.59949	0.02266	0.13701	0.00194	0.999473048	1308.2	20.11	827.7	11	63
20_01	c	1.52485	0.02179	0.15492	0.00219	0.989251051	968.7	21.53	928.5	12.2	96
20_02	r	1.50652	0.02311	0.15368	0.0022	0.933211936	960.4	24.61	921.6	12.27	96
21_01	c	1.41189	0.02198	0.14477	0.0022	0.976151623	952.1	23.23	871.6	12.39	92
21_02	m	1.57452	0.02825	0.14743	0.00229	0.865723778	1134.1	29.31	886.5	12.84	78
22_02	c	1.17046	0.02089	0.11841	0.00185	0.875389804	982.5	29.47	721.4	10.66	73
23_01	c	1.71297	0.02523	0.17124	0.0025	0.9912137	1001.6	21.42	1018.9	13.74	102
23_02	r	1.61695	0.02603	0.16269	0.00233	0.88964652	988	27.15	971.7	12.92	98
24_01	c	1.58299	0.02077	0.16165	0.00206	0.971254818	958.4	21.61	965.9	11.45	101
25_01	c	1.59651	0.02087	0.16281	0.00207	0.972609401	961.1	21.6	972.4	11.48	101
25_02	r	1.53037	0.021	0.156	0.002	0.934291819	962	23.36	934.5	11.15	97
26_01	c	1.65256	0.02157	0.16528	0.00211	0.978068433	1000.8	21.31	986.1	11.65	99
26_02	r	1.70321	0.02386	0.16195	0.0021	0.925627186	1102.6	23.39	967.6	11.65	88
27_01	c	1.51494	0.01956	0.14549	0.00186	0.990162291	1082.7	20.53	875.6	10.46	81
27_02	m	1.58245	0.02153	0.15565	0.002	0.944423614	1034.7	22.42	932.5	11.14	90
28_01	m	1.46054	0.0212	0.15272	0.00198	0.893196206	909.8	25.47	916.2	11.08	101
29_01	c	1.4704	0.01952	0.153	0.00197	0.969907854	919.9	21.91	917.8	11.01	100
29_02	r	1.50429	0.02036	0.15271	0.00196	0.94829266	970.4	22.63	916.2	10.97	94
30_01	c	1.15405	0.01726	0.12655	0.00172	0.908761943	810.8	25.96	768.2	9.82	95
31_01	r	1.55795	0.02177	0.15878	0.00205	0.923959957	962.4	23.83	950	11.4	99
32_01	m	1.52059	0.02174	0.1577	0.00204	0.904796818	926.6	24.93	944	11.36	102
32_02	m	1.58053	0.02556	0.15925	0.00205	0.79600595	986	30.35	952.6	11.39	97
33_01	m	1.60747	0.02118	0.16561	0.00211	0.966969596	940.3	21.9	987.9	11.69	105
34_01	m	1.54482	0.02219	0.15876	0.00205	0.898945478	945.3	25.16	949.9	11.38	100
35_01	c	1.52329	0.01983	0.15665	0.00199	0.975848849	944	21.5	938.1	11.1	99
36_01	c	1.64852	0.02125	0.1657	0.0021	0.98317782	990.7	21.01	988.4	11.64	100
37_01	c	2.43093	0.03088	0.202	0.00256	0.997662751	1367	19.45	1186.1	13.72	87
38_01	c	1.63218	0.02079	0.16411	0.00208	0.995043007	990	20.64	979.6	11.5	99
38_02	r	1.50219	0.02204	0.15273	0.00197	0.87913415	967.3	25.91	916.3	11.04	95

Table 4. CG10-133 zircon age data.

Sample Name: CG10-133, charnockite
GPS Co-Ordinates: Latitude (N) 18° 4'16.85"
Longitude (E) 82°41'23.65"

Spot	Type	Pb207/U235	1σ	Pb206/U238	1σ	rho	Pb207/Pb206 Age (Ma)	1σ ± (Ma)	Pb206/U238 Age (Ma)	1σ ± (Ma)	Concordancy %
01_01	r	1.41222	0.01998	0.14782	0.00187	0.894160092	908.6	25.72	888.7	10.49	98
01_02	c	1.59364	0.02027	0.15357	0.00191	0.977830223	1076.5	21.4	921	10.69	86
02_01	c	9.28881	0.11422	0.21603	0.00272	0.976623652	3530.7	15.4	1260.9	14.43	36
03_01	c	1.41316	0.01821	0.14444	0.00182	0.977834371	956.9	21.9	869.7	10.24	91
04_01	c	1.53799	0.01935	0.15691	0.00195	0.987771591	960.8	21.3	939.6	10.89	98
04_02	r	1.34282	0.01917	0.13802	0.00176	0.893236236	945.4	25.67	833.4	9.98	88
05_01	c	1.3702	0.01878	0.14291	0.00186	0.949595614	914.7	23.38	861.1	10.51	94
05_02	r	1.26798	0.02122	0.13203	0.00174	0.787487464	918.4	31.71	799.5	9.91	87
06_01	c	1.64116	0.02337	0.16484	0.00211	0.898901407	992	25.32	983.6	11.67	99
06_02	r	1.4936	0.02484	0.15161	0.00201	0.797169957	970.3	31.16	910	11.25	94
07_01	c	1.5584	0.02013	0.15535	0.002	0.996675775	1007.3	20.92	930.9	11.17	92
08_01	c	3.32452	0.04771	0.24758	0.00326	0.91753275	1574.8	23.18	1426	16.82	91
08_02	r	1.42188	0.02105	0.14636	0.00192	0.886114153	941.9	26.3	880.5	10.8	93
09_01	c	1.55435	0.02087	0.15581	0.00201	0.960786956	996.1	22.55	933.4	11.2	94
09_02	r	1.42872	0.0226	0.14766	0.00196	0.839135109	933.6	28.9	887.9	11.01	95
10_01	c	1.57692	0.02238	0.1574	0.00213	0.953508249	1005.3	23.28	942.3	11.89	94
11_01	c	2.0732	0.02766	0.1808	0.00229	0.949349401	1273.3	21.89	1071.3	12.53	84
11_02	r	1.45236	0.02269	0.14648	0.00195	0.852110788	983.7	28.13	881.2	10.95	90
12_01	m	1.47546	0.02249	0.14894	0.00197	0.867746482	982.1	27.14	895	11.08	91
13_01	c	1.55276	0.02068	0.15912	0.00206	0.972067114	951.3	22.11	951.9	11.47	100
13_02	r	1.47693	0.0224	0.14824	0.00196	0.871771283	993.7	26.92	891.1	10.99	90
14_01	c	1.32314	0.01774	0.13833	0.00183	0.986704017	909.9	21.58	835.2	10.38	92
14_02	r	9.09718	0.11756	0.19711	0.00259	0.983471283	3638.9	15.47	1159.8	13.94	32
15_01	c	1.3998	0.01814	0.09993	0.0013	0.996147911	1653.5	18.7	614	7.63	37
15_02	r	1.44263	0.02166	0.14815	0.00199	0.894639208	946.6	26.08	890.6	11.16	94
15_03	c	1.5829	0.02129	0.14215	0.00186	0.972845553	1215.7	21.23	856.8	10.51	70
16_01	c	1.74446	0.02456	0.152	0.00204	0.953277259	1274.7	22.32	912.1	11.41	72
16_02	r	1.45871	0.0275	0.15041	0.00217	0.765278107	938.4	35	903.3	12.13	96
17_01	c	1.52528	0.01992	0.15464	0.00201	0.995255206	972.9	20.84	926.9	11.25	95
17_02	r	1.45763	0.02321	0.14757	0.00201	0.855401757	975.8	28.14	887.3	11.31	91
18_01	c	1.58544	0.02152	0.16118	0.00215	0.982731445	967.4	21.67	963.3	11.93	100
18_02	r	1.50151	0.02328	0.1522	0.00208	0.881442396	973.4	26.85	913.3	11.64	94
19_01	c	1.48934	0.01841	0.15297	0.00181	0.957221343	946.5	22.23	917.6	10.09	97
19_02	r	1.52919	0.02731	0.15347	0.0019	0.693218042	993.5	35.09	920.4	10.63	93
20_01	c	1.59279	0.01892	0.13784	0.00158	0.964981996	1288.1	20.67	832.4	8.98	65
20_02	c	1.89695	0.02341	0.13191	0.00158	0.970585585	1702.2	19.81	798.7	8.99	47
21_01	c	1.47699	0.0194	0.14966	0.00183	0.930938891	974.2	23.27	899	10.27	92
22_01	c	1.53696	0.02209	0.15483	0.00192	0.862805617	986.1	26.35	928	10.7	94
22_02	r	1.45635	0.02433	0.15086	0.00187	0.741978215	929.2	32.37	905.8	10.48	97
23_01	m	1.52832	0.02496	0.15628	0.00193	0.756177276	955.6	31.77	936.1	10.78	98
24_01	c	1.57549	0.01929	0.16156	0.00196	0.990844836	949.7	20.93	965.4	10.89	102
25_01	c	1.6825	0.02249	0.15676	0.00197	0.940148784	1143.2	22.71	938.8	10.98	82
26_01	c	1.47939	0.01863	0.15316	0.00181	0.938432502	930.4	22.93	918.6	10.14	99
27_01	c	1.62684	0.02001	0.16328	0.00193	0.960997086	993.7	21.97	975	10.7	98

Table 5. CG10-142 zircon U-Pb age data.

Sample Name: CG10-142, megacrystic granitoid
GPS Co-Ordinates: Latitude (N) 17°51'51.80"
Longitude (E) 82°50'39.13"

Spot	Type	Pb207/U235	1σ	Pb206/U238	1σ	rho	Pb207/Pb206 Age (Ma)	1σ ± (Ma)	Pb206/U238 Age (Ma)	1σ ± (Ma)	Concordancy %
01_01	c	0.76644	0.01406	0.09209	0.00127	0.75176844	617.3	36.41	567.9	7.5	92
01_02	r	1.09368	0.01741	0.12018	0.00162	0.846787257	807	29.33	731.6	9.33	91
02_01	c	1.82701	0.02764	0.16115	0.00202	0.828559966	1252.2	27.36	963.1	11.21	77
02_02	r	1.45442	0.02126	0.14566	0.00192	0.901752803	998.3	25.43	876.6	10.82	88
03_01	c	1.31052	0.01698	0.13102	0.00165	0.971968782	1001.7	21.87	793.7	9.38	79
04_01	c	1.38468	0.02281	0.13938	0.00181	0.788319462	987.8	31.18	841.2	10.22	85
05_01	c	1.39419	0.02221	0.14083	0.00182	0.81124048	980.7	29.64	849.4	10.28	87
06_01	c	1.73617	0.02888	0.15604	0.00206	0.793645097	1214.4	30.02	934.7	11.51	77
07_01	c	1.36007	0.02975	0.13264	0.00185	0.637634058	1052.2	43.19	802.9	10.53	76
08_01	c	1.5477	0.02903	0.15727	0.00218	0.739010065	968.7	35.86	941.6	12.14	97
08_02	r	1.54505	0.02749	0.15324	0.00212	0.777555712	1018.2	32.91	919.1	11.85	90
09_01	c	1.08044	0.02148	0.11702	0.00162	0.696339928	836.8	39.39	713.4	9.33	85
10_01	c	1.0893	0.01974	0.11563	0.00156	0.744482388	878.6	34.74	705.4	9.04	80
10_02	r	1.20621	0.01771	0.12813	0.00166	0.882392129	877.3	26.45	777.2	9.48	89
11_01	c	1.04909	0.01995	0.11589	0.00159	0.721474538	795.6	37.17	706.9	9.2	89
12_01	c	1.39538	0.02047	0.14268	0.00186	0.888637211	955.6	26.01	859.8	10.47	90
13_01	c	0.87963	0.01538	0.10057	0.00134	0.762043996	723.2	34.11	617.7	7.85	85
13_02	r	0.80852	0.01267	0.08747	0.00113	0.824391432	839.5	29.45	540.6	6.72	64
14_01	c	1.61761	0.02477	0.16432	0.00216	0.858442363	969	27.55	980.7	11.94	101
15_01	c	1.53861	0.02634	0.15051	0.00209	0.811136063	1045.8	31.02	903.8	11.7	86
16_01	c	1.41874	0.02444	0.13977	0.00187	0.776656986	1031.3	32.14	843.4	10.58	82
17_01	c	1.03228	0.01504	0.11209	0.00145	0.887872919	831.7	26.43	684.8	8.4	82
17_02	r	0.97253	0.01379	0.10558	0.00137	0.915119164	831.9	25.12	647.1	7.97	78
18_01	c	1.02156	0.01779	0.11145	0.00149	0.767704572	821.7	33.47	681.2	8.63	83
19_01	c	1.34977	0.01924	0.13833	0.00179	0.907802465	951	24.93	835.2	10.15	88
19_02	r	1.34893	0.01906	0.13754	0.00178	0.915919909	961.3	24.49	830.8	10.11	86
20_01	c	1.61025	0.02553	0.14214	0.00191	0.847538722	1249.6	27.39	856.7	10.76	69
21_01	c	0.84745	0.01233	0.09727	0.00126	0.89031284	714.8	26.53	598.4	7.42	84
22_01	c	1.41089	0.02045	0.14459	0.00189	0.901827324	950.9	25.31	870.6	10.67	92
22_02	r	1.00224	0.01502	0.11084	0.00145	0.872917669	793.2	27.22	677.6	8.44	85
23_02	c	1.21723	0.01742	0.13053	0.0017	0.910045445	857.6	25.27	790.9	9.68	92
24_01	c	1.61082	0.0242	0.16243	0.00214	0.876958771	984	26.52	970.3	11.88	99
25_01	c	1.49582	0.02092	0.15275	0.00198	0.926833295	958.2	24.05	916.4	11.08	96
26_01	c	1.4763	0.03804	0.12876	0.00197	0.593771529	1273.1	49.45	780.8	11.23	61
27_01	c	1.53518	0.02965	0.15491	0.00213	0.711925839	983	37.14	928.4	11.89	94
28_01	c	1.29055	0.02656	0.14021	0.00195	0.675775413	830.3	40.4	845.9	11.05	102
29_01	c	1.59901	0.02808	0.16222	0.00221	0.775786027	971.9	32.68	969.1	12.28	100
30_01	r	1.46798	0.02537	0.15304	0.00215	0.812892608	915.7	31.48	918	12.02	100
30_02	c	1.43314	0.02273	0.15017	0.00209	0.87751043	905.1	27.67	901.9	11.72	100
32_01	c	1.3125	0.02219	0.14051	0.00191	0.804022391	862	31.89	847.5	10.78	98
33_01	c	1.36746	0.02353	0.13749	0.00188	0.794656503	990.8	31.86	830.5	10.64	84
34_01	c	1.44192	0.03212	0.11797	0.00177	0.673546085	1397.5	41.33	718.9	10.19	51
34_02	r	0.66798	0.01268	0.08371	0.00115	0.723710218	525.3	38.72	518.2	6.83	99
35_01	c	1.51629	0.03928	0.15404	0.00234	0.586398889	969.2	51.62	923.6	13.08	95
36_01	c	1.30749	0.02391	0.14076	0.00193	0.749785178	849.3	35.18	848.9	10.91	100
37_01	c	1.57835	0.02783	0.1619	0.00224	0.784677641	949.3	32.59	967.3	12.44	102
38_01	m	1.01891	0.03384	0.11701	0.00195	0.501784339	713.7	69.36	713.3	11.24	100
39_01	c	1.52523	0.03779	0.15693	0.00235	0.604394265	942.8	48.58	939.7	13.09	100
40_01	c	1.57982	0.02346	0.16363	0.00224	0.921859398	929.2	25.04	976.9	12.41	105
41_01	c	1.56494	0.03108	0.15988	0.00232	0.730651914	957.3	37.31	956.1	12.88	100
42_01	m	1.26808	0.02494	0.13642	0.00196	0.730513473	850.6	37.7	824.4	11.1	97
43_01	c	2.43822	0.04118	0.17858	0.00255	0.845461642	1605.8	27.86	1059.2	13.95	66
43_02	r	0.98286	0.01595	0.1139	0.00157	0.849389527	694.1	30.03	695.4	9.07	100
44_01	c	1.56697	0.0245	0.16009	0.00222	0.886917792	957.2	26.83	957.3	12.35	100

45_01	c	1.07137	0.02129	0.1163	0.00168	0.72693133	831.9	38.14	709.3	9.68	85
46_01	c	1.45527	0.02209	0.15051	0.00208	0.910428491	932.2	25.75	903.8	11.68	97
47_01	c	1.27024	0.02058	0.13428	0.00187	0.859549096	886.9	28.71	812.2	10.65	92
48_01	c	1.5941	0.03064	0.16186	0.00233	0.748933377	969.7	35.95	967.1	12.94	100
49_01	c	1.46522	0.04847	0.15366	0.00268	0.527234455	903.8	66.54	921.4	14.98	102
50_01	m	1.46747	0.02435	0.15323	0.00213	0.837733857	912.5	29.97	919.1	11.92	101
51_01	c	1.24965	0.0251	0.13427	0.00196	0.726761235	853.6	38.65	812.2	11.12	95
52_01	c	1.11085	0.03398	0.12097	0.00197	0.532378601	825.6	62.1	736.2	11.33	89
53_01	c	1.48975	0.02642	0.15312	0.0022	0.810161015	945	32.09	918.4	12.29	97
54_01	c	1.6036	0.02345	0.14731	0.00205	0.951644697	1171.1	23.16	885.9	11.53	76
54_02	r	1.48881	0.02503	0.15467	0.00221	0.849893711	923.2	29.59	927.1	12.36	100
55_01	r	0.74092	0.01236	0.09255	0.00132	0.854968975	532	31.48	570.6	7.78	107
55_02	r	0.94537	0.01721	0.10946	0.00162	0.812981226	696.3	33.68	669.6	9.42	96
56_01	r	1.48181	0.02477	0.15471	0.00229	0.885489898	913.4	28.41	927.3	12.81	102
57_01	c	1.42588	0.02626	0.14995	0.00225	0.814749877	898.9	33.06	900.7	12.64	100
58_01	c	1.55157	0.03077	0.16129	0.00239	0.747195653	922	36.95	963.9	13.24	105
58_02	r	1.55374	0.02668	0.15946	0.00236	0.861891831	948.8	29.6	953.8	13.13	101
59_01	c	1.49608	0.0233	0.15088	0.0021	0.893689212	983.8	26.7	905.9	11.75	92
59_02	r	1.423	0.02273	0.14955	0.00212	0.887472507	899.5	27.39	898.5	11.91	100
60_01	c	0.91424	0.01486	0.10278	0.00142	0.850004334	758.9	29.57	630.7	8.33	83
60_02	r	0.98512	0.01881	0.11189	0.00161	0.753589681	737.1	36.48	683.7	9.34	93
61_01	c	0.74362	0.01353	0.09094	0.0013	0.785672709	578.7	35.05	561.1	7.66	97
62_01	r	1.32791	0.0254	0.14107	0.00214	0.793074584	877.1	35.03	850.7	12.07	97
63_01	c	1.3451	0.02198	0.14272	0.00199	0.85328699	879.6	29.14	860	11.2	98
64_01	r	1.30282	0.0213	0.14028	0.00195	0.85024418	849.2	29.39	846.2	11.02	100
65_01	c	1.45191	0.02876	0.15129	0.00219	0.730776725	917	37.53	908.2	12.24	99
66_01	c	1.50029	0.02952	0.15347	0.00223	0.738482539	954.8	36.91	920.4	12.45	96

Table 6. CG10-087 monazite U-Pb age data.

Sample Name: CG10-087, megacrystic granitoid
GPS Co-Ordinates: Latitude (N) 18° 3'44.99"
Longitude (E) 82°35'6.04"

Spot	Pb207/U235	1σ	Pb206/U238	1σ	rho	Pb207/Pb206 Age (Ma)	1σ ± (Ma)	Pb206/U238 Age (Ma)	1σ ± (Ma)	Pb207/U235 Age (Ma)	1σ ± (Ma)	Concordancy %
01_01	1.62691	0.02745	0.16806	0.00256	0.902810884	935.7	27.38	1001.4	14.14	980.7	10.61	98
01_02	1.5681	0.02397	0.16092	0.00235	0.955352312	948.1	23.37	961.9	13.06	957.7	9.48	100
01_03	1.71009	0.02709	0.16673	0.00247	0.935175597	1052.9	24.05	994.1	13.63	1012.3	10.15	102
01_04	1.61148	0.02552	0.16406	0.00242	0.931444341	965.8	24.54	979.3	13.4	974.7	9.92	100
02_01	1.57798	0.02589	0.16149	0.00243	0.917128275	954	25.98	965.1	13.47	961.6	10.2	100
02_02	1.63339	0.02751	0.1648	0.00249	0.897101209	982.7	26.93	983.4	13.81	983.2	10.61	100
03_01	1.60225	0.02433	0.16301	0.00236	0.953423664	965.6	23.13	973.5	13.11	971.1	9.49	100
03_02	1.5153	0.03154	0.15766	0.00243	0.740494242	919.8	38.52	943.7	13.51	936.6	12.73	99
04_01	1.57457	0.02496	0.16133	0.00236	0.922814183	951.2	25.06	964.2	13.12	960.2	9.84	100
04_02	1.54429	0.02303	0.15733	0.00226	0.963234031	963.1	22.9	941.9	12.61	948.2	9.19	101
05_01	1.56797	0.02494	0.16012	0.00237	0.930559323	958	24.96	957.4	13.16	957.6	9.86	100
06_01	1.55542	0.0227	0.16115	0.00225	0.956696158	929	23.34	963.1	12.51	952.6	9.02	99
07_01	1.49832	0.02402	0.15404	0.00229	0.927328369	944.4	25.23	923.5	12.78	929.7	9.76	101
08_01	1.56198	0.02638	0.15865	0.00237	0.884522627	969.2	27.68	949.3	13.19	955.3	10.45	101
08_02	1.59803	0.02642	0.16059	0.00238	0.896418011	990.4	26.73	960	13.21	969.4	10.33	101
09_01	1.4883	0.02187	0.15309	0.00223	0.991287749	943.2	21.38	918.3	12.44	925.6	8.92	101
10_01	1.50979	0.02439	0.15446	0.00229	0.917749583	954.9	25.48	925.9	12.77	934.4	9.87	101
11_01	1.13695	0.02097	0.12464	0.00189	0.822142879	811.9	32.44	757.2	10.83	771.1	9.96	102
11_02	1.04633	0.01917	0.1131	0.00171	0.825239619	841.5	31.98	690.7	9.92	727.1	9.51	105
12_01	1.34111	0.02265	0.14211	0.00212	0.883298343	882.9	27.86	856.6	11.98	863.7	9.82	101
13_01	1.462	0.02445	0.15317	0.00228	0.890081232	906.2	27.37	918.7	12.75	914.8	10.08	100
13_02	1.48602	0.02334	0.15178	0.00224	0.939630862	958.4	24.09	910.9	12.54	924.7	9.53	102

Table 7. LA-MC-ICPMS results for Lu/Hf isotope analyses.

Sample no.	Analysis no.	Interf. corr.	Total Hf beam (V)	$^{176}Hf/^{177}Hf$	2 se	exp. factor[1]	2 se	$^{178}Hf/^{177}Hf$	2 se	$^{176}Yb/^{177}Hf$	$^{176}Lu/^{177}Hf$	Age (Ma)	$^{176}Hf/^{177}Hf$ Initial	2 se	**$e_{Hf}(t)$**	T_{DM} (Ga)	T_{DM} crustal	$^{176}Hf/^{177}Hf$ using Hf corr.	2 se
CG10-006	01_01	Yb	5.13349	0.28203	0.00004	0.83991	0.00452	1.46731	0.00006	0.03866	0.00065	956.7	0.28202	0.00004	-5.37909	1.70	2.17	0.28206	0.00002
CG10-006	03_01	Yb	2.74958	0.28203	0.00005	1.03380	0.00522	1.46733	0.00007	0.04481	0.00085	963	0.28202	0.00005	-5.46812	1.71	2.18	0.28203	0.00003
CG10-006	05_01	Yb	6.61378	0.28198	0.00003	0.92315	0.00407	1.46736	0.00007	0.04234	0.00090	965.5	0.28197	0.00003	-7.20443	1.78	2.30	0.28202	0.00002
CG10-006	05_02	Yb	6.75036	0.28203	0.00003	0.96593	0.00338	1.46731	0.00005	0.06161	0.00107	1053.6	0.28201	0.00003	-3.54949	1.72	2.13	0.28209	0.00002
CG10-006	06_01	Yb	6.47159	0.28202	0.00002	0.93388	0.00337	1.46731	0.00006	0.02863	0.00057	930.3	0.28201	0.00002	-6.47314	1.72	2.22	0.28203	0.00002
CG10-006	07_01	Yb	6.20621	0.28205	0.00003	0.92989	0.00344	1.46727	0.00006	0.05851	0.00098	1087.3	0.28203	0.00003	-2.09903	1.69	2.07	0.28211	0.00002
CG10-006	09_01	Yb	6.61612	0.28199	0.00003	0.93066	0.00362	1.46724	0.00006	0.03263	0.00057	949.4	0.28198	0.00003	-6.94522	1.75	2.27	0.28203	0.00002
CG10-006	16_01	Yb	6.78362	0.28201	0.00003	0.95384	0.00338	1.46726	0.00005	0.06572	0.00107	980.4	0.28199	0.00003	-6.09309	1.76	2.24	0.28211	0.00002
CG10-006	16_02	Yb	8.17350	0.28200	0.00002	0.94074	0.00302	1.46730	0.00005	0.02779	0.00053	980.4	0.28199	0.00002	-6.05959	1.74	2.24	0.28202	0.00001
CG10-006	17_01	Yb	7.96877	0.28203	0.00003	0.81030	0.00313	1.46727	0.00005	0.07697	0.00130	957.2	0.28201	0.00003	-5.91529	1.73	2.21	0.28213	0.00002
CG10-006	18_01	Yb	7.26005	0.28203	0.00002	0.94524	0.00350	1.46724	0.00005	0.03786	0.00062	925.6	0.28201	0.00002	-6.35734	1.71	2.21	0.28205	0.00002
CG10-006	21_01	Yb	6.80972	0.28205	0.00002	0.93794	0.00331	1.46723	0.00005	0.05441	0.00090	931.9	0.28204	0.00003	-5.37631	1.68	2.15	0.28210	0.00002
CG10-006	22_01	Yb	6.73955	0.28206	0.00003	0.94604	0.00347	1.46728	0.00005	0.04812	0.00080	968.3	0.28205	0.00003	-4.1654	1.67	2.11	0.28208	0.00002
CG10-006	25_01	Yb	8.14464	0.28201	0.00002	0.81819	0.00323	1.46724	0.00005	0.07428	0.00122	971.7	0.28198	0.00002	-6.43704	1.77	2.25	0.28210	0.00002
CG10-006	25_02	Yb	8.26255	0.28200	0.00003	0.81378	0.00334	1.46725	0.00005	0.02400	0.00048	916.5	0.28199	0.00002	-7.32345	1.74	2.27	0.28201	0.00002
CG10-006	26_01	Yb	8.86673	0.28212	0.00002	0.87579	0.00306	1.46725	0.00005	0.07266	0.00120	978.3	0.28210	0.00002	-2.11466	1.60	1.98	0.28219	0.00001
CG10-006	26_02	Yb	9.33984	0.28205	0.00002	0.84166	0.00279	1.46722	0.00004	0.02849	0.00053	965.3	0.28204	0.00002	-4.422	1.67	2.12	0.28207	0.00001
CG10-044	08_02	Yb	8.90918	0.28200	0.00002	1.06029	0.00320	1.46730	0.00006	0.00491	0.00007	975.9	0.28200	0.00002	-5.91256	1.73	2.22	0.28201	0.00002
CG10-044	18_01	Yb	3.61831	0.28199	0.00005	0.94601	0.00562	1.46717	0.00007	0.02934	0.00052	944.7	0.28198	0.00005	-7.08588	1.75	2.27	0.28201	0.00003
CG10-044	20_01	Yb	3.89162	0.28194	0.00002	0.90675	0.00484	1.46723	0.00007	0.00192	0.00003	967.2	0.28194	0.00002	-7.94368	1.79	2.34	n/a	
CG10-044	23_01	Yb	4.70285	0.28195	0.00006	0.91183	0.00775	1.46719	0.00011	0.05806	0.00105	903.7	0.28193	0.00006	-9.79622	1.84	2.41	0.28201	0.00004
CG10-044	24_01	Yb	4.59922	0.28190	0.00005	0.96279	0.00505	1.46729	0.00009	0.03477	0.00064	954.1	0.28189	0.00005	-10.2687	1.89	2.48	0.28197	0.00003
CG10-044	25_01	Yb	2.80476	0.28201	0.00006	0.98032	0.00509	1.46731	0.00007	0.03618	0.00067	999.9	0.28200	0.00006	-5.26293	1.73	2.20	0.28207	0.00003
CG10-044	25_02	Yb	3.43279	0.28198	0.00002	0.96438	0.00483	1.46724	0.00007	0.01026	0.00018	955.6	0.28197	0.00002	-7.08983	1.76	2.28	n/a	
CG10-044	27_01	Yb	9.67274	0.28200	0.00002	1.08637	0.00279	1.46726	0.00005	0.07507	0.00118	975.3	0.28198	0.00002	-6.56414	1.77	2.26	0.28207	0.00001
CG10-044	29_01	Yb	9.25875	0.28206	0.00002	1.07613	0.00308	1.46731	0.00006	0.03730	0.00056	976.8	0.28205	0.00002	-3.92654	1.66	2.10	0.28210	0.00002
CG10-087	02_01	Yb	9.28330	0.28206	0.00002	0.93244	0.00309	1.46727	0.00005	0.04993	0.00081	948.1	0.28204	0.00002	-4.7865	1.67	2.13	0.28210	0.00002
CG10-087	03_01	Yb	9.64156	0.28197	0.00002	0.92239	0.00328	1.46726	0.00005	0.01254	0.00020	917.5	0.28197	0.00002	-8.21042	1.77	2.32	0.28197	0.00001
CG10-087	04_01	Yb	8.50598	0.28205	0.00002	0.90042	0.00299	1.46730	0.00005	0.06580	0.00107	987.3	0.28204	0.00002	-4.24986	1.69	2.13	0.28212	0.00002
CG10-087	12_01	Yb	8.88074	0.28199	0.00002	0.89053	0.00313	1.46725	0.00005	0.03445	0.00057	978.5	0.28198	0.00002	-6.45847	1.76	2.26	0.28201	0.00001
CG10-087	32_01	Yb	8.95686	0.28200	0.00001	0.96566	0.00307	1.46730	0.00006	0.00442	0.00007	926.6	0.28200	0.00001	-6.75986	1.72	2.24	n/a	
CG10-087	34_01	Yb	8.94994	0.28196	0.00001	0.90058	0.00312	1.46728	0.00005	0.00269	0.00004	945.3	0.28196	0.00001	-7.72514	1.77	2.31	n/a	
CG10-087	35_01	Yb	9.14626	0.28200	0.00003	0.89190	0.00331	1.46726	0.00006	0.02731	0.00043	944	0.28199	0.00003	-6.86348	1.74	2.26	0.28202	0.00002
CG10-087	38_01	Yb	8.35435	0.28196	0.00002	0.86642	0.00377	1.46724	0.00007	0.01195	0.00019	990	0.28196	0.00002	-6.9978	1.78	2.30	0.28198	0.00002
CG10-133	01_01	Yb	8.53819	0.28200	0.00001	0.88314	0.00302	1.46724	0.00005	0.00150	0.00002	908.6	0.28200	0.00001	-7.19031	1.72	2.25	n/a	
CG10-133	04_01	Yb	7.19822	0.28208	0.00003	0.81113	0.00373	1.46727	0.00007	0.05899	0.00095	960.8	0.28207	0.00003	-3.75309	1.65	2.07	0.28212	0.00002
CG10-133	06_01	Yb	6.79468	0.28204	0.00002	0.80684	0.00401	1.46725	0.00006	0.03042	0.00052	992	0.28203	0.00002	-4.36624	1.69	2.14	0.28204	0.00002
CG10-133	06_02	Yb	7.64158	0.28198	0.00001	0.81274	0.00324	1.46729	0.00006	0.00155	0.00002	970.3	0.28198	0.00001	-6.46483	1.74	2.25	n/a	
CG10-133	15_02	Yb	7.03892	0.28200	0.00003	0.77656	0.00402	1.46730	0.00007	0.00673	0.00010	946.6	0.28200	0.00003	-6.36253	1.72	2.23	0.28200	0.00002
CG10-133	17_01	Yb	7.08010	0.28200	0.00002	0.79089	0.00341	1.46728	0.00006	0.00148	0.00002	972.9	0.28200	0.00002	-5.9362	1.72	2.22	n/a	
CG10-133	24_01	Yb	7.85528	0.28199	0.00003	0.83157	0.02258	1.46726	0.00005	0.06657	0.00118	949.7	0.28197	0.00003	-7.55252	1.79	2.31	0.28204	0.00002
CG10-133	26_01	Yb	6.93609	1.46727	0.00007	0.79524	0.00385	1.46727	0.00007	0.02879	0.00048	930.4	0.28198	0.00003	-7.56457	1.76	2.29	0.28202	0.00002
CG10-133	27_01	Yb	6.47124	0.28204	0.00003	0.80133	0.00365	1.46726	0.00006	0.04925	0.00085	993.7	0.28202	0.00003	-4.50655	1.70	2.15	0.28210	0.00002
CG10-142	01_01	Yb	6.40149	0.28198	0.00004	0.85205	0.00693	1.46728	0.00007	0.06354	0.00102	617.3	0.28197	0.00003	-14.9025	1.79	2.51	0.28207	0.00002
CG10-142	08_01	Yb	4.45029	0.28193	0.00004	0.77094	0.00541	1.46724	0.00007	0.03609	0.00060	968.7	0.28192	0.00003	-8.6156	1.83	2.39	0.28195	0.00002
CG10-142	10_02	Yb	8.50082	0.28191	0.00001	0.93781	0.00344	1.46732	0.00006	0.00411	0.00005	877.3	0.28191	0.00001	-11.2345	1.84	2.48	n/a	
CG10-142	12_01	Yb	8.96945	0.28191	0.00002	0.89489	0.00354	1.46727	0.00007	0.01724	0.00025	955.6	0.28190	0.00002	-9.70511	1.86	2.45	0.28192	0.00002

Table 8. Major element compositions, trace element concentrations, and rare earth element compositions for the granitoid suite.

		Megacrystic orthogneiss	Charnockite		Megacrystic granitoid	
Element		CG10-006	CG10-044	CG10-133	CG10-087	CG10-142
SiO_2	(wt.%)	64.8	65.9	64	63.2	62.8
TiO_2		0.735	1.145	1.1	1.165	1.405
Al_2O_3		14.7	14.4	15.3	15.6	15.5
Fe_2O_3t		6.41	7.38	6.6	8.06	7.65
MnO		0.08	0.1	0.08	0.12	0.12
MgO		0.76	1.71	1.53	1.68	1.49
CaO		2.9	3.76	4.16	3.4	3.1
Na_2O		2.15	1.62	2	1.86	1.82
K_2O		6.1	3.42	3.3	3.62	4.48
P_2O_5		0.24	0.31	0.3	0.34	0.44
LOI		0.46	0.24	0.39	0.29	0.37
Be		2.5	1.5	2	1.5	2
Sc		10	15	15	20	20
V		25	85	75	90	85
Cr		<20	40	40	35	30
Zn		100	110	80	95	90
Ga		18.5	19	18	19	20
Rb		195	135	115	100	190
Sr		195	165	140	105	105
Y		21	41	25.5	55	75
Zr		450	335	365	375	650
Nb		20	19.5	8	20.5	33
Mo		1.3	1.4	1.6	1.6	1.6
Sn		<10	<10	<10	<10	<10
Cs		0.9	0.3	0.2	0.2	0.6
Ba		1400	1000	700	800	850
Hf		11	9	10	10	18
Ta		<2	<2	<2	2	3
Th		2.3	7.5	23	18.5	95
U		0.4	0.3	0.4	0.6	1.5
La		43.5	65	80	60	180
Ce		75	125	170	115	385
Pr		10	15	20	15	43.5
Nd		36.5	60	75	55	160
Sm		6.5	10.5	12.5	11	27
Er		2.4	4.5	2.4	6.5	8.5
Eu		2.1	2.2	2	1.95	2.4
Gd		6	10	10	11	22
Tb		0.8	1.4	1.15	1.75	2.9
Dy		4.6	8	6	11.5	16.5
Ho		0.86	1.55	0.94	2.2	3
Tm		0.3	0.6	0.3	0.9	1.1
Yb		2	4.2	1.75	6	7.5
Lu		0.28	0.6	0.24	0.8	1